- **THERMAL CONDUCTIVITY OF CARBON NANOTUBES AND ASSEMBLIES**

Pengyingkai Wang [1], Rong Xiang [1], Shigeo Maruyama [1,2]

[1]Department of Mechanical Engineering, the University of Tokyo, 7-3-1 Hongo, Bunkyo Tokyo 113-8656, Japan;

[2] Energy Nano Engineering Lab., AIST, 1-2-1 Namiki, Tsukuba, Ibaraki 305-8564, Japan

I. INTRODUCTION

The history of carbon nanotube can be traced back to 1879 when Thomas A. Edison used it as filament in electric heated light bulb. Carbon fibers are macroscale analog of carbon nanotubes. The research work proceeded slowly but steadily over the following years and in 1890, vapor grown carbon filaments was established, which is a far-reaching synthesizing method. Driven by the need for strong, stiff and light weight materials in 1950's, preparation for filamentary carbon materials has received intense study and similar methods spread to materials like Si and iron. To further improve the purity of filaments, synthesized carbon fiber with catalytic chemical vapor deposition (CVD) was achieved during the 1960's and early 1970's [1]. Vapor grown carbon fibers have smaller diameters and CVD method is further optimized with greater control. However, the real breakthrough was done by Sumio Ijima [2] in 1991, he synthesized the first hollow carbon nanotube (CNT) by soot of arc discharge. In 1993 he synthesized a single-shelled carbon nanotube with diameter of 1 nm [3]. Since then, this theoretical 1-D material has sped up the research in related scientific branches. Owing to its marvelous electrical, thermal, and optical properties, CNT has been intensively studied [4, 5] and also has aroused related commercial activities. Various new tube structures are displayed in Figure 1.

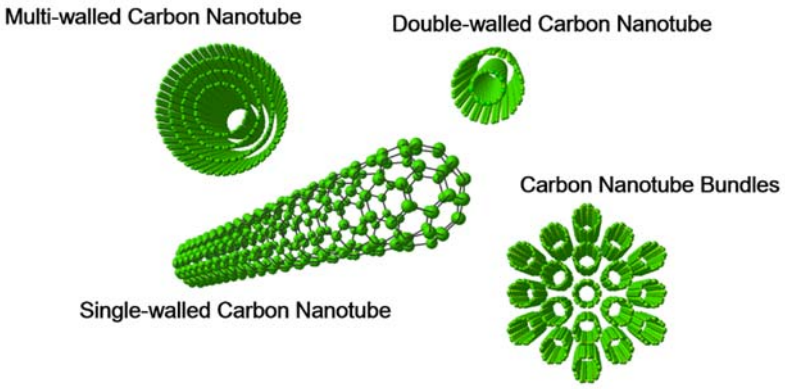

Figure 1-1 Carbon nanotube related 1-D carbon materials that have been extensively studied during the recent years.

The microelectronic industry has enabled devices with smaller volume but faster operating speeds Materials with outstanding electrical and thermal performance have become important in application Among the vast candidates, carbon nanotube is one remarkable option. Carbon nanotube film is one of potential candidate for solar cells as transparent conductive film [6-8]. It is stable, flexibile and harmless. Thermal property is another advantage of carbon nanotube. Savas *et al*. [9] has suggested unusual high thermal conductivity of an isolated (10, 10) carbon nanotube to be around 6600 W/mK at room temperature. Despite the fact that carbon nanotubes have these attractive properties, the understanding of energy transport in this material is necessary. In macroscale energy heat transfer, the state of a system can be described comprehensively by a phase point and the motion of the system can be predicted by Hamilton's equations. In contrast to macroscale, carbon nanotube has a one dimensional crystal structure, the energy carriers should be taken into consideration. But microscale objects obviously have some similarities with macroscale systems Macroscale models need some modifications to allow them to be applied to microscale situations. The first way is to modify classical methods like Fourier's law and Newton's law to make them fit micro systems. After that, Liouville and Boltzmann equations are adopted as a more universal description of a nonequilibrium state. At the same time, near-equilibrium equations (Landauer equation) can be used to simplify the mechanism in heat transfer. Another very powerful approach is molecular dynamic (MD) simulations, which are becoming more accurate thanks to the fast improvement of computing technology.

Several excellent review papers have summarized the benchmarks of carbon nanotubes and closely related graphene mechanical, electrical, and thermal properties [10-13]. In this work, we will discuss basic methods towards attaining thermal properties of carbon nanotubes and recent progress on carbon nanotube composites. This review paper will start by quickly going through some basic solid state physics concepts such as electrons, lattice vibrations, phonons and heat capacity. With this background knowledge, a basic review of theoretical and basic experimental methods will be discussed. Recent progress and key finding will be addressed in detail. Next we will talk about bundles and contacts, which are not widely discussed in the existing literature. Finally, promising thermal management using carbon nanotube components will be presented.

II. MICROSCOPIC VIEW OF CARBON NANOTUBES

A. STRUCTURE OF SINGLE-WALLED CARBON NANOTUBE

1. Geometry structure

To understand the structure of carbon nanotubes, it is easy to think of a sheet of graphene rolled up into a seamless cylinder and adding two terminations to the ends. The terminations, which is a hemisphere of a fullerene, fits perfectly to the long cylindrical nanotube. The rolling up a carbon nanotube is described by a rolling vector or chirality vector C_h, which divides carbon nanotubes into three groups: zigzag, armchair and chiral, shown in Figure 2-1 [14]. The name of the structure originates from the shape of the cross section ring, shown at the edge of the carbon nanotube in the picture. Zigzag and armchair are symmetrical structures and the chiral nanotube, which is common and abundant, lacks this feature.

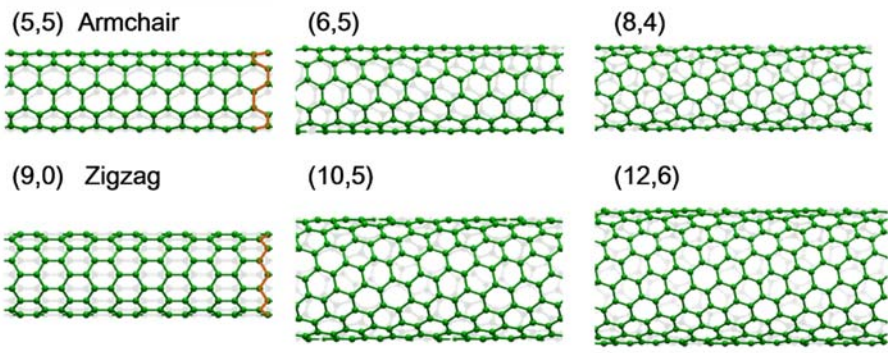

Fig 2-1 Carbon nanotubes with different chirality. (5, 5) is featured by the red line shown at the end of the tube. (9, 0) is named by the zigzag structure at the tube end shown by read line. The other four chiral structures are popular carbon nanotubes and are widely studied.

2. Chiral vector C_h

A chiral vector is the only one parameter to define a carbon nanotube, shown as vector OA in Figure 2-2, representing the lattice structure of graphene. The distance between two carbon atoms is $a_0 = 1.42$ Å. Perpendicular to OA is OB, the direction of the axial called translational vector T. Moving OB along OA until point O and point A coincide defines the position of B as B'. If we cut OABB' and roll it up to make O and A coincide and B and B' coincide, a carbon nanotube will be formed. Setting unit

vectors of the lattice as a_1 and a_2, as shown in Figure 2-2, we can use a_1 and a_2 to express C_h:

$$C_h = na_1 + ma_2 \equiv (n,m), \quad (n, \ m \in \text{integer}, 0 \leq |m| \leq n) \tag{2-1}$$

$$a_1 = \left(\frac{\sqrt{3}}{2}\, a, \frac{1}{2}\, a\right), a_2 = \left(\frac{\sqrt{3}}{2}\, a, -\frac{1}{2}\, a\right) \tag{2-2}$$

Now many properties can be deduced from the chiral vector (n, m). For zigzag structure carbon nanotubes, $m = 0$, and $C_h = (n, 0)$. For armchair structures, $m = n$, and all other vectors correspond to chiral structure carbon nanotube. The diamtere of the carbon nanotube, d, is calculated through C_h:

$$d_t = \frac{L}{\pi}, L = |C_h| = \sqrt{C_h \cdot C_h} = a\sqrt{n^2 + m^2 + mn} \tag{2-3}$$

where a is the lattice constant, $|a| = |a_1| = |a_2| = a_0 \cdot \sqrt{3} = 1.42 \times \sqrt{3} = 2.46$ Å . For example, chiral vector OA is (4, 1) in Figure 2-2, so the diameter of this carbon nanotube is $d_t = 3.59$Å.

The chiral angle θ is defined as the cross angle of C_h and a_1, it defines the spiral symmetry of nanotube. With the hexagonal symmetry of honeycomb lattice taken into consideration, $0 \leq |\theta| \leq 30^\circ$. θ can be calculated through the following equation:

$$\theta = \arccos\left(\frac{C_h \cdot a_1}{|C_h| \cdot |a_1|}\right) = \arccos\left(\frac{2n+m}{2\sqrt{n^2+m^2+nm}}\right) \tag{2-4}$$

Zigzag structures have $\theta = 0^\circ$ and armchair structures to $\theta = 30^\circ$. Chirality and nanotube diameter affect thermal property significantly, and will be discussed in detail in section 3.4.

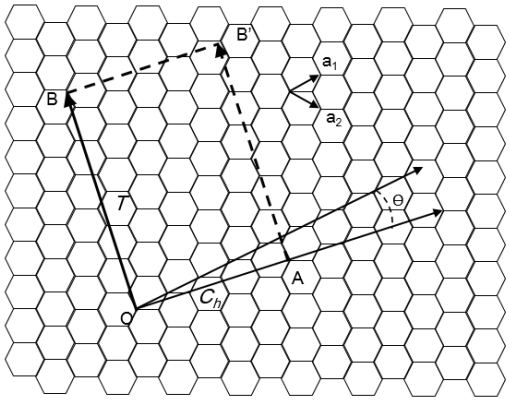

Fig 2-2 Lattice structure of graphene. OA, OB denotes the chiral vector and translational vector, respectively.

3. Translational vector T

Vector OB in Figure 2-2 is perpendicular to chiral vector C_h and is defined as the translational vector. Similar to the chiral vector, a translational vector can be expressed in terms of unit vectors a_1 and a_2:

$$\mathrm{T} = t_1 a_1 + t_2 a_2 \equiv (t_1, t_2), \quad (t_1,\ t_2 \in \text{integer}) \tag{2-5}$$

where

$$t_1 = \frac{2m+n}{d_R},\ t_2 = -\frac{2n+m}{d_R} \tag{2-6}$$

with d_R the greatest common divisor of $(2m+n)$ and $(2n+m)$. If we define d as the largest common divisor of *n* and *m*,

$$d_R = \begin{cases} \mathrm{d} & if\ n-m\ is\ not\ a\ multiple\ of\ 3\ \mathrm{d} \\ 3\mathrm{d} & if\ n-m\ is\ \ a\ multiple\ of\ 3\ \mathrm{d} \end{cases} \tag{2-5}$$

Therefore, the definition of different structure of carbon nanotube by diameter d_t and height of *T* simplify to:

$$\text{Zigzag: } |C_h| = na,\ \ T = \sqrt{3}a, \quad \theta = 0 \tag{2-6}$$

$$\text{Armchair: } |C_h| = \sqrt{3}na,\ \ T = a, \quad \theta = 30^{\circ} \tag{2-7}$$

The physical meaning of translational vector *T* is the unit length of the carbon nanotube along the axial direction. Now, the unit cell of the 1D carbon nanotube is rectangular OABB' as shown in Figure 2-2 can be defined by C_h and *T*. The area of the nanotube unit cell is $|C_h \times T|$ and the area of a single hexagon is $|a_1 \times a_2|$, thus the number of hexagonals in one unit cell of carbon nanotube *N* is calculated by:

$$\mathrm{N} = \frac{|C_h \times T|}{|a_1 \times a_2|} = \frac{2(n^2+m^2+nm)}{d_R} = \frac{2L^2}{a^2 d_R} \tag{2-8}$$

Since each hexagon contains two carbon atoms, the number of carbons N_c is N_c=2*N* for a nanotube with chirality C_h.

B. ELECTRONICAL PROPERTIES OF CARBON NANOTUBE

1. Chemical bonding

One significant way in which carbon materials different from other materials is that carbon atoms have many possible electron states by hybridization of atomic orbit. Each carbon atom has six electrons which occupy $1s^2$, $2s^2$, $2p^2$ atomic orbits. The first two electrons, also called core electrons, are bonded tightly with the core, while the other four electrons are bonded relatively weaker. The energy difference between $2s^2$ and $2p^2$ is smaller than the binding energy of chemical bonds, therefore their electronic wave function can mix with each other. In carbon, there are three possible hybridizations: *sp*, sp^2, sp^3. When the carbon atom uses one $2s^2$ electron orbit to mix with two $2p^2$ electron orbits, the result is three sp^2 orbits and one single 1p orbit. Two of these three sp^2 orbits form two covalent bonds with two hydrogen atoms by *s*- sp^2 orbit overlap, and the remaining one sp^2 orbit overlaps with the sp^2 of another carbon atom to form a σ bond. These three sp^2 bonds are in the same plane with 120°angles. The remaining two *2p* electrons of the two carbon atom form a π bond. Thus there are two bonds between carbon atoms, one is a σ bond and one is a π bond. But a π bond is of lower energy so it is easily broken to mix with other atoms and form new molecules, for example:

$$H_2C = CH_2 + Cl_2 \rightarrow Cl - CH_2 - CH_2 - Cl \tag{2-9}$$

sp hybridization (like C_2H_2) and sp^3 hybridization (like CH_4) orbits can be explained in similar ways.

2D-graphene has tightly packed carbon atoms with three sp^2 orbits forming 3 σ bonds and one *2p* orbit forming a π bond. As stated before, carbon nanotube can be treated as graphene rolled into a cylinder, they have the same chemical bonds.

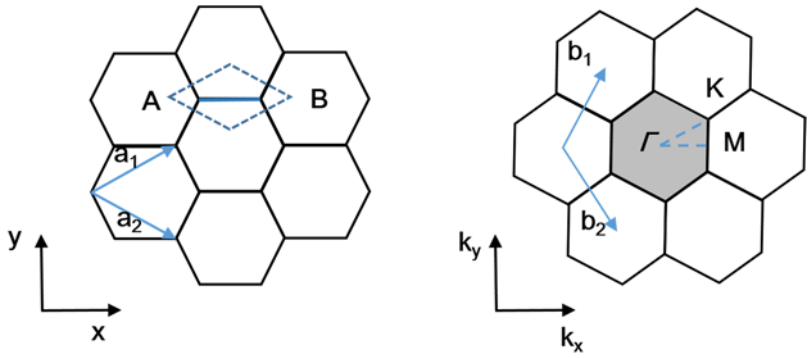

Figure 2-3. Unit cell and Brillouin zone of graphene in real space and in momentum space. Dotted line and shaded

part denote first Brillouin zone in real space and momentum space, respectively.

2. Electrical properties of carbon nanotubes

Another impressive characteristics of carbon nanotube is that the chirality decides electrical conductivity. To better understand this unique electronic property, we first look at the momentum space of graphene. Figure 2-3 shows the unit cell of graphene in real space (lattice) and in momentum space (reciprocal lattice). We use a_1 and a_2 as the unit vectors in the Cartesian *x*-*y* coordinate, with a representing the lattice constant of graphene. Correspondingly, in the $k_x - k_y$ coordinate in reciprocal space, the unit vectors are defined as

$$b_1 = \left(\frac{2\pi}{\sqrt{3}a}, \frac{2\pi}{a}\right), b_2 = \left(\frac{2\pi}{\sqrt{3}a}, -\frac{2\pi}{a}\right) \tag{2-10}$$

The first Brillouin zone is selected as a gray hexagon as shown in Figure 2-3, and *Γ*, *K* and *M* denote three high symmetry points at the center, corner and the center of the edge, respectively. Similar to the basis vector in real space, (C_h and T), reciprocal space has basis vectors defined as K_1 and K_2 through following equations:

$$C_h \cdot K_1 = 2\pi; \quad T \cdot K_1 = 0 \tag{2-11}$$

$$C_h \cdot K_2 = 0\,; \quad T \cdot K_1 = 2\pi$$

Therefore, K_1 and K_2 can be obtained as:

$$K_1 = \frac{1}{N}(-t_2 \cdot b_1 + t_1 \cdot b_2) \tag{2-12}$$

$$K_2 = \frac{1}{N}(m \cdot b_1 - n \cdot b_2) \tag{2-13}$$

From the above equations, one can see the size of Brillion zone is inverse with unit cell size in real space. Thus the Brillion zone for SWNT is much smaller than that of graphene, and becomes a cutting line on the reciprocal lattice of graphene as shown in Figure 2-4(a). T and the N wave vectors μK_1 (μ=0,1,2…,N-1) , which are related to the quantized wave vectors from the periodic boundary conditions on C_h, lead to N electronic energy band (one π band and one π^* band), and 6N branches of phonon dispersion relation, where N is given by equation (2-8). Along the axial direction, if the length of the carbon nanotube is infinite, there will be continuous wave vectors. However, for a finite length carbon nanotube, the distance between wave vectors is $2\pi/L_t$, where L_t is the length of carbon nanotube.

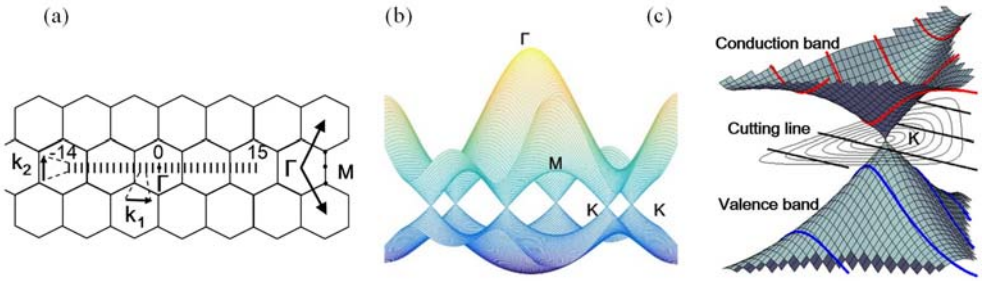

Fig 2-4: (a) The first Brillion zone of a carbon nanotube (5, 5) is represented by line segments parallel to K_2. Corresponding to C_h and T, K_1 and K_2 are reciprocal lattice vectors. (b) π band and π* band for graphene of the first Brillouin zone. (c) The calculated constant energy contours for the conduction band and valence band for 2D graphene layer. The two bands touch in the K point. Solid curves are the cutting lines for (7, 5) carbon nanotube. (Figure 2-4 (c) was originally plotted by Professor Yuhei Miyauchi at Kyoto University)

As mentioned before, 2D graphite has a π energy band and it is very important in determining the solid state properties. The basis function for 2D graphite is provided by Bloch functions only considering the nearest-neighbor interaction [4], from which the energy dispersion relation of two-dimensional graphite containing a π band and a π^* band can be deduced. The energy dispersion relation is given as:

$$E_{g2D}(\vec{k}) = \frac{\varepsilon_{2p} \pm t\omega(\vec{k})}{1 \pm s\omega(\vec{k})} \tag{2-14}$$

where the + signs in the numerator and denominator together give bonding π energy and – signs gives anti-bonding π^* energy. While the function $\omega(\vec{k})$ is given by:

$$\omega(\vec{k}) = \sqrt{1 + 4\cos\frac{\sqrt{3}k_x \cdot a}{2}\cos\frac{k_y \cdot a}{2} + 4\left(\cos\frac{k_y \cdot a}{2}\right)^2} \tag{2-15}$$

The energy dispersion relation of 2D graphite is plotted in Figure 2-4(b), with $\varepsilon_{2p} = 0$, t = 0.29 eV and s = 0.129. The upper half is the π^* anti-bonding band and the lower half is the π energy bonding band, shown in Figure 2-4 (b). Figure 2-4 (c) show the calculated constant energy contours for the conduction band and valence band for a 2D graphene layer. The two bands touch at the K point, meaning a zero gap here. Thus whether the allowable and discrete wave vectors of CNT can or cannot pass through the *K*-point will result in a metallic or a semiconducting CNT, and this is decided by chirality (*n*, *m*). With increasing diameter, the band gap will decrease and result in more allowable wave vectors for the circumferential direction, indicating the CNT are transforming from 1D to 2D. Therefore, to

observe 1D quantum effects, the CNTs must have small enough in diameters.

It is possible to define a vector $\overrightarrow{YK}$ as expressed below:

$$\overrightarrow{YK} = \frac{2n+m}{3} K_1 \tag{2-16}$$

If the length of the vector $\overrightarrow{YK}$ is a multiple of the length of K_1, the nanotube is metallic. Particularly, all armchair nanotubes denoted by (n, n) are metallic and zigzag nanotubes denoted by (n, 0) are metallic only when n can be divided by three. Of course the conductivity of carbon nanotubes can be judged by their density of state at the Fermi level, which will be discussed later. One thing worth mentioning is that calculation reveals that one third of carbon nanotubes are metallic and two thirds are semiconducting. As stated above, when $2n+m=3q$, where q is an integer, the carbon nanotube is metallic, whereas it is semiconducting if not [4]. As a result, a map of carbon nanotubes based on the electronic properties is demonstrated in Figure 2-5.

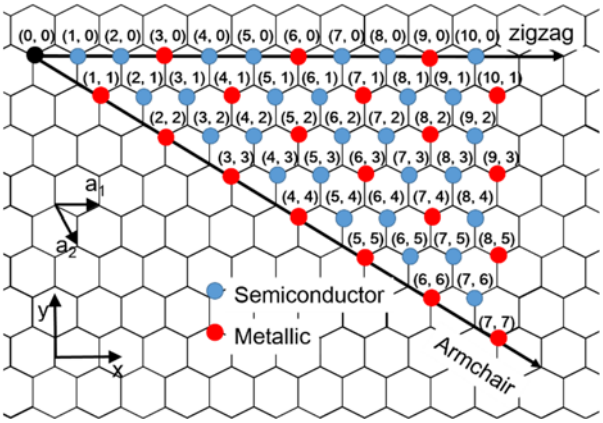

Figure 2-5. Period table of electrical conductivity for SWNT. Blue and red dots referring to semiconductor and metallic SWNT respectively.

It is important to introduce the concept of electron density of state (eDOS), the origin of the difference between metallic and semiconducting SWNTs. Using a tight binding model, the eDOS of metallic (5,5), (9, 0) and semiconducting (10, 5) nanotube are shown in Figure 2-6. The nanotube structures are plotted by eDOS in accordance with Figure 1-1. The van Hove singularities (vHSs) in the picture are introduced by the one-dimensional quantum confinement. At the Fermi level, the eDOS of semiconducting nanotube (10, 5) is zero and the energy difference between the two vHSs near Fermi level is the band gap. Therefore the 2D graphene forming this SWNT is a zero-gap semiconductor. And correspondingly,

the eDOS of metallic (5, 5) and (9, 0) SWNTs are very small.

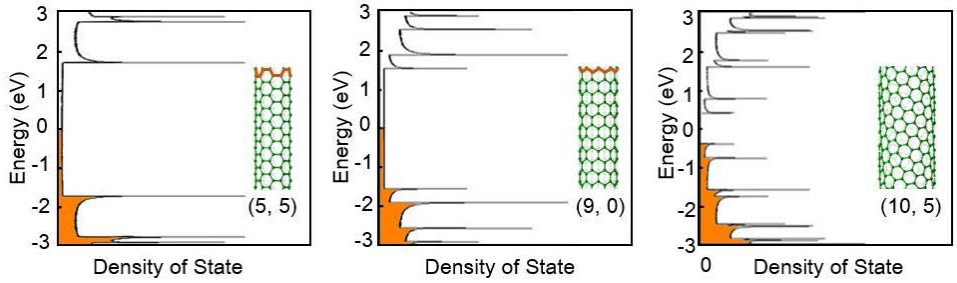

Figure 2-6 Electron density of state for (5, 5), (9, 0) and (10, 5) carbon nanotubes. (10, 0) has semiconductor behavior and (5, 5), (9, 0) have metallic behavior.

C. VIBRATIONS AND PHONONS

We start with imaging a one-dimensional chain containing N atoms with the interatomic force simplified as a spring constant. Using Newton's equation of motion to describe the i^{th} atom in the chain as:

$$m_i \cdot \ddot{\partial}_{xl} = \frac{\partial(\sum_{i_2}^{K}(\delta_{i+1}-\delta_i)^2)}{\partial x_i} \tag{2-17}$$

where m_i and x_i are the mass and coordinate of i^{th} atom, K is the spring constant, δ is the displacement from balance position, and $\sum_i \frac{K}{2}(\delta_{i+1}-\delta_i)^2$ is the total potential of the chain.

For any coupled system, there are normal modes in which all particles move at the same frequency forming a collective oscillation [16]. The solution to the frequency is:

$$\omega = 2\sqrt{\frac{K}{m}}\left|\sin(\frac{Ka}{2})\right| \tag{2-18}$$

with a as the lattice constant for 1D chain, or the distance between successive masses at rest. The energy of a system oscillating at frequency ω is $\hbar\omega(n+\frac{1}{2})$, where n is a non-negative integer. The lowest excitation energy for such system is $\hbar\omega$, and all possible excitations occur in energy units of $\hbar\omega$. Each excitation by a step up the harmonic oscillator excitation ladder is known as a phonon; or a phonon is a discrete quantum of vibration.

Determining the phonon dispersion relation in a SWNT is not easy as for a 1D chain, but it can be

obtained from that of a 2D graphene sheet through the zone folding approach [4] as shown in Figure 4-8 (a):

$$\omega_{1D}^{m\mu}(k) = \omega_{2D}^{m\mu}(k)\left(k\frac{\mathrm{K}_2}{|\mathrm{K}_2|} + \mu\mathrm{K}_1\right), \left(\begin{matrix} m=1,\ldots,6 \\ \mu=0,\ldots N-1, \end{matrix} and\ -\frac{\pi}{T} < k \leq \frac{\pi}{T}\right) \quad (2\text{-}19)$$

In the above equation, left term denotes the phonon dispersion relation of one-dimensional SWNT, $\omega_{2D}^{m\mu}(k)$ is that of 2D graphene and $\left(k\frac{\mathrm{K}_2}{|\mathrm{K}_2|} + \mu\mathrm{K}_1\right)$ describes the quantized wave vectors in the circumferential direction resulting from periodic boundary conditions. *m* represents the six phonon modes of the two carbon nanotubes in a graphene unit cell, each of which has three-dimensional vibration. As mentioned above, there are $2N_c$ carbon atoms in the unit cell of a SWNT, the total vibration degree of this system is $6N_c$, and therefore the phonon dispersion relation of SWNT consists of $6N_c$ branches for each unit cell.

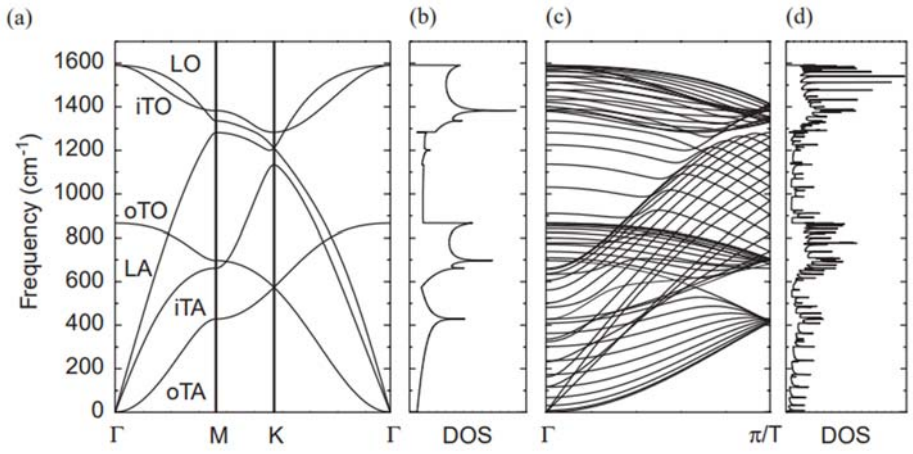

Figure 2-7 (a) Phonon dispersion relations of graphene sheet, six phonon modes in the order of increasing energy are out-of-plane transverse acoustic (oTA), in-plane transverse acoustic (iTA), longitudinal acoustic (LA), out-of-plane transverse optic (oTO), in-plane transverse optic (iTO) and longitudinal optic (LO), respectively. (b) The phonon density of states of graphene sheet. (c) Calculated phonon dispersion relations of (10, 10) armchair SWNT, including 120 degrees of freedom and 66 distinct phonon branches. (d) Corresponding phonon density of states for (10, 10) SWNT.

In Figure 2-7 (a), 3 branches originating from *Γ* are the acoustic modes, the order of increasing energy is: out-of-plane transverse (oTA) mode, in-plane tangential (iTA) mode and in-plane radio (LA) mode. Corresponding density of state is plotted in Figure 2-7 (b). Dispersion relation of a (10, 10) carbon

nanotube is plotted in Figure 2-7 (c). For $2N_c$= 40, there should be 120 vibration degrees of freedom, yet only 66 phonon branches are observed because of the degeneracies of some modes. Different from 2D graphene, all the acoustic phonon dispersion relations around Γ have linear relations to *k*, we'll talk more in detail in section 3. Worth mentioning is that there is a fourth acoustic mode for carbon nanotubes [4] relating to the rotation around the tube axis, called the twisting mode (TW). But the velocity of this mode is the same with in-plane TA mode. The phonon density of state for a (10, 10) carbon nanotube is shown in Figure 2-7 (d), similar to that of 2D graphene because phonon dispersion relation of SWNT is calculated from the dispersion relation of graphene by the zone folding method. But for SWNT, there are numbers of peaks which are not seen in 2D graphene, reflecting the unique effects from 1D quantum confinement.

D. THERMAL TRANSPORT IN CARBON NANOTUBE

Energy exchange is the result of random motion of material particles in the system. Such material particles can be electrons, atoms, and molecules in gases, liquids and in solids. But for different types of system, the energy carriers are different. For example, in metals, energy is conducted by free electrons and phonons. But in semiconductors, the energy is mainly carried by phonons because the free electron density in semiconductor is much smaller than in metals, ~10^{18} cm^{-3} and ~10^{23} cm^{-3}, respectively. The heat capacity from phonon contribution is expressed as [15]:

$$C_{ph} = \int_0^\infty \frac{k_B\left(\frac{\hbar\omega}{k_BT}\right)^2 \rho(\omega) e^{\hbar\omega/k_BT} d\omega}{\left(e^{\frac{\hbar\omega}{k_BT}}-1\right)^2} \tag{2-20}$$

In the formula, $\rho(\omega)$ is phonon density of state derived from the phonon dispersion relation. For isolated SWNT, the four low-frequency acoustic phonons mentioned above are expected to dominate heat transfer at low temperatures. The dispersion relations for these four acoustic phonons are linear, therefore a linear relationship between C_{ph} and temperature (at low temperatures) can be expressed as:

$$C_{ph} = \text{const}\,\frac{k_B^2 T}{\hbar v}, T \ll \frac{\hbar v}{k_B d_t} \tag{2-21}$$

where v and d_t are averaged velocity of sound and the diameter of SWNT, respectively. At higher temperature, optical phonons will be excited and the total heat capacity will deviate from the linearity with temperature. Even though these four high-energy phonon modes have significant weight, the contribution from the optical phonons cannot be completely nullified [17].

For metallic SWNTs, heat capacity contributed by electrons is considered to vary linearly with temperature but its impact is two orders of magnitude lower than phonons since the Fermi velocity is a hundred times smaller than sound velocity. As in semiconducting SWNTs, the contributions of electrons at low temperature is quite small and is expected to depend on temperature exponentially [15].

Thermal conductivity of phonons in a 1D system is expressed as a summation over all phonon modes and polarizations:

$$\kappa_{ph} = \sum C v^2 \tau \tag{2-22}$$

C, v and τ are specific heat capacity, phonon group velocity in the axial direction of SWNT and the relaxation time of a given phonon mode, respectively. The thermal conductivity of free electrons can be determined from the electrical conductivity σ by the Wiedemann-Franz law:

$$\frac{\kappa_{el}}{\sigma} \approx L_0 = 2.45 \times 10^{-8}\,(V/K)^2 \tag{2-23}$$

The total thermal conductivity can be obtained by adding κ_{ph} and κ_{el} together. However, the contribution to heat transfer from phonons is much larger than from electrons at all temperatures in SWNTs. In the following sections, heat transfer is only considered for phonons.

III. THEORETICAL MODELING

Until now, the basic information about the energy carriers and the ways to dealing with these carriers has been developed. In this section, we'll focus on modeling heat transfer from a microscopic view. The first and simplest way is to explain thermal transport using modified classical continuum models like Fourier's law is to relate the local temperature gradient with local heat flux:

$$q = -\kappa \cdot \nabla \mathrm{T} \tag{3-1}$$

where κ is the thermal conductivity, q is local heat flux with unit of [W/m^2], and ∇ is an operator that:

$$\nabla \mathrm{T} \equiv \frac{\partial T}{\partial x}\hat{x} + \frac{\partial T}{\partial y}\hat{y} + \frac{\partial T}{\partial z}\hat{z} \tag{3-2}$$

It describes the heat conduction through a medium which is caused by temperature gradient because the random motion of energy carriers. Fourier's law yields an infinite speed of energy propagation throughout the medium, which actually is quite slow. Kittle and Kroemer [18] put up an average velocity

of thermal energy propagation rate, indicating the existence of a time scale for finite speed thermal transport. After that, Joseph and Preziosi introduced Catteneo's equation and addressed it with a more applicable solution containing the relaxation time of heat carriers, τ.

Other continuum thermal models that deal with heat transfer as equilibrium and nonequilibrium systems also exist, but the thermal properties can be influenced by microscale phenomena. Defects, such as boundary scattering and surface scattering make heat carriers in 1-D materials behave differently from their bulk counterparts. So proper models should be used to accurately describe heat carriers in carbon nanotube.

As previously mentioned, thermal transport in carbon nanotubes is by the lattice vibration, or the phonon transport and sometimes includes electron transport if the sample is metallic. Let's call these energy carriers. If energy carriers can move through a material with negligible resistance caused by scattering, the material is a ballistic conductor. Otherwise the energy carriers experience a diffusive transport. But CNTs act as ballistic conductors or as diffusive conductors depending on several conditions. It is a ballistic conductor when the mean free path is longer than the nanotube length and the wavelength of the dominant phonon is smaller than nanotube diameter. Diffusive transport occurs when CNT length is longer than the phonon mean free path and the diameter on CNT is larger than phonon wave length. Also, high temperature will increase the scattering rate for both electron and phonon with in the carbon nanotube, thus leading to diffusive transport.

At an atomic level, there are ways to determine how atoms composing the system interact with each other and how phonons are transported in a medium: molecular dynamic (MD) simulation (Sec. A) and phonon transport theory (Sec. B). Molecular dynamics simulations allow the observation of atoms dynamic evolution of a system on the basis of choosing proper potential equations. As long as a proper model is set up, parameter influences like length, diameter, chirality, and temperature could be investigated. Phonon transport in a medium often involves a dispersion relation, scattering between phonons and boundary, relaxation time, phonon mean free path, and these have to be measured or calculate with some kinetic equations like the Boltzmann equation.

Ballistic transport happens in an ideal situation, but variations in temperature or tube length may alter the heat transfer to diffusive regime. To smoothly cross from a ballistic regime to a diffusive regime, some modification methods have been adopted to extend the effectiveness of Landauer model [19, 20], which will be discussed in detail in the following sections (Sec. C).

A. MOLECULAR DYNAMIC SIMULATIONS

Simulations involve a suitable model, accurate interatomic potential and properly chosen conditions. CNT modeling methods could be organized into three groups: atomistic modeling, continuum modeling and nanoscale continuum modeling. Atomic modeling includes molecular dynamic (MD) simulation, Monte Carlo and *ab initio* methods [21]. The nanoscale simulation method is an ongoing method and is not computationally intensive as atomic modeling. MD simulation is a powerful way to solve thermal transport in carbon nanotubes based on suitable interatomic potentials. Some proper interatomic potentials for many-body materials like silicon and carbon nanotube have been proposed [22-26], and used vastly. Total potential is expressed as the summation of all the chemical bonds [27]:

$$\Phi = \sum_i \sum_{j(i<j)} f_c(r_{ij})\{V_R(ij) - b_{ij}^* V_A(r_{ij})\} \tag{3-3}$$

Here we mainly review the molecular dynamics simulation approach. MD simulation could be classified into the following categories: equilibrium molecular dynamics (EMD), nonequilibrium molecular dynamics (NEMD) and homogeneous nonequilibrium molecular dynamics (HNEMD).

EMD method is based on linear response of Green-Kubo formula, when simplified along the axis of heat conduction in a 1-D situation is expressed as [28]:

$$\kappa = \frac{1}{V k_B T^2} \int_0^\infty < J_z(0) J_z(t) > dt \tag{3-4}$$

where J_z is the axial component of heat current, V is the volume. NEMD is derived from Fourier's law with a given temperature gradient or heat flux. Thermal conductivity is related to thermal gradient as:

$$J_\alpha = -\sum_\beta \kappa_{\alpha\beta} \frac{\partial T}{\partial x_\beta} \tag{3-5}$$

in the formula, $\partial T / \partial x_\beta$ is the thermal gradient and α, β denotes the direction of heat current [29]. The HNEMD method uses an external field as a phantom temperature gradient or heat flux and the thermal conductivity is determined to be:

$$\kappa = \lim_{F_e \to 0} \lim_{t \to \infty} \frac{<J_z(\vec{F}_e, t)>}{F_e T V} \tag{3-6}$$

in which $\vec{F}_e$ is the external field. This method has been shown to be computationally efficient [28].

Results of many reported molecular dynamic simulations on thermal transport in carbon nanotubes

are summarized in Table 3-1. In the table, all the measurements were at room temperature (around 300 K) unless otherwise stated. Applied temperature for Maruyama *et al*. [30, 31] and Moreland and Chen were the same, with mean temperature at 300 K and temperature gradient of ΔT=20 K. For single-walled carbon nanotubes, most researchers treated the cross sectional area as a hollow cylinder. Then the cross sectional area here is calculated with $\pi d\delta$, where d is diameter and δ=0.34 nm is the van der Waals distance between graphene layers. With the parameters in Table 3-1, thermal conductivity of carbon nanotube s for a cross sectional area defined as $\pi d^2/4$ could be easily calculated. In order to avoid the ambiguity of cross sectional area, Yao *et al.* [32] referred to thermal conductance instead of thermal conductivity. Ref. [43] is the theoretical calculated result listed in Table 3-1 as a reference.

Table 3-1 Molecular dynamics simulation summary

Ref	chirality	D (nm)	L (nm)	Type	potential	Boundary condition	κ W/m K	Converged with length?
[33]	(10, 10)	1.36	< 40	EMD	Brenner 2nd	periodic	2980	> 10 nm
[9]	(10,10)	1,36	2.47	HNEMD	Tersoff	periodic	6600	Not mentioned
[34]	(5, 5)	0.68	Aspect ratio of 10-20	NEMD	Tersoff–Brenner	periodic	2250	Not investigated
	(8, 8)	1.08					--	
	(10, 10)	1.36					1700	
	(12, 12)	1.63					--	
	(15,15)	2.03					1700	
	(10,0)	078					2250	
[30]	(5, 5)	0.68	6-404	NEMD	Tersoff-Brenner	Free	140-500	No
	(10, 10)	1.36					270-380	
[31]	(5, 5)	0.68	6-404	NEMD	Simplified Brenner	Free	130-510	No
	(8, 8)	1.08					150-290	
	(10, 10)	1.36					180-300	
[35]	(10, 10)	1.36	--	HNEGK	homogeneous Green–Kubo method and Brenner	periodic	2200	
	(11, 11)	1.49	30				3500	

	(10,13)	1.56	29		potential		1000	
	(20, 0)	1.57	26				7500	
[36, 37]	(10, 10)	1.351	2.477-39.632	EMD	[a]AIREBO	periodic	890	Yes (>20 nm)
	(18, 0)	1.404	2.145-34.320				820	
	(14, 6)	1.387	3.813-30.504				790	
[38]	(10, 10)	1.36	50-1000	NEMD	Brenner	periodic	215-831	No (Sign of converge)
[39]	(10, 10)	1.351	<350	NEMD	[b]REBO	periodic	350	Yes (>250)
[32]	(5, 5)	0.68	6-80	EMD	Tersoff	periodic	$1\text{-}4\times10^{23}$	No
	(10, 10)	1.36					$\sim10^{23}$	
	(15, 15)	2.03					$\sim10^{22}$	
[40]	(5, 5)	0.686	2-100	NEMD	Tersoff	Free	960	No
	(9, 0)	0.714					880	
	(10, 0)	0.794					770	
[41]	(10,. 0)	0.794	0.5-200	EMD	Tersoff	periodic	7000	Yes
[28]	(10,10)	1.36	5-40	EMD	REBO potential and Lennard Jones potential	Free	16-120	No
				EMD		Periodic	18-140	
				HNEMD		--	240-375[c]	
[42]	(10, 0)	0.8	3000				2314	
	(10,10)	1.4					2436	
[43]	(10, 10)	1.36	24.5	NEMD	Tersoff-Brenner and Lennard Jones potential	periodic	6000	No
[44]	(5, 5)-(21,21)	0.7-2.9	50	NEMD	Optimized Tersoff	Free	507-1913[b]	No
	(9, 0)-(36, 0)						233-1964 [b]	

[a]AIREBO: adaptive intermolecular reactive empirical bond order.

[b]REBO: reactive empirical bond order.

The definition of sample length would result in ambiguity with diverse boundary conditions: free boundary conditions, periodic boundary conditions and rigid boundary conditions. Free boundary conditions or infinite long conditions are employed to investigate the length dependence of thermal conductivity of carbon nanotubes, with longer cell providing more accurate representation, as in [30-31]. In NEMD simulations, periodic boundary conditions are very common, with lengths of heating and cooling regions. Sample lengths could be defined as between the two heat bath [45, 46], overall length including the two heating regions [38, 47] or length between the center of the two heating regions [44, 48, 49]. Zhigilei *et al.* discussed the influence of boundary condition in detail [50].

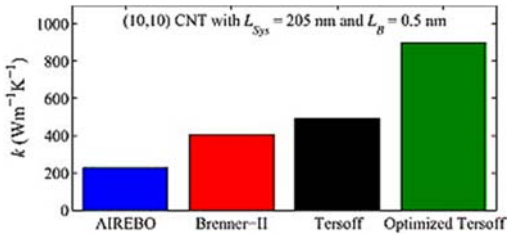

Figure 3-1. Comparison among four different calculated thermal conductivities for a of (10, 10) single-walled carbon nanotube with NEMD simulation [50].

Classical MD simulation methods have poor agreements with experimental data at temperatures lower than 500 K [28]. The reason is quantum effects, which are of great importance for materials with high Debye temperatures like carbon nanotube and diamond. With increasing temperature, the difference between a quantum-corrected method and a classical MD simulation decreases, but at room temperature, the quantum effects must be considered [28, 31]. Different quantum correction methods have been adopted yet this application is still under discussion in the literature [33, 28]. However, thermal conductivity at lower temperature is dominated by long wave length phonon [36, 37], MD simulation still provides valuable predictions of thermal properties of carbon nanotube.

(10, 10) carbon nanotube structures predominate the laser-oven grown SWNTs, and many reports have simulated SWNT with this chirality with calculated thermal conductivity values in a wide range from 16 W/m K [28] to 6600 W/m K [9]. Yao *et al*. [32] attributed their extremely high thermal conductivity to the very high-frequency phonon modes and the same vibration modes for SWNT with different length. Besides the boundary conditions mentioned above, simulation methods and interatomic potential lead to the variation of simulated results. For the NEMD method, Tersoff-Brenner thermal conductivity ranges from 380 to 6000 W/m K [30, 34, 43]. Brenner potentials are on the order of 180-

800 W/m K [31, 38]. For chirality of (10, 10) using Brenner- potentials with comparable CNT lengths, NEMD methods give 180-831 W/m K [31, 38], EMD methods give 2980 W/m K [33] and HNEMD methods give 2200 W/m K. Similarly, simulation with REBO potential result in 350 W/m K [39]. Ref 43 solved BTE instead of using the MD simulation method. The results are shown here as a comparison of thermal conductivity of (10, 10) chirality carbon nanotubes simulated with MD method. Zhigilei *et al*. [50] made comparison among four different interatomic potentials, shown in Fig 3-1. All of the simulations were NEMD and other parameters were identical.

In recent years, simulation works have expanded the field for use of carbon nanotube. Research on enhanced thermal properties of carbon nanotubes, interface phonon transport between carbon nanotube and other materials, structure optimized carbon nanotube thermal management devices have been fruitful [51-54].

B. PHONON BOLTZMANN TRANSPORT EQUATION

Thermal conductivity in real materials is limited by inharmonic transport of phonons. To fully understand the thermal properties of a system, the solution of the Boltzmann transport equation (BTE), which describes steady-state phonon transport, is needed. For systems with small and constant temperature gradients, a time-independent linearized Boltzmann equation is established to investigate the thermal properties of materials. As a consequence of the extreme difficulty in finding a full solution for the Boltzmann equation, many simplification methods with varying complicity are explored and fit with experimental measurements [55, 56].

In general, the equation is solved to describe phonon distributions and thus determine the thermal conductivity. Chantrenne and Barrat [57] developed an analytical model for calculate thermal conductivity in one direction:

$$\kappa_x = \sum_k \sum_p C(k,p) v^2(k,p) \tau(k,p) cos^2(\theta_x(k))$$

with k as the wave vector, p denotes the polarization, v is the group velocity, $\tau(k,p)$ is the relaxation time, and $\theta_x(k)$ is the angle between x direction and wave vector. This expression can be transformed into an integral form containing group velocity, relaxation time and density of state through a phonon dispersion curve. Recent progress in light scattering could be adopted to measure frequencies of phonon at special point in the Brillion zone [58] and thus group velocity could be derived. The most critical part in the formula is the phonon life time, τ, involving scattering mechanism in phonon transport.

Scattering of phonons includes boundary scattering, defect scattering and three-phonon Umklapp scattering, thus the total relaxation time can be calculated as:

$$\tau^{-1} = \tau_B^{-1} + \sum_j \tau_D^{-1} + \tau_U^{-1} \tag{3-7}$$

where τ_B^{-1} is the boundary scattering, $\sum_j \tau_D^{-1}$ is the summation of defect (vacancy, impurity, isotope etc.), and τ_U^{-1} is due to three-phonon Umklapp scattering. Among these, Umklapp scattering is of special importance because Umklapp scattering is not momentum conserving and provide intrinsic thermal resistance that will confine the thermal current [59]. Normal phonon scattering may change the direction of scattered phonon, but the direction of heat flus is unchanged, thus the normal phonon scattering is not influential for thermal transport [58].

Approximation of relaxation time for Umklapp scattering has been widely presented and obtained good agreement with measured data. Chantrenne and Barrat [57] gave the following:

$$\tau_U^{-1}(\omega) = A\omega^2 T^{\xi} \exp(-B/T) \tag{3-8}$$

with A, B and ξ fitting parameters for thermal conductivity of bulk materials. Their model agrees well with solid argon and even sound for single graphene sheets, but is not applicable for carbon nanotubes. Yan *et al*. [60] derived the Umklapp process relaxation time from first-order perturbation theory as:

$$\tau_U^{-1} = \frac{4\gamma^2 h}{3} \sum_{q'} \frac{F(\omega, v_g, N_0)}{\rho} \tag{3-9}$$

where $F(\omega, v_g, N_0) = [\omega\omega'\omega''(N_0' - N_0'')/v_g^2]\delta(\omega + \omega' - \omega'')$, γ is the Grüneisen parameter, h is the Planck constant, ρ is the mass density, and N_0' and N_0'' are equilibrium occupancies of q' and q'' phonons. Wang, Tang, Zheng *et al.* [61] gave the following formula about the first-order and second-order Umklapp scattering for longitudinal branch of 1D CNT:

$$\tau_{1,U}^{-1} = \frac{A\omega^2 T}{T_0}, \ \tau_{2,U}^{-1} = \frac{32}{27}\gamma^4 (\frac{T}{T_0})\omega_b \tag{3-10}$$

with $A = 4\pi a\gamma^2/v$, $T_0 = Mv^2/k_B$, M is the atomic mass, and γ is the Grüneisen parameter, and a^3 represents the atom volume. Their wave vector model included the normal scattering process and showed excellent agreement with experimental data using the 3- ω method [61].

Treatment of relaxation time from boundary scattering can be roughly divided into two groups, one is derived from Casimir limit [57, 60, 61], taking into consideration the surface roughness:

$$\tau_B^{-1} = v(k,p)\frac{1-s}{L(k)} \tag{3-11}$$

where *s* represents the fraction of all phonons scattered by the boundary surfaces (s $\in[0-1]$), *L(k)* is the distance a phonon can travel between two boundary surfaces. Another way is to treat the relaxation time for boundary scattering as a constant, as in Ref. 58 and 62, boundary scattering relaxation time is set to equal 50 ps. Models with this value have been shown to match with experimental and theoretical works [29].

Though relaxation time approximation (RTA) has shown significant usage in understanding phonon transport, however recent studies have shown this method is not sufficient in describing nonequilibrium transport. The RTA method treats normal scattering and Umklapp scattering processes identically, thus underestimating the real thermal conductivity. Also for low temperature systems where Umklapp scattering is frozen or systems with weak Umklapp scattering, the RTA method fails to properly describe these systems. Many researchers have attempted full solutions of the Boltzmann equation for phonon transport and this has lead to some progress.

The Mingo and Broido [62] model includes normal and Umklapp scattering as well as ballistic and diffusive terms. Relaxation times are determined using an iterative method. With this method, they analyzed thermal conductivity of (10, 10) nanotubes and found that the thermal conductivity converges with length only when second order Umklapp scattering is added to the model. Then, in 2007, Broido *et al*. [63] treated the inharmonic interatomic force constants (IFCs) using density function perturbation theory (DFPT). This method shows excellent agreement for silicon and germanium, and is predicted to be applicable for carbon nanotubes. Lindsay *et al*. [64] used optimized empirical interatomic potentials and found that only acoustic phonon scattering won't provide thermal resistance and the traditional RTA method leads to a poor solution to BTE. Although they discussed chirality and length dependence, the model gave a relatively low thermal conductivity of 600 W/m K for SWNT compared with experiment results, which is around 3000-3500 W/m K. After revising the Tersoff and Brenner potentials, the agreement of acoustic phonon branches was improved [64], but is still lower than measured valves (1950W/m K). Another method is the real space displacement method, in which IFCs matrix is created by fitting force and displacement data through density function theory (DFT) [65- 67]. In this real space method, selection of harmonic and inharmonic IFCs depends on the cutoff length, and determines the number of surrounding shells considered of a certain atom. Tian *et al*. [68, 69] calculated cubic IFCs derived from lower order IFCs, and revealed that the contribution from optical phonon is not negligible

and accounts for up to 20% of the thermal conductivity in Si nanowire. Maris and Tamura [70] give thermal conductivity for a uniform cross-section rod as:

$$\kappa = \frac{\hbar^2}{16\pi^3 kT^2 A} \oint dl \sum_j \iiint \vec{v}_{\overrightarrow{kj}} \cdot \hat{e}(l) n_{\overrightarrow{kj}} \times (n_{\overrightarrow{kj}} + 1) \Lambda^2_{\overrightarrow{kj}} \hbar\omega_{\overrightarrow{kj}} k^2 dk dcos\theta d\Phi \tag{3-12}$$

where A is the cross sectional area and $\hat{e}(l)$ denotes the vector perpendicular to the surface. The integral is around the boundary of the rod.

C. LANDAUER METHOD

Compared with other materials, carbon nanotubes show a strong ballistic thermal transport owing to its relatively long mean free path over submicron length scale [71]. Rego and George [72] investigated thermal transport in quantum wires and predicted thermal conductivity at low temperatures in all dielectric materials. Rego *et al*. [72] showed that at low temperature, only acoustic branches phonons are excited and these phonon contribute to the quantum thermal conductance to the system. For one dimensional conductors, the Landauer theory serves as the basis for driving the quantum ballistic thermal conductance. Yamamoto and coworkers [71] applied the theory to a one-dimensional system sandwiched between a hot and a cold bath with ideal transmission and adiabatic at the contact region. Conditions were set to be $\Delta T \equiv T_{hot} - T_{cold} \ll T \equiv (T_{hot} + T_{cold})/2$. Thus thermal conductance can be written as:

$$G_{ph} = \frac{Q_{ph}}{\Delta T} = \frac{k_B^2 T}{2\pi\hbar} \sum_m \int_{x_m^{min}}^{x_m^{max}} d_x \frac{x^2 e^x}{(e^x - 1)^2} \tag{3-13}$$

where *m* denotes the phonon branches, $x = \hbar\omega/k_B T$, $T = (T_{hot} + T_{cold})/2$. Independent of the exact phonon mode, at low temperature around 10 K, each branch of four acoustic phonons contribute equally to the total thermal conductance, and

$$G_{ph} = \frac{\pi^2 k_B^2 T}{3h} \tag{3-14}$$

As previously discussed, dispersion relation show four acoustic phonon modes at low temperature in carbon nanotubes, and the four modes contribute to total thermal conductance. This result is similar to Rego *et al*. [72] for thermal conductance of quantum wire, and many other investigation on low temperature phonon thermal conductance have confirmed that $G = 4G_{ph}$. In their studies, Yamamoto *et al*. [71,73] calculated the universal behavior of low-temperature thermal conductance and showed that thermal conductance is characterized by lowest optical band energy gap of $\hbar\omega_{op}$, which only depends on

the radius of SWNT. Specifically, for a (10, 10) carbon nanotube, the lowest energy gap is 2.1meV. In their work, Yamamoto and coworkers also applied the equations mentioned above to electrons in metallic nanotubes. From their calculation, quantized thermal conductivity caused by electrons could spread from near 0 K to up to room temperature. When treating low-temperature systems, thermal conductance quanta from electron should be taking into serious consideration [71], while at high temperatures when phonons give relatively high thermal conductance, the contribution of electrons is negligible.

In section 2.4 we provided results of earlier research on the dispersion relation of four acoustic phonons that have linear dependence on temperature. This once widely accepted relation [71, 73-75] has been challenged given the fact that conventional elastic theory neglects the fact that carbon nanotube is hollow, not a solid wire, and widely adopted zone folding method fails to treat the bending bond in the nanotube. Therefore, there are some discrepancies in the phonon dispersion relation. In 1999, Sánchez-Portal compensated for the deficiencies of the zone folding method with *ab initio* calculation [76], and found that phono dispersion relations of transverse acoustic phonon modes have quadratic curves. Similar results were obtained by simulation works of Popov and coworkers [77-79]. They adopted Born's perturbation technique together with a lattice dynamical model to show that phonon dispersion increase as the square of the wave number. Mahan and Jeon [80] further developed a theoretical underpinning by using a force model with properly treated symmetry rules between carbon atoms in nanotubes.

As temperature increases to several degrees Kelvin, optical phonon modes are onset as heat carriers, depending on the lowest optical phonon energy, which is found to be uniquely determined by the nanotube diameter [71, 73]. Thermal conductance calculation of SWNT should extend from low-temperature to higher temperature by including these optical phonon channels. The total number of phonon modes is three multiplied by the carbon nanotube number in the unit cell (or in a shell of multi-walled carbon nanotube), expressed as below:

$$N_{ph} = 3 \times N_C = 3 \times \frac{4(n^2+m^2+mn)}{d_R} \tag{3-15}$$

where (n, m) is the chirality, d_R is as in section 2.1.3, is the greatest common divisor of $(2m+n)$ and $(2n+m)$. It is clear that total thermal conductance is the summation of the quantum thermal conductance contributed by each phonon mode in the ballistic regime $G_{ph} = N_{ph} \cdot G_{ph}$. For SWNT bundles, similar method can be used. Shang, Ming and Wang [20] derived equations to calculate thermal

conductance of CNT bundles:

$$G_{bundle} = \sum_D N_{tube} G_{tube} \tag{3-16}$$

where D denotes the diameter of the tubes in the bundle, N_{tube} is the tube number inside the bundle. One thing worth mentioning is that theoretical [60] and experimental [81] works have demonstrated that thermal conductance perpendicular to tube axial is small enough to ignore. The percentage of CNTs' contribution to bundle thermal conductance is expressed as $\sim\pi\,\overline{D}/w_{bundle}$, where $\overline{D}$ is the mean diameter of SWNT in bundle and w_{bundle} is the bundle width.

When the length of CNT is larger than phonon mean free path, thermal conductivity converges to a constant value, indicating a diffusive transport regime [33, 82]. Shang, Ming and Wang [20] extend ballistic models to diffusive regimes using a piecewise functions to feature thermal conductance of the two processes. With L indicating the length of CNT and l representing the phonon mean free path, thermal conductance should obey the following equations:

$$G = \begin{cases} N_{ph} \cdot G_{ph} & for\ l \le L \\ N_{ph} \cdot G_{ph} \cdot \frac{l}{L} & for\ l > L \end{cases} \tag{3-16}$$

One thing need to be recalled is that the assumption for Landauer theory is the perfect transmission and adiabatically connection between the CNT and two bathes. In this condition, phonon could travel freely without scattering by defects or boundary. Inspired by electronics transport in mesoscopic systems [57], Wang and coworkers [19] modified energy transmission ζ cover from ballistic to diffusive regimes:

$$\zeta = \begin{cases} 1 & Ballistic\ regime \\ \frac{l}{l+L} & Ballistic - Diffusive\ regime \\ \frac{l}{L} & Diffusive\ regime \end{cases} \tag{3-17}$$

A theoretical scheme that seamlessly crosses over from fully ballistic to fully diffusive transport was derived by Yamamoto *et al*. [83] with the following result:

$$G = \sum_v \int_{\omega_v^{min}}^{\omega_v^{max}} \frac{d\omega}{2\pi} \hbar\omega \left[\frac{\partial f(\omega,T)}{\partial T}\right] \frac{\Lambda_v(\omega)}{L+\Lambda_v(\omega)} \tag{3-18}$$

where v is the phonon mode, $f(\omega,T)$ is the Bose-Einstein distribution function for phonons at an average temperature T between hot and cold baths, and $\Lambda_v(\omega)$ is mean free path. Equation (3-18) derives the ballistic conductance for $L \ll \Lambda_v(\omega)$ and the Boltzmann-Peierls equation for $L \gg \Lambda_v(\omega)$. Three- phonon Umklapp scattering in the low frequency regime where $\hbar\omega/k_BT \ll 1$ was expressed as:

$$\Lambda_v(\omega) = c_v A/\omega^2 T \tag{3-19}$$

In this formula, c_v is a parameter representing the curvature effect of a CNT (used as 0.65 in this reference) and A is the coupling constant for graphene. Adopting the equation for thermal transport in CNT provides thermal conductance as:

$$\mathrm{G_{CNT}} = \frac{k_B}{2\pi}\sum_v \Omega_v \left[\arctan\left(\frac{\omega_v^{max}}{\Omega_v}\right) - \arctan\left(\frac{\omega_v^{min}}{\Omega_v}\right)\right] \tag{3-20}$$

where $\Omega_v(L) = \sqrt{c_v A/TL}$ can be regarded as a length-dependent characteristic frequency. Yamamoto *et al*. [83] determined interfacial resistance as κ_{int}^{-1} by fitting to experimental data as 0.09K/nW, therefore the total thermal conductance is $\kappa^{-1} = \kappa_{\mathrm{CNT}}^{-1} + \kappa_{int}^{-1}$. For (3,3) and (5,5) CNTs, the analytical model results are in excellent agreement with nonequilibrium MD simulation.

D. KEY FINDINGS

A variety of research was conducted on the influence of chirality, length, temperature and defects on thermal conductivity of carbon nanotubes. This issue will be discussed in the following.

1. Temperature dependence

Several efforts to reveal the temperature dependence of thermal conductivity of carbon nanotubes by varying temperature from low to high, and phonons have shown varying behavior from ballistic to diffusive. In the ballistic transport regime, thermal conductivity shows a linear relationship with temperature in a certain range, resulting from a linear increase in specific heat [71, 73]. Thermal conductivity becomes a maximum at around 320 K [84], a substantially higher value compared with bulk crystals, which indicates suppressed three-phonon scattering over a wide temperature range [85].

Below 30 K, the mean free path is energy-independent [81] and the only resistance from boundary scattering remains constant [60, 62].Therefore thermal conductivity could be calculated from kinetic theory as $\kappa = \sum C v^2 \tau$. It is obvious that thermal conductivity increases with temperature as the specific heat increases with phonon modes. As mentioned in section 3.3, at low temperature, only the four acoustic phonon modes are excited and each mode contributes a quantum phonon thermal conductance G_{ph} and the total thermal conductance is a radius-independent value, $G = 4G_{ph}$. However, this ballistic transport region is not as large as expected. Hone *et al*. [86] found this limit up to 8 K, and Chalin *et al*. [87] found the linear dependence region is within a quite narrow range from 3 to 6 K. That is because low-energy bending modes are excited above 6 K and could cause a deviation from a linear relationship.

With the contribution of these lowest-energy bending modes, phonon thermal conductance is further enhanced by and displays a non-linear temperature dependence [87]. For <75 K, the main contribution to phonon thermal conductance is from acoustic and bending modes [87]. Ballistic transport dominates up to room temperatures, as phonon-phonon scattering is negligible and phonon mean free path is determined by boundary scattering [13]. In this region, thermal conductivity $\kappa \sim T$ is observed [87, 88].

Starting from lowest optical mode which contributes to thermal conductance, phonon transport starts to transfer from 1-D to 2-D behavior [84]. The temperature at which lowest optical phonon mode is excited depends on the energy gap, which is determined by nanotube radius [71, 73]. Yamamoto *et al*. [71, 73] scaled low-temperature phonon thermal conductance with the lowest optical mode, $\tau_{op} = k_B T/\hbar\omega_{op}$, and found low-temperature phonon transport is characterized by the optical phonon energy gap. Shown as Figure 3-2 (a). Hata *et al*. [89] further extended analysis to higher temperatures and found the excitation of optical phonon modes are influenced by chirality. For zigzag and chiral SWNTs, phonon modes increase from four to six immediately at a lower energy while the transmission coefficient stays at four for a wider range of energy [89]. From reported work, the temperature dependence at 100 K is T^3 [68] and $T^{1.5}$ up to 200 K [13, 84]. For MWNTs, this trend was found to be $T^{2.5}$ for <50 K and $T^{2.01}$ for >50 K [90].

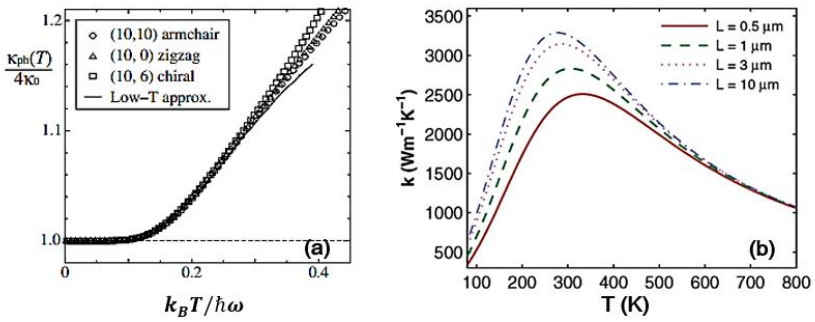

Figure 3-2. (a) Thermal conductance as a function of temperature scaled by the energy gap of the lowest optical mode [71]. (b) Intrinsic thermal conductivity of SWNT over 100-800 K temperature range. The length difference is observable in the picture, and chirality may lead to variations up to 20% difference between SWNT. [88]

At higher temperature, thermal conductance decreases as Umklapp scattering dominates. First order Umklapp scattering leads to a T^{-1} trend and second order Umklapp scattering results in a T^{-2} trend, shown in Figure 3-2 (b) [88]. Pop *et al*. [88] attribute this to the onset of second order of Umklapp scattering above around 300 K. High temperatures excite optical phonons with small group velocity,

providing scattering channels for acoustic phonons. Yet these optical phonons contribute to about 20% thermal conductivity at room temperature [68]. Given the discussion above, the highest thermal conductance for carbon nanotube could be reached at the balance point of increasing phonon population and the increasing scattering rate accompanying higher temperatures. Reported works gave a possible temperature range from 150-400 K for maximum thermal conductance of CNT [34, 35].

2. Length effect

Thermal conductivity is a function of several parameters including length, diameter, temperature, etc. and is expected to crossover from the ballistic regime to the diffusive conduction regime when SWNT length exceeds that of phonon mean free path. For a nanotube, this crossover phenomenon could be observed with different lengths at various temperatures. In order to clarify length effect, the following discussion is based on room temperature unless otherwise mentioned. Different MD simulations were used to estimate the influence of sample length on thermal conductivity. It is now a common sense that at shorter lengths, thermal conductivity diverges with carbon nanotube length. Similar divergence is also observed in other low-dimensional lattices [85, 91]. When the tube length L is smaller than the phonon mean free path, l_0, heat conduction shows a significant ballistic behavior, and the thermal conductance is constant. Thus thermal conductivity is proportional to L [92]. This arises from the fact that a longer nanotube has more phonon modes with long wavelengths and smaller wavelengths, providing new heat carriers which are less likely to be scattered by inelastic scattering [13, 28]. Under this condition, a wider range of optical phonons could also contribute to thermal conductivity together with acoustic phonons [92]. A power law can be used to fit these analyses as $\kappa \sim L^{\alpha}$, for $\alpha \sim 1$ with ballistic transport [49, 19]. Following purely ballistic transport there occurs a long quasi-ballistic heat conduction phenomenon, with a slower increase in the thermal conductivity [19, 62, 93]. This quasi-ballistic heat conduction could exceed a micrometer [93], and even reach millimeter at 10 K [62].

For longer carbon nanotubes, there's still debate on whether the thermal conductivity will converge or not. Some research work reported unlimited thermal conductance with increasing carbon nanotube length [19, 28, 30, 31, 38, 45, 49, 93, 94] while others obtained a saturated thermal conductivity when sample length reaches a certain threshold value [50, 61, 83, 95-98]. One reason for the unlimited thermal conductivity could be the small length of sample used. For the majority of the simulations with unlimited thermal conductivities, the simulated sample lengths were shorter than several micrometer. But for very long carbon nanotubes with length of 100μm [49], simulations showed a $\alpha = 0.21$ dependence on sample length. Another possibility could be the simulation parameters, as mentioned before. Some researchers

mentioned the physically unreal periodic boundary conditions used in simulations [28, 93], which eliminates boundary scattering and ignores the contribution from phonons with wavelengths longer than the cell size. Chirality is also worth mentioning. Maruyama attributed the divergence to chirality by performing simulations on (5, 5) and (10, 10) carbon nanotubes. The latter showed a nearly constant thermal conductivity independent of length. Simulation results also indicated that for longer CNTs, the thermal conductivity should reach a saturation.

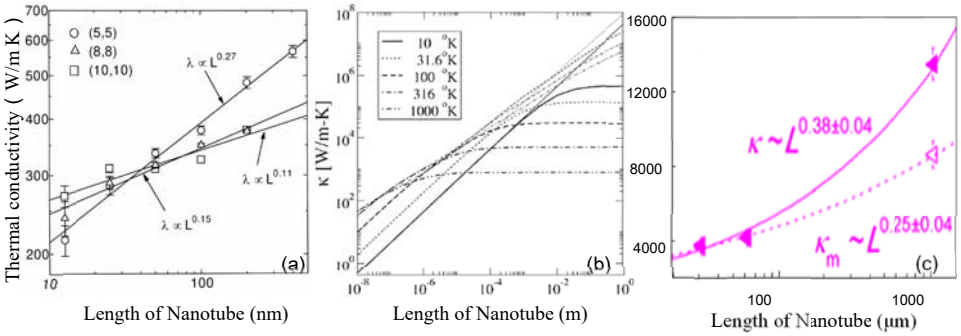

Figure 3-3 Calculated thermal conductivity versus nanotube length at different tube length. (a) Three simulated carbon nanotubes exhibit ballistic thermal transport to over 400 nm. (b) NGR in the figure is nanographene ribbon. Thermal conductivity increases at a decreasing rate. (c) Thermal conductivity of a 1.039 mm SWNT. (Open symbol are measured thermal conductivity and solid symbols are corrected ones.)

Different from the ballistic transport regime, the power law diffusive regime demonstrates $\kappa \sim L^{\alpha}$ with $\alpha < 1$. Theoretical and simulation works have given a range of 0.12-0.4 [30, 62, 40]. Figure 3-3 (a) shows the length dependence of thermal conductivity for different nanotubes [31].From the picture, it is obvious that all of the three simulated carbon nanotubes exhibit ballistic thermal transport to over 400 nm length and chirality influences the power law, with (5, 5) nanotube having the highest thermal conductivity over the other two nanotubes. Mingo and Broido [62] analyzed thermal conductivity of a (10, 10) nanotube and found that thermal conductivity converges with length only when second order Umklapp scattering is added to the model, shown in Figure 3-3 (b). Without second order Umklapp scattering, thermal conductivity would increase with length for CNTs without saturation. Lee *et al*. [99] measured thermal conductivity with length from 2 μm to 1.039 mm, and found no saturation occurred. According to their research, 8638 W/m K is the lower bound for millimeter-long CNT, shown in Figure 3-3 (c). With full solution of BTE, Lindsay predicted saturated thermal conductivity for nanotubes longer than 1000 mm. Yamamoto *et al*. [83] used length-dependent characteristic frequency $\Omega_v(L) = \sqrt{c_v A/TL}$, where A=3.35 $\times 10^{23}$ m K/s^2 is the coupling constant for graphene, T is temperature. The position where $\Omega_v(L)$ falls

is increasing with increasing L. By comparing $\Omega_v(L)$ with phonon frequencies, seamless crossover from ballistic regime to quasi-ballistic regime and then to diffusive regime is possible.

3. Chirality and diameter effect

Chirality and diameter have been extensively studied by different methods including both theory and experiment. Although chirality and diameter are closely related parameters，the impact of chirality has been mysterious for long time. In MD simulations, it is relatively easy to model SWNTs with different chirality, but there has not been good control experimentally. And there still remains discrepancy among simulation works and theoretical analysis.

First we talk about the influence of diameter. Thermal conductivity dependency on nanotube diameter is the result of diameter dependence scattering and changes in number of conduction channels [13]. Many researchers reported thermal conductivity decreasing with increasing diameter [19, 57, 60, 100]. Osman and Srivastava found small diameter nanotubes have higher thermal conductivity than larger ones. Yan *et al*. [60] obtained a n^{-2} dependence for thermal conductivity for both (n, n) and (n, 0) carbon nanotubes, while Wang and Wang [19] deduced a n^{-1} dependence. Despite the differences, the two relationship both describe an inverse relation between thermal conductivity and diameter. Shiomi and Maruyama [100] included the tube length and reported a trivial influence of diameter dependence on thermal conductivity for short SWNTs, and an inverse conductivity relationship with increasing diameter when tube length is long enough.

However, other studies lead to a different conclusion. Qiu *et al*. [44] reported that thermal conductivity increases with increasing diameter, owing to curvature that shortens the relaxation time. Cao *et al*. [49] derived the following formula for zigzag and armchair carbon nanotubes:

$$\kappa(L,d) = \kappa_g(L) \times (1 - e^{-0.185d/a_0}) \tag{3-21}$$

where $\kappa_g(L)$ is the thermal conductivity of graphene with same length L and a_0 is the graphene lattice constant. Cao *et al*.[101] believed that breathing mode phonons are very sensitive to diameter and a large diameter has more active low-frequency modes that contribute to higher thermal conductivity. When $d \to \infty$, SWNT becomes graphene and the thermal conductivity of SWNT equals that of graphene. That is, single layer graphene is the upper limit for free-standing SWNTs at room temperature. The same conclusion was drawn from Boltzmann transport equation solutions for SWNTs with diameters from 1-8 nm [42]. However, different from a simple trend, Lindsay *et al*. [42] calculated a non-linear relation

between thermal conductivity and diameter from BTE. They found that the thermal conductivity of carbon nanotube exhibits a minimum for modest diameters. SWNT with small diameters have higher thermal conductivity. This is because the inherent curvature violates the selection rule, and this strongly restricts the phonon-phonon scattering. Yue *et al*. [102] found a slightly non-linear relationship for thermal conductivity with respect to diameter. With this relationship, thermal conductivity of single layer graphene is the lower limit, different from the conclusion of Lindsay.

For chirality impact, several works found no significant influence [19, 40, 62, 71, 73]. Yamamoto *et al*. found that diameter is the only factor that affects the lowest optical phonon mode [72, 74]. The density of state of phonons in SWNTs doesn't change much with varying chirality, suggesting a relatively trivial impact [13, 40].

However, other modeling studies reported obvious effects of chirality [20, 9, 35, 36, 60]. This may be explained by different bond structures in different chirality specimens [13]. Based on the chirality effect, efforts have been exerted to find out carbon nanotube chirality with optimal thermal properties. Osman and Srivastava [34] found that zigzag nanotubes have the highest thermal conductivity because stretching of sigma bond in armchair and chiral carbon nanotubes would shorten the phonon mean free path, thus confining thermal conductivity. Similar conclusions are reached by Zhang *et al*. [35], ranking of thermal conductivity from low to high in nanotubes with similar diameters but different chirality is chiral nanotube, armchair and zigzag structures. This could be attributed to more phonon modes in zigzag SWNT than in armchair structures in the ballistic regime [20]. In contrast, Feng *et al.* [103] discussed the impact of chiral angle from 0-30° with NEMD simulations. Results showed that chirality influence is obvious for short SWNTs and large-diameter SWNTs. For longer SWNTs, the chirality influence is replaced by diameter influence. Through simulation, armchair SWNTs have been found to have larger thermal conductivity than zigzag structure with comparable diameters at room temperature, consistent with the findings of Yan *et al.* [60].

4. Defect and vacancy

Defects like isotopes, dislocations and grain boundaries influence thermal conductivity of carbon nanotubes. However, the well-established methods for tracking specific phonon modes are not able to accurately include the above mentioned defects. To fully understand defects effect on thermal property, the key factor is the potential modes, which could properly describe the defect structure and to reveal phonon reaction.

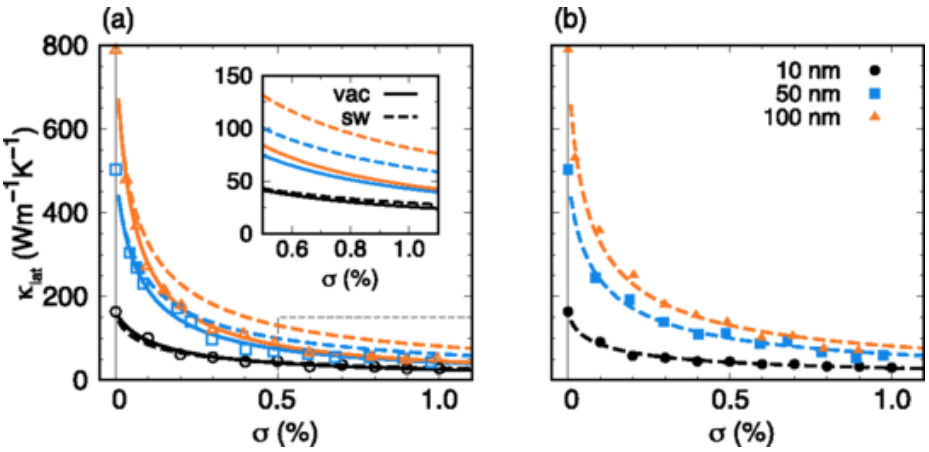

Figure 3-4 Thermal conductivity decrease with increasing defect concentration for 10 (black circle), 50 (blue square), 100 (orange triangle) nm CNTs. (a) vacancy, (b) SW. Solid and dashed lines are fitting curves for vacancy and SW defects.

Sevik *et al*. [104] used NEMD simulations to distribute single vacancy, double vacancy and Stone-Wale (SW) for zigzag carbon nanotubes. By calculating the drop of the mean free path, Sevik *et al*. [104] found that for defective carbon nanotubes, high frequency phonon modes are greatly suppressed within 1 μm while low frequency phonons maintain ballistic transport, yielding an almost unchanged thermal conductivity. The calculated mean free path decayed with factor of ω^{-2}, indicating a Rayleigh scattering mechanism [105]. Menuier *et al*. [106] pointed out that semiconducting tubes are more sensitive to disorder and result in a shorter mean free path. Ohnishi *et al*. [107] found an over 50% reduction for CNTs with vacancy in range of 0.06 % to 0.14 % and SW in the range 0.078 % to 0.11 % for 10-100 nm CNTs, as shown in Figure 3-4. Comparing the decrease caused by vacancies and SW, Ohnishi *et al*. [107] suggested that vacancies have a greater effect than SW because the absence of C-C bonds diminish short phonon-waves. To mitigate the influence of defects, Ivanov *et al*. [106] annealed MWNT arrays at 2800 ℃ for 2 hours and the sidewall defect was greatly reduced.

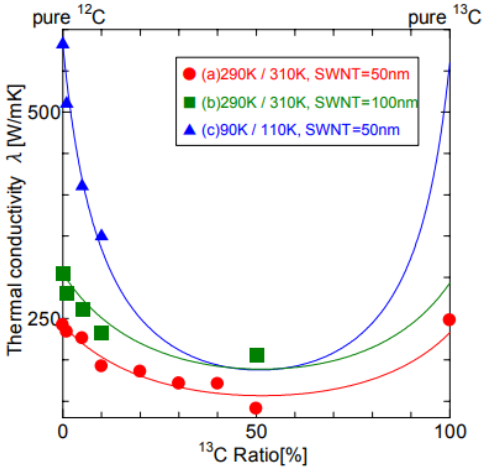

Figure 3-5 Effect of ^{13}C isotope on thermal conductivity of SWNT.

Isotopes were assumed to have smaller effect for higher mass system [58]. For example, 99.999% ^{12}C diamond has thermal conductivity 4 times larger than 99.9% ^{12}C, while ^{235}U isotope has little effect on UO_2 [58]. Zhang and Li [40] valued the effect of ^{13}C and ^{14}C isotopes on thermal conductivity of ^{12}C carbon nanotubes. Thermal conductivity decreases with isotope concentration at a decreasing rate, and the decrease percentage is similar to that of diamond [40]. Maruyama and Shiomi calculated the thermal conductivity of carbon nanotube from pure ^{12}C to fully ^{13}C nanotubes. Simulation results are shown in Figure 3-5 [108]. It can be seen from the picture that the general trend of the simulation is that thermal conductivity decreases as the ratio of ^{13}C increases as a result of phonon scattering. Green and red curves in the picture represent 50 nm and 100 nm nanotubes at 300 K, and variation of the thermal conductivity between the two results is almost constant. This phenomenon could be explained that the additional long wavelength phonons contributed by longer nanotubes are not influenced by the isotope, whose influence is localized within relatively short atomic length scale. Li *et al.* [109] observed a similar phenomenon by adding ^{13}C isotopes randomly to pure ^{12}C CNT and agreed on the explanation that the isotope effect is caused by phonon localization. However Savić *et al.* [110] suggested this is caused by diffusive phonon scattering instead of unobservable phonon localization. Feng *et al.* [111] investigated the doping effect in CNTs with N, B and K atoms. The doping effect showed a similar decrease as with isotopes without changing the temperature at which maximum thermal conductivity occurs.

IV. SIMULATION AND EXPERIMENT

A. EXPERIMENTAL METHODS

Thermal measurement techniques at the nanoscale level can be divided into two groups: (1) using external heat sources to generate temperature gradients along the nanotube, and (2) applying dc current into the nanotube, or a self-heating method to estimate the thermal properties. Here, several methods will be covered to illustrate the merit and shortcomings of each method.

1. External heat source

1.1 Suspended thermometer

A representative example of this method was put forward by P. Kim *et al* [107], and this method is revised by other researchers [112, 134], shown in Figure 4-1 (a) [134]. Though the detailed structures may have little difference, the working principle remains the same. First, the assumptions involved using this method should be clarified:

(1) The temperature on either of the two membranes is uniform.

(2) The heat exchange between the two membranes is caused by thermal radiation or convection are negligible.

(3) Connecting parts of the beams and substrate have the same temperature, which is a constant value in experiment.

The principle of this method is to apply dc current in one of the serpentine membranes, there will be joule heating and, thus this membrane serves as a heater. Part of the heat will be conducted to the environment by the beams connecting the membrane and the substrate. Part of the heat will be conducted to another membrane, called the sensing membrane, and will cause a temperature rise which will also dissipate to the environment through the beams connected with it. The schematic picture of this process is illustrated as in Figure 4-1 (b).

The thermal conductance of the nanotube bridging the two membranes can be expressed as:

$$T_h = T_0 + \frac{G_b + G_s}{G_b(G_b + 2G_s)} P, \text{and } T_s = T_0 + \frac{G_s}{G_b(G_b + 2G_s)} P_s$$

where P is the Joule power applied to the resistor R_h. By measuring the variation of two membranes' electrical resistance as a function of P, the temperature on the two membranes can be determined and further the thermal conductance of bridging nanotubes at temperature T_0 can be calculated.

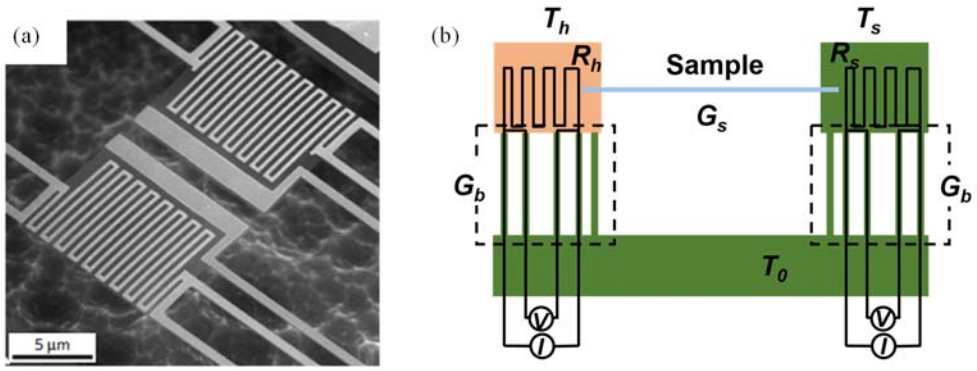

Figure 4-1. (a) A representative SEM image of the suspended microstructure used for measuring the thermal conductivity. (b) Schematic diagram and thermal resistance circuit of the device.

Samples of carbon nanotubes were put across the two membranes and the pictures of several experiment samples are shown in Figure 4-1. The measurement results show a multi-walled carbon nanotube (MWNT) of 14 nm diameter, 2.5 μm length and with a thermal conductivity over 3000 W/m K at 320K. The sample showed a $T^{2.5}$ dependence below 50 K and T^2 above 50 K. In 2009, Pettes *et al*. [113] measured the thermal conductivity of individual SWCNTs, double walled carbon nanotubes and MWCNTs and the thermal conductivity of SWCNTs was around 600W/Km at room temperature.

1.2 T-type nano sensor

Fujii *et al*. [114] reported using a T-type nano sensor to measure the thermal conductivity of a single CNT. The structure of the T-type sensor is shown in Figure 4-2. The working principle is: after supplying current to the nanofilm sensor (NS), heat will partly be conducted to heat sink (HS) and dissipated to the ambient through NS and HS. If the contact resistance is neglected, the thermal conductivity of CNT can be calculated as

$$\lambda_{f0} = \frac{L_f L_h \lambda_h A_h (L_h^3 q_v - 12 L_h \lambda_h \Delta T_v)}{L_{h1} L_{h2} A\{12 L_h \lambda_h \Delta T_v - q_v (L_{h1}^3 + L_{h2}^3)\}}$$

where L_f is the length of the sample, L_h is the length of the nanofilm, L_{h1} and L_{h2} denote the lengths

of left and right side of the nanofilm from the connecting point of sample and nanofilm, A_h and A_f are the cross section areas of nanofilms and CNT samples, q_v is the heat generation rate and λ_h is thermal conductivity of Pt nanofilm. The author used two ways to define the cross section area:

$$A_f = \pi d_0^2/4 \quad \text{and} \quad A_f = \pi(d_0^2 - d_1^2)/4$$

where d_0 is the outer shell diameter and d_i is the diameter of the inner lumen.

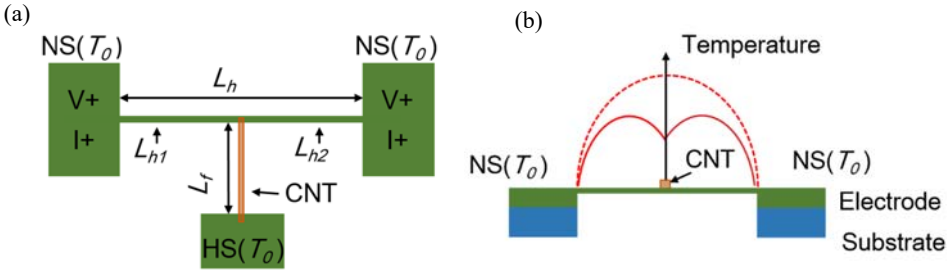

Figure 4-2. (a) Schematic diagram of the nanosensor. (b) Temperature distribution along the nanofilm sensor.

Through measurement and calculation, the thermal conductivity for a diameter range of 9.8 nm and a length 3.7 μm MWCNT is 2069 W/mK. For a 16.1 nm diameter sample, thermal conductivity showed an asymptote near 320 K, this tendency is repeated with other observations [112], which is assumed to be caused by the onset of three phonon Umklapp scattering.

1.3 Four-probe method

Kim *et al*. [115] reported a four probe method not only to measure the intrinsic thermal conductivity of the sample but also the contact resistance. Figure 4-3 (a) demonstrates the structure of the four probe device. One of the four Pt beams (*i* th) is electrically heated by a direct current, and the other three (*j* th) are heated with energy transported by the sample. Temperature distributions in *i* th and *j* th beams are shown in Figure 4-3 (b). The thermal resistance circuit of the measurement device when the Pt beam serves as a heating beam is plotted in Figure 4-3 (c). After the four Pt beams serve as heaters one by one, a 4×4 matrix could be obtained and a sample resistance (R_2) together with thermal contact resistance ($R_{c,2}$ and $R_{c,3}$) could be calculated. This four probe method could obtain an overdetermined matrix and previously only three of the equations are used to derive the three unknown parameters mention above.

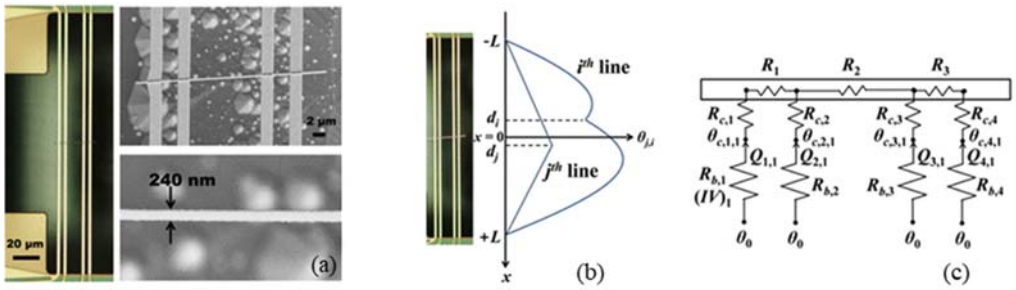

Figure 4-3. (a) An optical micrograph (left) and a SEM graph (right) of the 240 nm wide Si nanowire sample assembled across the four Pt/ Si_3N_4 beams. (b) Schematic diagrams of temperature profiles of the *i* th heating beam and the *j* th thermometer beam. (c) Thermal resistance circuit of the measurement device. Sample resistance, R_2, and thermal contact resistance $R_{c,2}$ and $R_{c,3}$ will be derived from the measurement.

A Si nanowire sample was measured with the four probe method and the measurement data agreed well with theory derived by Wang and Mingo [116]. Kim *et al*. [117] further improve this method with data reduction and further validated this latest four-probe thermal transport measurement method for application on thin films and nanostructures.

2. Self-heating method.

Methods using external heat sources to investigate the thermal transport in CNTs including $3-\omega$, Raman thermography and dc thermal bridge methods. All these methods start from the same point that when the CNT absorb energy, it generates a temperature gradient along itself and by analyzing temperature profile, thermal information is extracted.

2.1 $3-\omega$ method

Schematics of the $3-\omega$ method are shown in Figure 4-3. Choi *et al*. [118] deposited a single carbon nanotube along the four metal contacts, as shown in Figure 4-4 (b). The black trench made by focused ion beams (FIB) prevented the nanotube from touching the substrate. The outer two electrodes supplied a sinusoidal current $I_0 \sin(\omega t)$ and as the current passes through, joule heat is generated. The joule heat generated is proportional to $[I_0 \sin(\omega t)]^2$, and thus a lock-in amplifier, which is denoted as V in Figure 4-3 will detect a small 3ω signal $V_{3\omega}$. Choi *et al*. [119] obtained thermal conductivity of individual MWCNTs which outer diameter is about 45 nm to be 650-830 W/m K at room temperature

with measurement error ± 6%.

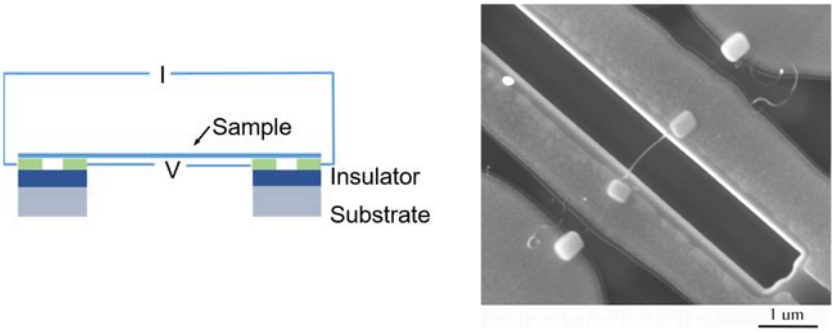

Figure 4-4. (a) Schematic diagram of a 3-ω method measurement device. (b) Picture of a prepared sample on the measurement device.

One limitation of this method is that measured sample should be electrically conductive and has a linear electrical response. According to a recent study about the thermal transport mechanism, Bachtold *et al*. [120] suggested that MWCNTs are diffusive conductors, metallic SWCNTs are ballistic conductors over several microns, while the semiconducting SWCNTs have large barriers along their length.

Lu *et al*. [121] established the conduction equation along the suspended sample:

$$\rho C_p \frac{\partial}{\partial t} T(x,t) - \kappa \frac{\partial^2}{\partial x^2} T(x,t) = \frac{I_0^2 \sin^2 \omega t}{LS} [R + R'(T(x,t) - T_0)]$$

where C_p, κ, R and ρ are specific heat, thermal conductivity, electric resistance and mass density of the sample at the substrate temperature T_0. The symbol $R' = (\frac{dR}{dT})_{T_0}$, L is the length of the sample between voltage contacts and S is the area of the cross section of sample. The 3ω voltage signal is expressed as: $V_{3\omega} = 4I^3 LRR'/\pi^2 \kappa S$ (low frequency) and thus $\kappa = 4I^3 LRR'/\pi^4 V_{3\omega} S$. But the simplification and approximation will introduce errors with this method, several improved methods [122-124] were developed to improve the accuracy.

Accuracy of the measured result depend on the proper chose of ac current to short circuit the contact area, yet the contact resistance causes further uncertainty in calculating thermal conductivity. To enhance the reliability of this method, the four-point 3-ω method was developed [118]. Compared with the two-point method, this improved method eliminates the contribution of contact resistance in calculating thermal conductivity and enables the accurate measurement of the first and third harmonic signals. The thermal conductivity of MWCNT (outer diameter ~20 nm, length 1.4μm) at room temperature (24.4℃) is 300±20 W/mK.

2.2 Optical methods

An optical method for measuring thermal transport was demonstrated by Hsu.*et al*. [125] . In this method, the optical information can both act as heater or sensor. When using a focused laser beam to heat the sample, it becomes an energy source. As a sensor, the temperature profile is measured by optical properties like Raman shift. Chiashi *et al*. [126] used three different wavelength lasers to heat various bundled SWNT samples and observed the Raman shift of the G^+ peak frequency shift over a wide temperature range from 4-1000 K. The measured result shows that: Raman shift frequency decrease and peak width broadens with increasing temperature. An advantage of this method is that it provides information about contact resistance and ballistic/diffusive phonon transport. Yet the energy absorption from the incident laser was unknown.

Hsu *et al*. [127] further enhanced this method by using two laser measurements. Temperature at the heated point was determined by the Raman G band shift and the temperature of the two ends were calculated by the electric resistance change via temperature coefficient. The optical absorption of 7.4-10.3 nm diameter bundles is between 0.03-0.44 % in 0.4μm diameter spot, and thermal conductivity of three measured samples range from 118-683 W/m K. Another novel technique to address the above mentioned challenge was developed by Li *et al*. [128] in which the sample was heated by electricity and the temperature at the heated point and two ends were determined by shift of shifts in G band Raman frequency. In this way, thermal conductivity can be determined independently from contact thermal resistance. Thermal conductivity of a SWCNT (1.8 nm in diameter and 41 μm in length) was measured to be 2400 W/m K and a MWCNT (outer diameter 8.2 nm and 32 μm in length). Optical means can act both as heater and as sensor, Hsu *et al*. [127] used one laser beam as heater and one laser to measure spatial temperature spreading along SWCNT bundles in both vacuum and in air. Measured results of SWCNT bundles are comparable to Ref.126, range from 16-163 W/m K. Because of unavoidable defects in the sample, temperature along the sample is not strictly linear. With Raman investigations, spatial thermal conductivity measurements are possible [128, 129]. This problem can be solved by reducing the self-heating current.

During electrical self-heating, especially for high-bias voltage, Joule heating will cause nonequilibrium transport in suspended SWCNTs [110, 130-132]. In high-bias experiments [131], electrons excite optical phonons, which act as the main scattering source and thus decrease the electron mean free path and suppresses ballistic phonon transport. Generation of hot phonons can be detected directly from a Raman scattering experiment. Theoretical analyses of acoustic and optical phonons

generated by Joule heating are contained in [129-133].

According to Pop *et al*. [131], the effect of nonequilibrium phonons can be minimized by a substrate that has close vibration modes with the sample and thus shortens the lifetime of optical phonons. The same conclusion of the positive effect was verified earlier by Lazzeri *et al*. [134]; that a heat sink would increase scattering length and decrease the occupation temperature of optical phonons. On the other hand, on-substrate measurements may cause other problems. Wang *et al*. [61] observed 30-40% of the heat generated dissipated to the substrate, thus the impact of substrate cannot be eliminated. And substrate-sample interaction may also suppress some phonon modes and impact boundary scattering [134].

C. Comments on experimental methods

Because of the extreme difficulty in measuring nanoscale materials, there are still some short comings with these methods. The most critical issue is the thermal contact resistance between the sample and the substrate. And this will further complicate the modeling of phonon transport in such systems. According to Rego and Kirzenow, for wires with small enough diameter, extremely smooth connections will ensure reflectionless contact [72]. P. Kim *et al* [84] measured the thermal conductance at the junction between the CNT and the substrate to be $5 \times 10^{-7}\mathrm{W/K}$ at room temperature and the total thermal conductance of the sample is $1.6 \times 10^{-7}\mathrm{W/K}$. About 68% of the thermal conductivity is contributed by the intrinsic thermal conductivity of CNT. A similar result was obtained on a 66-nm-diameter MWCNT by Yang *et al* [135], they found contact thermal resistance can contribute up to 50% of the total effective thermal resistance. According to P. Kim *et al* [84], outer walls of MWCNTs have greater contribution in thermal transport than do the inner walls. Therefore, studies on MWNT usually consider the outer most wall. Though the analysis and calculation were for MWCNTs, this conclusion is applicable to SWCNTs as well

Cahill *et al*. [58] calculated the thermal resistance per unit area to be in the range of $(1-3) \times 10^{-8}$ $\mathrm{m^2K/W}$. Pop *et al*. [110] estimated the thermal contact resistance by $A_c = dL_c$, where d=1.7 nm, $L_c = 2\,\mu m$. This resulted in a thermal contact resistance of $(3-9) \times 10^6$ K/W, leading to ~10% uncertainty of the total thermal conductivity. Matthew *et al*. [136] measured a higher SWNT film-substrate resistance (about 33-46 $\mathrm{mm^2}$ K/W) by nanosecond thermos reflectance thermometry. This value is higher because the measured result contains residual volumetric resistance. Using experimental methods can also separate intrinsic thermal resistance from contact thermal resistance. According to Hsu *et al*. [125], thermal contact resistance and the intrinsic thermal resistance of CNTs can be calculated by

measuring the temperature profile, and the calculated ratio ranges from 0.02 to 17 depending on the contact conditions and the sample quality.

If the contact resistance can be eliminated, true thermal conductivity could be higher. A conventional method to avoid the influence of contact thermal conductivity is by depositing metallic drops on the tube-substrate contact area. In this way, the sample will be sandwiched between the metal and substrate, and decrease the thermal contact resistance. Choi *et al*. [119,118] used the $3-\omega$ technique with deposited Pt on the tube-substrate contact region by EB method. The measurement results on several MWCNT samples of different lengths and diameter implied negligible contact resistance. Pettes *et al* [113] measured three samples after Pt-C deposition, compared with no deposition result, the contact resistance was about 12-54% of the total thermal resistance.

A second problem is related to the sample preparation, as the suspended thermometer is of rather small size, it is challenging to put the sample at the right place. One method is to grow CNT right on the structure [112, 129, 130, 137]. The advantage of this preparation method it provides clean samples. But the sample cannot be selected and number of CNTs is difficult to control. Another method is to put grown samples on the structure whether by spin coating a solution containing CNTs [112, 119, 122], placed by a nano-probe [107, 137] or use a PMMA to transfer CNTs [138]. But the selectivity of using a CNT solution is not satisfying because commercially purchased CNT samples have different sizes in diameter and length [122]. Kodama *et al*. [134] introduced a selective way by first spin-coat samples on a substrate and then fabricated the structure for a selected sample.

V. CNT-CNT BUNDLES

Measured results on thermal properties of mesoscopic and bulk materials like CNT bundles, mat and films composed of CNTs seem to lose the outstanding performance that single CNTs showed. Despite the quasi-one-dimensional physical property [4], the advantage of high thermal conductance of CNT is suppressed by packing fraction, interface resistance between CNTs, boundary resistance between CNTs and substrate as well as defects [13]. Take graphene as an example, experiments and simulations on single-layer graphene shows higher thermal conductivity than few layers [91]. Measured thermal conductivity of single-layer graphene could reach up to 5000 W/m K [11, 12], while increasing the layers reduces the thermal conductivity to about 1000W/m K [139-141]. Similar results happened for carbon nanotubes. Single-walled carbon nanotube have rather high thermal conductivity, surpasses that of CNT

mats whose thermal conductivity are only tens of W/m K. Heo [142] measured thermal conductivity of randomly packed CNT mat with thermal conductivity ranging from 0.12-0.20 W/m K. Comparably low values were also observed by Prasher *et al*. [143], with measured thermal conductivity ranging from 0.155-0.194 W/m K. The low thermal conductivity of CNT films was thought to stem from the large contact thermal resistance between individual CNTs.

Weak nonbonding van der Waals interactions among CNTs is responsible for the spontaneous self-assemble into interconnected bundles and mats [60,144]. Figure 5-1 shows a transmission electron microscopy observation of SWNTs packed in a hexagonal bundle. Simulations by Volkov *et al*. [145] applied tubular potential for thousands of nanotubes with micrometer length and showed the interaction between CNTs is the driving force for nanotube alignment and bundle generation. Feng *et al*. [146] observed bundle formation when annealing horizontally aligned SWNTs. But when the density of SWNTs is low, the formation is highly suppressed. A similar phenomenon is observed in CNT films, mats and fibers [144, 147, 148]. To fully elucidate the heat transport process in these materials, accurate models are needed to address the inter-CNT contact resistance and to link it with the different performance from a single CNT to its bulk counterparts. In this section we will discuss efforts to account for the interface influence in CNT bundles and discuss thermal performance of CNT bundles.

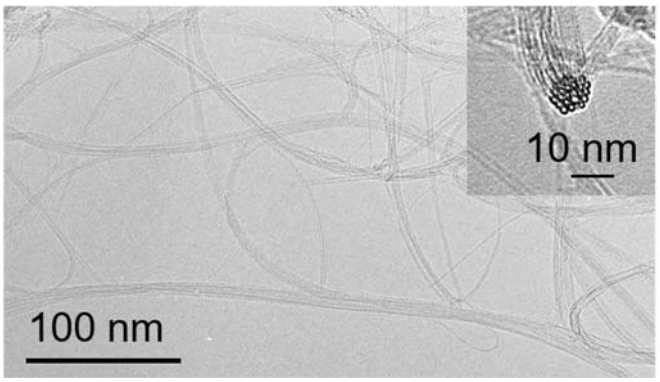

FIG.5-1 TEM image of SWNTs organized into bundles. Insect is cross sectional view of a SWNT bundle,

A. MODELING OF CNT BUNDLES

A CNT bundle is a collection of CNTs tightly packed in a parallel, arrangement. Its thermal property is related to a single carbon nanotube yet more complex. Hone *et al*. [108] used specific heat to clarify the thermal properties of SWNT bundles, and found a cross over from 3D to 1D behavior for strongly coupled bundles and from 3D to 2D for weakly coupled bundles. The cross over regime depends on the

relation between transverse Debye energy and the lowest optical phonon sub-band energy. (As shown in Figure 5-2) The phonon structure of a strong coupled bundle shows 3D characteristic at low temperature and reflect the isolated SWNT property at higher energies [108]. However, weakly coupled ropes may have little influence on thermal conductivity of each SWNTs in the bundle, therefore, SWNT in a weakly coupled bundle showed linear temperature dependence at low temperatures [108].

Sauvajol *et al*. [149] calculated a phonon dispersion relation for identical, infinitely long SWNTs hexagonally packed into a bundle by a valence force field together with Lennard-Jones potential to describe van der Waals inter-tube interactions. Parameters adopted are the same as Lu and Yang [150]. Assumptions in their calculation was that each SWNT remains circular despite the inter-tube interaction and all SWNTs are identical in the hexagonal lattice. Figure 5-2 illustrates some atom vibration modes for isolated tubes and tube in bundle at low and high frequency. It is obvious that inter-tube interactions lead to noticeable frequency shifts for low frequency modes. However, for high frequency modes, frequency differences are not significant, only about 0.1-2% [151, 152]. It is worth mentioning that the *liberation* of twisting mode at k=0, the intertube interaction gives rise to a non-zero frequency (measured to be range from 2 to 6meV [153]), implying a loss of twist in the bundle, different from isolated SWNTs.

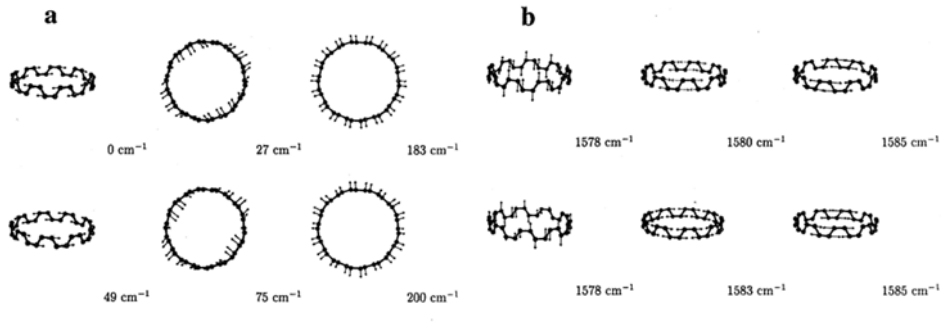

Figure 5-2. Sketch of the atomic displacements for specific vibration modes of (9, 9) SWNT isolated (upper row) and in a bundle (lower row). (a) is low frequency modes, (b) is high frequency modes.

For SWNTs in bundles, the vibrational density of state (VDOS) at zero frequency has non-zero VDOS, while SWNT VDOS is zero [149]. For (10, 10) SWNTs in bundles, the phonon dispersion relation is shown in Figure 5-3. When the energy is above 15 m eV, the profile of energy is similar to the dispersion curve for an isolated SWNT [149]. This relation verifies the results from Hone *et al*. [108].

Yan *et al*. [60] started from the kinetic model of thermal conductivity:

$$\kappa = \sum_q C_q v_{gq}^2 \tau_q = \sum_q C_q v_{gq}^2 \frac{\tau_{bq}\tau_{Uq}}{\tau_{bq} + \tau_{Uq}}$$

where C_q and v_{gq} are specific heat and group velocity of q phonons. τ_q denotes the relaxation time, expressed by the combination of boundary scattering process, τ_{bq} and three phonon umklapp scattering processed, τ_{Uq}. The relaxation time of boundary scattering process τ_{bq} is taken as 50 ps [101], and for the Umklapp process, the relaxation time is derived from first perturbation theory:

$$\frac{1}{\tau_{Uq}} = \frac{4\gamma^2 h}{3} \sum_{q'} \frac{F(\omega, v_g, N_0)}{\rho}$$

with the selection rule:

$$q + q' = q'' + G$$

$$\omega + \omega' = \omega''$$

where γ is the Grüneisen parameter, $F(\omega, v_g, N_0) = [\omega\omega'\omega''(N_0' - N_0'')/v_g^2]\delta(\omega + \omega' - \omega'')$ with N_0' and N_0'' the occupancies of the q' and q'' phonons. *h is* the Planck constant and ρ is the mass density. With the phonon dispersion relation calculated by Sauvajol *et al*. [149], Yan *et al*. [60] calculated the thermal conductivity of a (10, 10) carbon nanotube bundle in axial and perpendicular directions, as shown in Figure 5-4. Consistent with Yan *et al*. [60], Zhigilei *et al*. [154] reached the same conclusion that inter-tube interaction plays a negligible role by performing NEMD simulation on thermal conductivity of CNT in a bundle. However, from simulation results on graphene and graphite, Berber *et al*. [9] predicted a reduction of thermal conductivity when a CNT is brought to form a bundle.

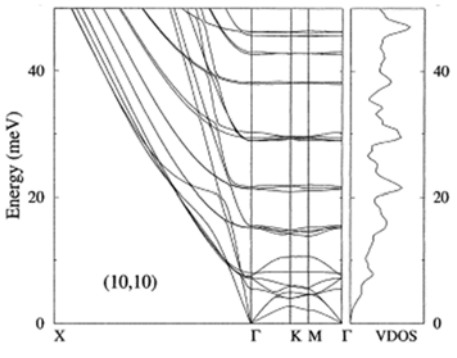

Figure 5-3. Phonon dispersion relation of a (10, 10) SWNT in a bundle

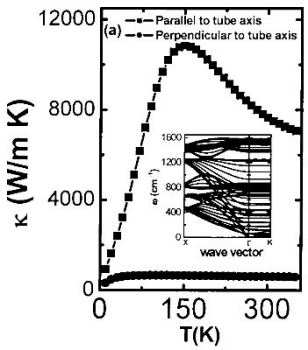

Figure 5-4. Thermal conductivity of (10, 10) carbon nanotube bundle in axial direction and perpendicular direction.

As stated in the model of Sauvajol, the assumption is that all tubes in the bundle are identical. But in experiments, bundles could consist of CNT with different chirality [155] and diameters [156]. Shang, Ming, Wang [20] provided a formula for calculating the total thermal conductance of CNT bundle:

$$K_{bundle} = \sum_{D} N_{tube} K_{tube}$$

where D is the diameter of CNT, N_{tube} is the number of CNT with same diameter D, and K_{tube} denotes thermal conductivity of CNT with diameter D. Normally, D follows a Gaussian distribution with mean diameter of $\overline{D}$ and a standard deviation σ_D:

$$N_{tube} = \frac{N_{bundle}}{\sqrt{2\pi}\sigma_D} \exp\left[-\frac{1}{2}\left(\frac{D-\overline{D}}{\sigma_D}\right)^2\right]$$

where N_{bundle} is the total number of CNTs in the bundle. This formula can be extended to thermal calculation of mixed bundles of SWNT and MWNT, and also applicable for pure MWNT bundles.

Through MD simulation and theoretical models, Zhigilei *et al*. [50,154] found there is crossover from an intertube-conductance–dominant regime to an intrinsic-conducting-dominant regime. Bundle thermal conductivity is describing with two formulas:

$$\bar{\kappa}_b = f(N_s, B_i) g(\bar{\Delta}) \int_0^1 \int_{\bar{x}_1}^1 \frac{A(Bi, \bar{x}_2 - \bar{x}_1)}{Bi} d_{\bar{x}_2} d_{\bar{x}_1}$$

$$f(N_s, B_i) = 1 + \left[\frac{17}{14} + \left(\frac{f^0(N_s)}{2} - \frac{12}{7}\right)\exp(-0.2\sqrt{Bi})\right] \times \left\{1 + \tanh\left[-0.79\log_{10}\left(\frac{Bi}{2.7}\right)\right]\right\}$$

where N_s, B_i, A, $\bar{x}_2 - \bar{x}_1$ denotes the number of full shells, Biot number, and cross-sectional and relative displacement of CNT ends, respectively. $g(\bar{\Delta}) = [H(1-\bar{\Delta})]^2$ is the number of shells in the bundle and $f(N_s, B_i)$ is the thickness function. This theoretical model fits well with simulation work. Using this model, the thermal conductivity of CNT bundles in the length range from 20 nm to 4 μm demonstrate strong dependence on individual CNTs consisting of a bundle and the cross over from inter-tube-conductance-dominant regime to intrinsic-conducting-dominant regime is likely to occur [154].

B. CONTACT THERMAL RESISTANCE

The interfacial thermal resistance forms a barrier for heat carriers from different phases and prevents thermal transport. Because of the challenge in accurately modeling interfaces of CNT-CNT contact in bundles, MD simulations have been performed to analyze parameters that affect energy transport

between CNTs in bundle. Such parameters include, but are not limited to length, junction angle, pressure, chirality, tube-tube space and diameter. Such atomistic modeling is computationally costly and not applicable for systems with large number of atoms; atomic and mesoscopic simulation are used to explore the above mentioned parameters.

Chalopin *et al*. [157] has shown CNT interface conductance had an upper bound for all chirality; simulated values were below 100 pW/K for temperatures ranging from 5-1000 K [157]. Simulation results of Prasher *et al*. [143] were about 50 pW/K, and fall in this range. In reality, CNT-CNT junctions exist in large numbers in CNT materials thus the simulation of single junction always overestimates the thermal conductance [143, 158].With MD simulations, Maruyama *et al*. [159] calculated thermal boundary resistance between (5, 5) carbon nanotubes to be 6.46×10^{-8} m^2K/W. This result is slightly lower than [161] at the order of 10^{-7}, but comparable to experiment measurements. An order of magnitude inter-tube thermal resistance of 5.67×10^{-9} m^2K/W is calculated for overlap length ranging from 10-45 nm [50, 154]. This lower inter-tube thermal resistance was assumed to be a result of the usage of periodic boundary conditions rather than fixed boundary condition [50, 154]. Comparable values were obtained by similar simulation in [51] for 25-75 nm long CNTs, ranging from 4×10^{-9}-6×10^{-9} m^2K/W. According to Zhong and Lukes [160], inter-tube conductance is an overlap length dependent value. For overlap increases from 2.5 nm to 10 nm, intertube conductance decreases from 0.0065 W/mK to 0.0018W/m K for 20 and 40 nm long CNTs simulated. But Zhigilei *et al*. [50, 154] reasoned this is because both the model length and overlap length in Reference 161 is short. In the Zhigilei *et al*. [154] work, overlap lengths of 10 to 95 nm were calculated for 200 nm CNT models; no significant decrease was observed from the simulation result.

Contact density is a topic vastly discussed by many researchers but there has been no conclusion until now. Prasher and coworkers [143] showed that two junctions placed closer than the coherence length of phonon transport in CNT decrease the inter-tube thermal conductance more dramatically than single junction. On the other hand, Hu and Mc Gaughey [161] calculated a 20% drop of thermal conductance when neighboring junctions are separated 10-20 nm for 60 nm CNTs, but for other simulated results, neighboring junction has a negligible effect. Zhigilei *et al*. [50] found no relationship between inter-tube thermal conductance and the presence of neighboring junction.

Much research work has concentrated on the angle, θ, between CNTs and its effect on junction thermal conductivity. Through simulations on different CNT-CNT angles, Yang *et al*. [162] found that the junction is easier to form and stay stable for small angles. Zhigilei *et al*. [50] suggested that for $\theta \leq 35°$,

the van der Waals forces would overcome original force and form a complete alignment of the two CNTs. Chalopin *et al*. [157] obtained thermal conductance of the same order for θ = 90° and for aligned junctions [160], implying trivial effect from the angle θ. In sharp contrast, Evans [163] simulated a strongly cross angle dependence of thermal conductivity and showed thermal conductivity is largest for parallel tubes and they mentioned the relationship of angle and contact area. Zhigilei *et al*. [50] further converted this problem to a matter of interatomic inter-tube interactions per atom, defining the effective contact between CNTs, and the simulation results indicate the effective contact is enhanced between CNTs with small angles. Simulation results suggested that aligned bundle have thermal conductance higher than that of a randomly oriented CNT network. This is consistent with previous research [160, 164, 165].

Zhong and Luke [160] predicted from MD simulations that interfacial resistance increases with increasing tube-tube space and decreases with increasing contact area. This is further confirmed by other researchers [157, 143]. Zhigilei *et al*. [145] adopted a continuum approach describing interactions between graphite structures at mesoscopic levels depending uniquely on the distance between interacting objects. From the work of Zhigilei *et al*. [145], the heat conduction path in a bundle will depend strongly on the thermal transport direction. For a tightly packed bundle structure, the CNTs contact with each other contributes a circumferential bypass pathway to perpendicular conductivity, thus increasing thermal conductivity of the structure [145]. From Evans *et al*. [163], extra inter-tube pressure not only enhances the van der Waals bdingin and the stiffness decreases with tube-tube space, but also increases the effective contact area.

Junction thermal conductance would be enhanced with increasing CNT length [161]. This is because a longer CNT contributes more low-frequency acoustic phonons carrying heat in the system and high-frequency phonons must couple with low-frequency ones to transfer energy across junctions [157, 163]. But there is a convergence of values of such junction conductivities [157, 50, 161, 163] due to suppression of phonon frequencies above a few tens of terahertz, and this value varies with potential or boundary conditions. As reported by Zhiglei *et al*. [154], bundle thermal conductance has a rather complex dependence on individual CNT length inside, especially for current CNT materials of length range from ~20 nm to ~4 μm. As for decreasing length of CNT bundles, the conductivity drops significantly by increasing density of “free” CNT ends inside bundles.

Shang, Ming and Wang predicted thermal conductance of mixed CNT bundles could be further enhanced for high densities and larger bundle widths [20]. Popov *et al*. [78] found that with increasing

size, CNT bundles show T^3 dependence similar to that of graphite, indicating a crossover to a 3D behavior. However, Aliev *et al*. [166] used simulations together with the 3-ω method mentioned in Section 4 to investigate the bundle size effect on thermal conductivity of MWNT, observing a 75% drop of thermal conductivity in MWNT bundle than in single MWNT.

C. EXPERIMENTAL MEASUREMENTS

Despite the theoretical and simulation efforts mentioned above that suggested inter-tube interaction on defect-free CNT in bundle has little effect [50, 60,154], experimental results seem contradictory. It is already a universally accepted fact that weak inter-tube bonding leads to large contact resistance and confines energy transfer between carbon nanotubes in van der Waals contacts. In truth, experimental experience is not exactly in conflict with theoretical or simulation, because in real bundles, CNTs may not be well aligned, with unavoidable defects, packing densities, catalyst nanoparticles etc.

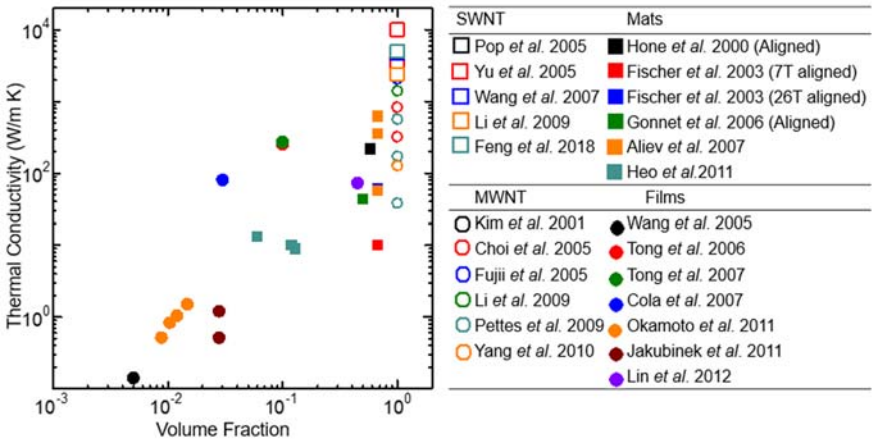

Figure 5-5 Thermal conductivity as a function of volume fraction for four kinds of CNT materials. Almost all of the carbon nanotube arrays and mats show relatively lower thermal conductivity than individuals. The highest thermal conductivity of aligned CNT arrays reported by Tong *et al*. shows a promising future in applications which take full advantage of high thermal conductivity of individual CNTs and exceeding 250 W/m K.

Randomly oriented CNT mats and films show rather low thermal conductivity [143, 167, 168]. In contrast, vertically aligned CNT (VACNT) arrays seem to have improved thermal performance. Figure 5-5 shows the thermal conductivity of bulk CNT materials as a function of volume fraction. Hone *et al*. [169] produced thick films of aligned SWNT arrays by suspending them in strong magnetic fields, yielding thermal conductivities over 200 W/m K in the parallel direction. Fischer *et al*. [170] and Gonnet

et al. [171] measured parallel thermal conductivity of about ~50W/m K and ~45W/m K respectively. Anisotropic ratio in the above mentioned references are ~3 to 9, indicating the morphology dependence of thermal conductivity, which is rather important for commercial applications in order to take advantage of carbon nanotube composite. This conclusion is also applicable for MWNT yarns and mats. Aliev *et al*. [172] determined thermal conductivity of MWNT mats and yarns and their findings show MWNT composites exhibit strong anisotropic thermal properties and high degree of long tube-tube overlap in yarns substantially reduces tube interconnection resistance.

In addition, compressive stress improves inter-tube contact and tube-substrate contact, thus reduce thermal resistance at interface [173]. Increasing packing density has the same beneficial effect [174]. But excessive compressive stress could cause buckling in the VACNT and reduce thermal conductivity. This is assumed to be caused by the breakdown of CNTs and increase of phonon scattering [174]. This result is further confirmed by simulation. Volkov *et al*. [175,176] investigated the buckling effect using atomistic and mesoscopic simulations. A 75% reduction in thermal conductivity of individual nanotubes were observed with buckling angle changing from 20 to 110°. For a CNT film, thermal conductivity was 20% lower when modeled with a buckling wrinkle [175].

Figures 5 and 6 show thermal conductance as a function of sample length for CNT bundles. Thermal conductivity of SWNTs with similar lengths are also plotted together. In the figure, solid symbols stand for SWNTs while hollow symbols denote SWNT bundles. The calculated thermal conductivity of lengths from several micrometers to tens of micrometers feature comparable or smaller magnitudes than the value for individual suspended SWNT, which are reported to range from 2400 to nearly 10000 W/mK [33-44]. This difference between SWNT and SWNT bundles is believed mainly stem from inter-tube interactions causing by strong phonon coupling at the inter-tube contacts. Influence of sample quality also makes sense to some degree because a combined structure and thermal conductance measurement has addressed the enhanced defect scattering of phonons which is inevitable in CNT samples. From the figure, an $L^{-\alpha}$ trend can be seen for SWNT bundles, which is a sign that sample length exceeds that of the phonon mean free path and is no longer the dominant parameter for thermal conductivity. But there exist some data that seem to conflict with the discussion above in reporting CNT thermal conductivity for samples with small lengths and small thermal conductivity. For example, the thermal conductivity of a 2.5 μm SWNT bundle measured by Feng *et al.* [146] is smaller than that of 5 μm SWNT bundle. But when it is considered that the size of the sample is large, namely thirteen SWNTs bundled together, it is apparent that the diameter that confines the thermal conductivity of SWNT bundle.

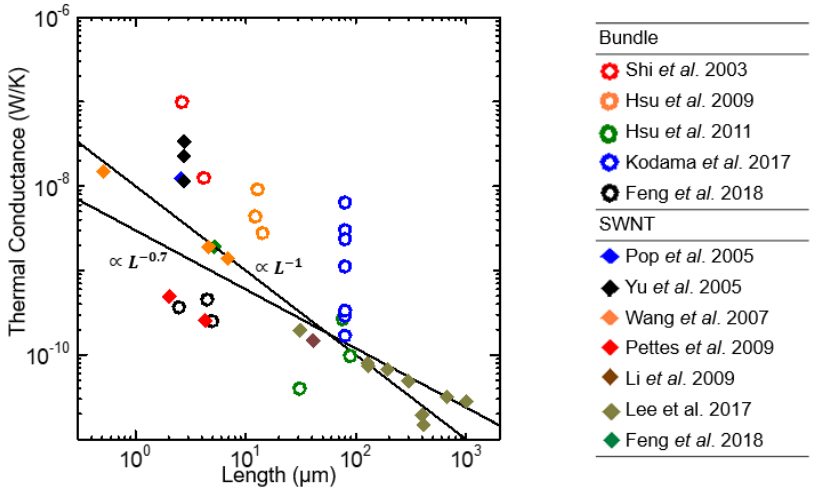

Figure. 5-6 Thermal conductivity as a function of sample length. The solid symbols represent individual suspended SWNT and the hollow symbol denotes suspended SWNT bundles.

Determining the exact number of SWNTs in a bundle is difficult even with TEM observation, therefore the bundle size effect is seldom discussed in reported works. Several researchers reported data that could help reveal this issue. Aliev *et al*. [166] used simulation together with the 3-ω method mentioned in Section 4 to investigate the bundle size effect on thermal conductivity of MWNT. They observed a 75% drop of thermal conductivity in MWNT bundles compared to a single MWNT. As shown in Figure 5-7 (a) and 5-7 (b), thermal conductivity is plotted as a function of bundle size and as a function as bundle diameter. These figure illustrate the bundle size effect. If these figures are assumed, the identical inter-tube forces, same packing morphology and same SWNT diameter, bundle size and bundle diameter could be treated equally. Unlike isolated SWNTs, CNT bundles could have diameters in a large range, therefore, the size dependence and diameter dependences can be observed more clearly.

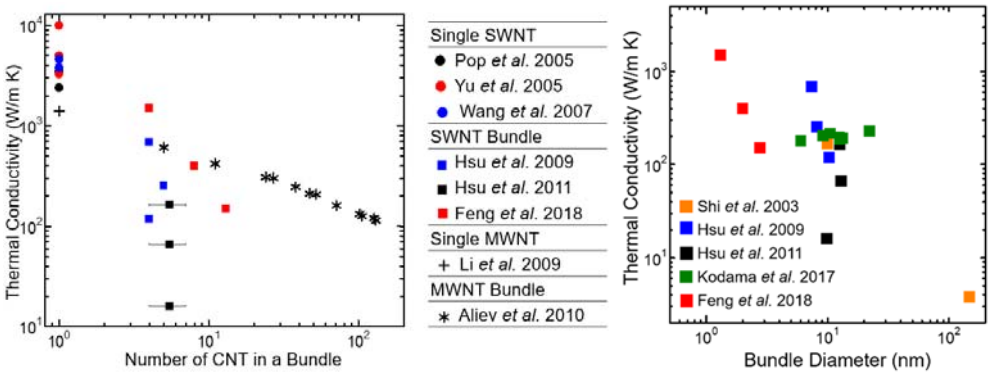

Figure. 5-7 (a) Thermal conductivity as a function of numbers of CNT in a bundle, and (b) thermal conductivity as a function of bundle diameter.

From the figure, thermal conductivity decreases with increasing bundle size and for CNT bundles, and this decrease is much quicker for SWNT bundles than MWNT bundles. This phenomenon is concluded to be a result of inter-tube interaction that strongly increase inelastic scattering involving phonons from neighboring SWNTs. As calculated in the work of Bagatskii *et al.* [168], radio thermal expansion of SWNT in a bundle increases with temperature and enhances the interaction with each other. This phenomenon was proved to strongly quench phonon modes in SWNTs thus leading to a very low thermal conductivity [146, 167]. Feng *et al*. [146] fitted experimental results with kinetic theory and the results indicate that the probability of scattering with neighboring SWNTs increases. From their experiment, thermal conductivity of bundles is related to the thermal conductivity of isolated SWNTs via the relation: $\kappa = \kappa_{is}(1/1+\sigma)$, where σ is related to the number of SWNTs in a bundle and is inversely proportional to temperature. With that model, at room temperature the thermal conductivity was reduced to 1/10 in a four-SWNT-bundle, 1/13 in a eight-SWNT-bundle and 1/15 in a thirteen-SWNT-bundle. Although the data shown in Figures 5-7 is at room temperature, similar trends are observed over a large temperature range. Experimental results measured by Kodama *et al*. [134] of bundle thermal conductivity with diameter from 6 nm to 22.2 nm seems to obey no rule. And from the Hsu *et al*. [125, 127] work, smaller diameters even have smaller thermal conductivity than larger ones. However, bundles containing five SWNTs have smaller diameters than bundles with four SWNTS, which indicates a loose packing morphology. According to simulation works [163, 166], reasonably tightly packed SWNTs would increase effective contact area and contribute a circumferential bypass pathway for phonon and thus increasing thermal conductivity. Recall what we discussed that theoretically, impact factors including inter-tube distance, angle, external pressure and these parameters can hardly be controlled or even measured or calculated in experiments. Assuming a perfectly well aligned morphology of CNT bundles is a simplification, experimentally observed CNT bundles often show a randomly bundling method, and are not strictly well aligned. Thus the portion to which thermal properties will be influenced by these factors could not be decided based on present experimental knowledge.

VI. CARBON NANOTUBE COMPOSITE

From section 3 to section 5, we discussed the thermal properties of carbon nanotube and bulk counterpart. However, the small size of carbon nanotube presents limitations and is not ideally applicable,

therefore seeking breakthrough from carbon nanotube composites is sought, like CNT-polymer composites, CNT-ceramic composites and CNT-metal composites. Up to now, the most extensively studied properties of carbon nanotube composite properties are mechanical and electrical [177-181]. In this review paper, we mainly focus on thermal related properties of carbon nanotube composites. Among the three kinds of composited mentioned, CNT-polymer composites have shown most promise for their thermal potential. Thus in this section, we'll talk about CNT-polymer composites.

A. CARBON NANOTUBE-POLYMER COMPOSTING PROCESS

Compositing processing of CNT-polymer composites usually fall in the following three classes: purification, dispersion and functionalization. Recent years have witnessed the progress in these processes [178, 179, 182, 183].

1. Purification

Mass produced CNTs usually contain impurities (carbon particles, catalyst particles or amorphous carbon) that prevent the full usage of their intrinsic properties. To remove the unwanted impurities. Physical separations including centrifugal separation, size exclusion, microfiltration or sonication are options [182, 184, 185]. Thermal annealing is an interesting way to transfer amorphous carbon into sp^2 carbon on the outer wall of a carbon nanotube [186]. Or oxidation in air, oxygen, water and H_2O_2 could etch the amorphous carbons [182, 186-190]. Removal of catalyst particles is achieved by reacting catalyst with acid or alkaline [191]. The procedures may be effective for certain kinds of impurities, thus the purify procedure is usually a sequential combination of many steps. To prevent secondary pollution, the purification process should be well tailored without causing damage to the raw CNT products. However, it is still a challenge to efficiently organize the existing procedures for purification of CNTs [186].

2. Dispersion

CNT in a polymer matrix acts as a filler to alter the mechanical, electrical, thermal and other properties of a polymer. Therefore, large interface areas is essential to guarantee effective reinforcement. The most common way is to mix the CNTs and polymers in a solvent and then evaporate the solvent. But there are extreme difficulties in properly distributing CNTs within the polymer matrix. One reason is that commercial CNTs are often fabricated in the form of bundles or entanglements instead of well-separated individual CNTs. Thus their mechanical, electrical or thermal properties will be diminished compared

with theoretical predictions [192, 193]. CNTs are of nanoscale dimension, and large number of CNTs exist within a very small volume. Take CNT and Al_2O_2 as example, for the same volume 1.0 mm^3 and 0.1 Vol. %, the two kinds of fillers has particles number of 4.42×10^8 and 1.9 respectively [194]. This brings about tremendous problem for uniformly disperse CNT particles in polymer matrix and further prevent the reinforcement in various properties.

Techniques like power ultra-sonication [194], calendaring [195, 196], ball milling [197], stir and extrusion [198, 199], and surfactant assisted processing [200] have been proven to disperse CNTs in polymer a matrix. Dispersion processes may cause change to the CNT sample, for example, bulk milling process could shorten the length of CNTs [179].

3. Functionalization

Before giving details about functionalization, it is necessary to mention that carbon nanotube dispersed with no treatment interact with the surrounding matrix mainly through van der Waals forces [185, 194], which are unable to transfer load through the CNT and polymer interface. To form a stable connection with the polymer, proper surface modification of CNTs should be carried out. Several functionalization methods have been developed, including, but not limited to: covalent functionalization, non-covalent functionalization, surfactants as supramolecular adducts, and defect functionalization [200-209].

Covalent functionalization is a chemical way of creating strong bonds between nanotubes and polymers via several existing approaches [200]. The translational symmetry will be changed from sp^2 to sp^3, and in this way the electronic and transport properties could be influenced [201]. Figure 6-1 (a) illustrates this process. Functional groups such as –COOH are created through oxidation as a precursor for further chemical reaction to form linkages with organic or inorganic chains [202]. Functionalization changes the CNT-CNT interface as well as CNT-polymer interface, and may change the thermal conductivity of CNT-polymer composite significantly.

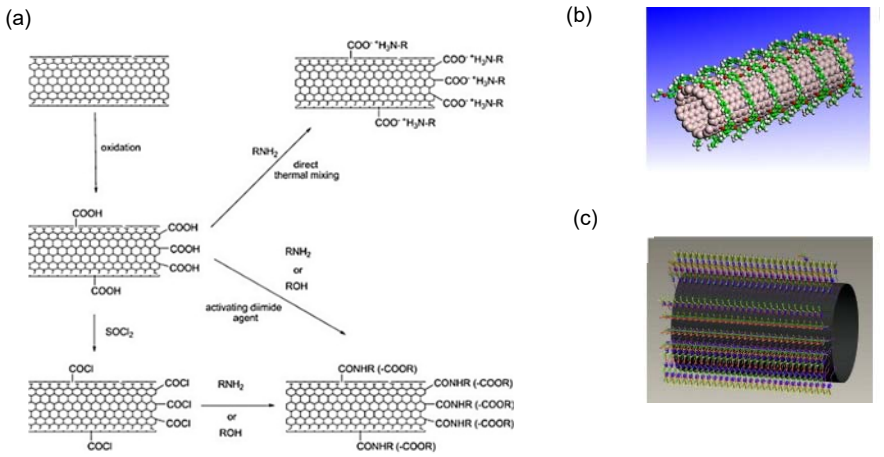

Fig 6-1. (a) Covalent oxidation of CNT and following reaction with amines and alcohols [177]; (b) and (c) are non-covalent methods (polymer rapping and surfactant adsorption) [194]

A non-covalent composite is a physical process that involves absorption and/or wrap of a polymer with the CNT together via π-stacking interactions [177, 203, 204]. Compared with covalent functionalization, this method doesn't destroy the surface of CNT side wall, and causes no change to CNT's properties. Schematics of two example of non-covalent method is shown in Figure 6-1 (b) and (c).

The secondary effect of functionalization is to make CNTs less likely to aggregate together and ensure better dispersion. Raw CNTs tend to aggregate together, forming clusters with dimension of several microns. CNTs with functional groups would distribute individually or within small clusters. Functionalization methods could be found in reported works such as [179, 183, 194, 205-209] and have been proven to effectively disperse CNT in polymer matrix.

4. Fabrication of CNT-polymer composite

To some extent, fabrication of CNT-polymer composites and dispersion processes largely overlap with each other. The most commonly used method is solution mixing [179, 194, 210]. Both CNTs and polymers are mixed in a solvent and sonification or other dispersion methods are adopted to get a satisfying homogeneous mixture. Lastly the solvent is removed by evaporation [211]. However, not all polymers are soluble. For insoluble polymers, CNT-polymer composites could be processed by melting a polymer and mixing it with CNT materials [194]. The composite could be melt many times to reach a

satisfying dispersion, but this process is not efficient and is limited to low filler concentration composites [194, 212]. For industry production, a relatively new, efficient and reliable approach called Latex technology is used. Latex is colloidal of dispersed polymer in an aqueous environment. CNT materials are dispersed in an aqueous surfactant solution, and then mixed with the Latex [194, 213]. The most tailored way to obtain high CNT weight fractions and high uniformity is with in situ polymerization. In this method, CNT are dispersed in a monomer and followed by polymerization reaction. In situ polymerization is the main way to fabricate epoxy-based nanocomposites [194, 210, 214, 215].

B. MODELING OF CARBON NANOTUBE-POLYMER COMPOSITES

1. Basic theoretical modeling

For heterogeneous system media, effective thermal conductivity can be expressed by the Maxwell-Garnett (MG) approximation [216]. This MG approach has been confirmed to be applicable for matrix based composites with low-filling ratios. Based on the conventional theory, modifications have been made to describe carbon nanotube-based composites.

Nan *et al*. [217] investigated effectivity thermal conductivity of CNT-based composites starting from a rigorous solution: $K_e = K^0 + \langle T \rangle (I + \langle GT \rangle)^{-1}$, where K_e denotes the effective thermal conductivity, K^0 is the constant part of the homogeneous value, T is transition matrix, I denotes unit tensor, and G is a Green's function. They made several simplifications and assumptions to the above equation including: ignore inter-particle multiple scattering, assume CNTs uniformly dispersed in the matrix, and assume effective CNT-matrix interface transport. The calculated effective thermal conductivity was given as:

$$\frac{K_e}{K_m} = 1 + \frac{f K_c}{3 K_m} \tag{6-1}$$

K_m, K_c and f in the formula are thermal conductivity of the matrix, thermal conductivity of SWNT, and the volume fraction of SWNT. As $K_c/K_m \gg 1$, the second part of the right side could be seen as enhanced thermal conductivity with addition of SWNTs into the system. However, compared with reported experimental works, formula 6-1 seems to overestimate the effect of SWNTs. The authors gave three possible reasons: waited to be improved composite quality, SWNT-polymer interfacial thermal resistance and aggregation or twist of SWNTs in composites. The effective media theory was used by many researchers to model composite with MWNTs fillers [218].

2. Basic simulation modeling

A CNT-polymer MD simulation model requires proper models for CNTs, polymers and the interactions between them [219]. Duong *et al*. [220] established a computational model based on Monte Carlo simulations. 90000 "hot" and "cold" walkers were release from opposite sides of the simulated cell and distributed randomly but uniformly on the surface. The walkers were dominated by Brownian motion. At the interface, walkers had a probability to move into the SWNT, otherwise they stayed in their previous position. Here we use an extended Monte Carlo model as a visual representation, as shown in Figure 6-2 [221]. A thermal equilibrium factor C_f was used as a sign of steady state which guaranteed that: (i) densities of hot walkers inside the SWNT and inside the matrix are equal; (ii) heat flux into the SWNT equals the heat flux from the SWNT to the matrix. After the whole process reach a steady state, composite thermal conductivity was calculated through the linear temperature slop. This model matched well with experimental works of Bryning *et al*. [222]. An off-lattice Monte Carlo model is also adopted to describe CNT multiphase model and investigate the heat transfer within the system [221].

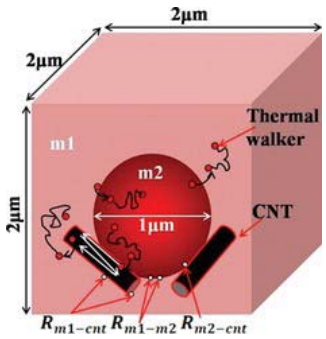

Figure 6-2 Schematic plot of the computational model. The pink part and black cylinder represent bulk medium and CNTs, respectively. Red dots are hot walkers and white dots represent boundary thermal resistance. The big red ball in the center is a third phase and is not discussed here.

Traditional effective-medium models could not accurately match with experimental data [223]. Foygel *et al*. [224] combined Monte Carlo simulations and the percolation theory to investigate the low-percolation-threshold (critical volume fraction) of carbon nanotube composites. The percolation model proved to be useful for predicting thermal conductivity of CNT networks in composites with high accuracy. Haggenmueller *et al*. [223] has shown that an effective media model could only fit experimental data up to 6 vol. % composites while percolation theory is accurate for composites with CNTs as high as 20 vol. %. In percolation theory, thermal conductivity increases with increasing fraction

value, and the critical fraction value is related to parameters including tube length, diameter, and alignment. The aspect ratio is defined as $a=l/d$ (l is the nanotube length and d is the tube diameter) and diminishes the critical fraction value as it increases. For fully aligned hard-core nanotubes, the critical fraction value is the maximum, 16%, for any aspect ratio. From this calculation, effective thermal conductivity of composites can be determined and calculation results agree well with experiment, and are quite accurate for CNT-oil suspension. Consistent with Foygel, Wang *et al*. [225] measured a 40% thermal conductivity improvement of chopped SWNT-epoxy compared with neat epoxy resins and this value was 20 % higher than pristine SWNT-epoxy composites. However, Shenogin *et al*. [226] suggested that large-aspect-ratios filled polymer composites are good conductors, even un-functionalized, and CNTs with aspect ratios smaller than 100 have little benefit on composite thermal conductivity.

3. Thermal resistance

As mentioned in 6.1.3, chemical bonds between CNTs and polymers not only change the structures of CNTs but also that of the polymer. For CNTs, sp^2 bond changing to sp^3 is a drawback for thermal conductivity since the changed C atom act as scattering center for heat carriers in the CNT and therefore lower the intrinsic thermal conductivity of CNTs [226]. On the other hand, chemical bonds linking CNTs and polymers decrease the interfacial resistance dramatically thus interface heat flow can be conducted effectively. The final effect of these two competing phenomenon is complicated. Enhanced thermal conductivity for CNT-polymer composites was observed [226], at the same time, slightly lower thermal conductivity was also observed for functionalization-induced defects in CNT-composites [227]. According to Gardea and Lagoudas [227], functionalization not only increases defects on CNT surfaces, but also breaks the symmetry of carbon nanotubes. The symmetry further influences phonon modes in carbon nanotubes, as discussed in section 2.

Nan *et al*. [228] further explore equation 6-1 and include interfacial resistance, yielding

$$\frac{K_e}{K_m} = 1 + \frac{fp}{3}\frac{K_c/K_m}{p+\frac{2R_kK_c}{d}} \tag{6-2}$$

where K_e and K_m denote effective thermal conductivity and thermal conductivity of the matrix. p is the aspect ratio, d is diameter and R_K is the interface thermal resistance known as Kapitza resistance. R_K value is of comparable magnitude with poly-crystals and other composite materials [229, 230], therefore it is one of the key factors for thermal conductivity of CNT-polymer composites. Nan *et al*. [228] plotted the degradation of enhanced thermal conductivity as a function of interface thermal resistance. Over a

80% drop of effective thermal conductivity was observed from that of a perfect interface to $R_k = 1 \times 10^7$.

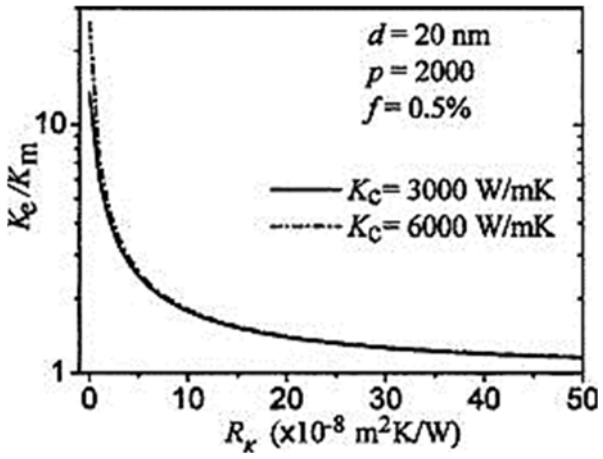

Figure 6-3. Effective thermal conductance enhancement as a function of interface thermal resistance.

Based on the diffuse mismatch model [231], Cahill *et al*. [232] discussed interface thermal conductance from phonon modes. For a given frequency phonon, thermal conductance is proportional to the density of state at the frequency both for the CNT and the matrix. Therefore, interface thermal resistance also arises from poor phonon coupling between the nanotube and the polymer, and from dampened phonon vibration matrix interaction [233]. Because phonon modes are related to tube length and diameter, they showed that for longer length and bigger diameter, interface thermal conductance would increase [232]. However, the increase will reach a constant and will not increase indefinitely. Although their model is for octane liquid, this method should be applicable to other systems. Moreover, from their simulation work, a 4 Å distance was found between octane and CNT for a large part of the octane simulated. This weak physical contact causes more interface resistance. However, physical contact depends on surface wettability and some composites were found with good conditions [234,235].

Another source of thermal resistance come from the contact thermal resistance. Thermal conductivity of SWNT networks in composites were quantified to be around 55 W/m K [236]. As discussed in Section 5, weak van der Waals force banded CNTs together and offer limited path ways for phonons. These contact parts not only become scattering sites for phonon propagating along carbon nanotube, but also act as a resistance route for phonon transport.

For CNTs that span the entire thickness of the composite, the CNT-matrix boundary resistance is lower than randomly dispersed CNT-composites. Long CNTs serve as pathways for phonon transport

through the composite. Therefore, CNT-matrix boundary resistance is critical for poorly aligned composites.

C. THERMAL CONDUCTIVITY OF CNT-POLYMER COMPOSITES

From the theoretical calculations of Nan *et al*. [217], effective thermal conductivity of CNT-based composite could be improved more than 500 times, depending on the thermal conductivity of the matrix and thermal conductivity of CNT filler. Experimental and simulation work have shown the improved thermal conductivity of polymers with CNT fillers. Choi *et al*. [237] obtained a 300 % improvement in thermal conductivity of SWNT-epoxy composites at room temperature with 3 wt % SWNT fillers. Biercuk *et al*. [238] observed a 125 % enhancement in thermal conductivity at room temperature for SWNT-epoxy composites. Marconnet *et al*. [239] got a higher increase of 18.5 for MWCNT-epoxy composites along the aligned direction. Thermal conductivity enhancement of CNT-polymer composites are shown in Figure 6-4. Though improvement levels for different polymers and CNT fillers vary a lot, CNT-composites displayed an observable enhancement for most of the measurements. Lower concentration of CNTs yield modest enhancement while higher concentrations yield larger improvement [239]. And what's more, the enhancement of thermal conductivity was measured to be very stable [240].

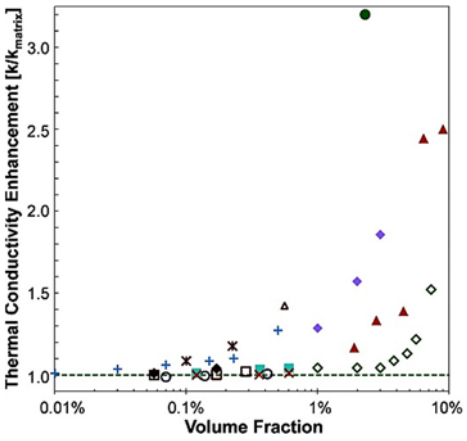

	Matrix	CNT Details	Reference
+	Epoxy (Epon 828)	HiPCO SWCNT	Bryning *et al.*[6]
✱	Epoxy (Epon 828)	Laser Oven Grown SWCNT	Bryning *et al.*[6]
●	Epoxy (Epon 862)	HiPCO SWCNT	Du *et al.*[23]
○	Epoxy (Bakelite L13i)	SWCNT	Gojny *et al.*[5]
■	Epoxy (Bakelite L13i)	DWCNT	Gojny *et al.*[5]
×	Epoxy (Bakelite L13i)	DWCNT-NH_2	Gojny *et al.*[5]
◆	Epoxy (Bakelite L13i)	MWCNT	Gojny *et al.*[5]
□	Epoxy (Bakelite L13i)	MWCNT-NH_2	Gojny *et al.*[5]
◆	Silicone	MWCNT	Hu *et al.*[8]
◇	Polymethylmethacrylate	SWCNT	Bonnet *et al.*[9]
▲	Polymethylmethacrylate	SWCNT	Guthy *et al.*[10]
△	Polyethylene	SWCNT	Haggenmueller *et al.*[24]

Figure 6-4. Thermal conductivity as a function of volume fraction for randomly dispersed CNT composites. Matrix materials in this chart fall into the range of 0.18-0.26 W/m K.

Theoretical predictions of thermal conductivity enhancement and results of earlier works are shown in Figure 6-5 [218]. It's easy to tell that despite the fact that thermal conductivity has been improved a lot, measurement never reached the theory prediction. The reason for these low values arise from

resistance, dispersion, functionalization, and alignment, quality of CNT and geometry of CNTs filler.

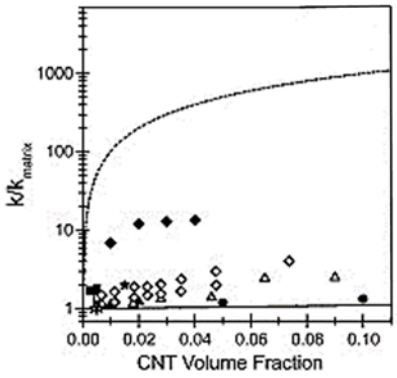

Figure 6-5 Theoretical predictions of thermal conductivity as a function of CNT volume fraction. Dotted and solid lines represent parallel model and series model prediction. Dotted symbols are measurement results.

Gardea and Lagoudas [227] calculated thermal enhancement as a function of fraction rate with different levels of dispersion. Figure 6-6 shows the effect of dispersion on composite thermal conductivity. Obviously, dispersed composites feature higher thermal conductivity. Comparing data of ten and five minutes milling time, the thermal conductivity was increased by 24% with five more minutes of dispersion treatment. Khare *et al*. 243 obtained an 8 % enhancement of thermal conductivity for disperse CNT-epoxy composites. Biercuk *et al*. [242] compared industry epoxy loaded with 1 wt % SWNT and carbon fibers without functionalization. The enhancements in thermal conductivity at room temperature were 125% and 40 % respectively. However, the enhancement with CNTs filler has a boundary when effectivity thermal conductivity no longer increase with weight fraction of CNT. As represented in Figure 6-5. For 5 min and 10 min dispersed samples, thermal conductivity stops increasing after the fraction rate exceeds 0.3 %. Moreover, it should be noted that fully dispersed CNTs with little or no contact with each other have proved to yield really low thermal conductivity [185]. This is because the high CNT-matrix thermal resistance would offset the superiority offered by carbon nanotubes.

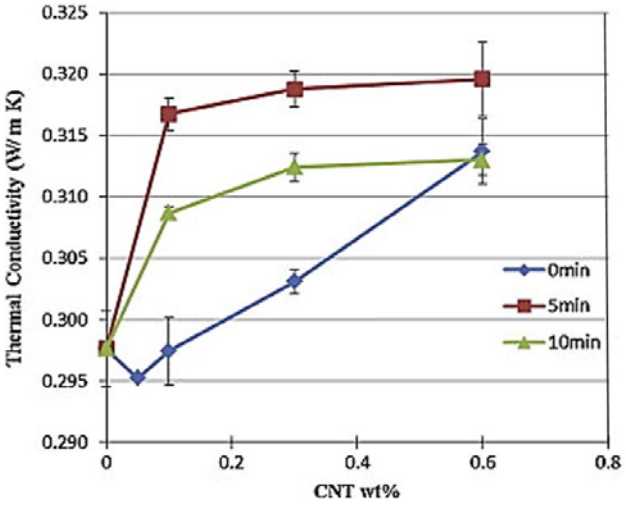

Figure 6-6. Thermal conductivity of CNT-epoxy composites with different ball-milled times as a function of weight percent.

Functionalization forms better connection between CNTs and matrix as well as benefit dispersion, and many works have confirmed the positive effect of functionalization [225, 226, 243-248]. Shenogin *et al*. [226] simulated the chemical bonding on tube-matrix boundary resistance. Thermal conductivity of functionalized SWNT-composites show an increase for nanotube ratios between 100 and 1000. Nonetheless, their simulation result also displayed negative impact of functionalization on SWNT intrinsic thermal conductivity compared with un-treated SWNT. Thermal conductivity of pure SWNT was 6000 W/m K, and with 1 % atoms in the tubed became functionalized, thermal conductivity drops more than threefold. Similarly, acid oxidization functionalization was found to lead to inferior thermal conductance of SWNT-epoxy composites [225]. This could be explained by composite thermal resistance, discussed in section 6.2.3, a side effect of functionalization is that it causes defects on nanotube side walls, and these defects significantly disrupt phonon ballistic conductance near the Fermi level [243]. Thermal transport in composites include ballistic transport in SWNT and diffusion in the matrix, hence the superiority of SWNT is offset by functionalization.

In order to form a highly effective thermal pathway for phonon transport, or enhance thermal conductivity in a desired direction, alignment of CNTs in composites is preferred. Alignment could be achieved by adding external forces, during fabrication and by using arrays as filler. Choi *et al*. [237] conducted 0, 15, 25 T magnetic alignment on CNT-epoxy composites for 4 hours. AFM images of

SWNT-epoxy composites after 25 T treatment confirmed that SWNTs in the composite formed bundles and aligned along the direction of the external magnetic field. Treated SWNT-epoxy composites with additional 10% improvement was measured [237]. Marconnet *et al*. [239] fabricated aligned carbon nanotube-polymer nanocomposites by infiltrated polymers on carbon nanotube arrays. Thermal conductivity was enhanced both in parallel and transverse directions of the CNTs, and increased non-linearly with the density of array.

Wei and coworkers [219] showed a 40% in thermal expansion coefficient for CNT-polyethylene composite with volume fraction about 8% using MD simulations. Compared with thermal expansion coefficients with frozen SWNT constraints and identical other parameters, the enhanced expansion coefficient was attributed to the phonon modes and Brownian motion of SWNTs. Similar with expansion coefficient, the diffusion coefficient of C atoms in polymer chains war found to be improved in composites, especially in the axis direction of SWNT.

Another obvious change of temperature-related property is glass transition temperature. Glass transition temperature is defined as a temperature at which the maximum damping factor is observed [246]. Both simulations and experiments [219, 246, 247] have observed an increase in the glass transition temperature T_g due to the reduced motion of polymer molecules with embedded CNT filler. Santos *et al*. [179] measured T_g 1 wt % MWNT-polymer composite with Raman and infrared spectroscopies and an increase of 40 ℃ of glass transition temperature was observed. However, one exception result was simulated by Khare *et al*. [241], T_g of nanocomposites with dispersed CNTs was ~66 K lower than neat cross-linked epoxy. This phenomenon was recovered by further functionalization.

D. OTHER CARBON NANOTUBE COMPOSITES

CNT and graphene could work synergistically to improve thermal conductivity of epoxy-composites. Shin *et al*. [240] demonstrated a multi graphene platelet/MWNT-epoxy composite, observed 146.9 % in thermal conductivity. MWNTs work as connections between two graphene platelets, resulting in a high contact area between the carbon structure and the epoxy matrix. Dispersing CNTs into metals and ceramics is more challenging, but recent advances enable in situ fabrication of such composites. More noticeable improvements are in the electrical properties and mechanical properties like strength and elastic modulus of such composites. Similar enhancement in thermal properties was also observed for CNT-metals and CNT-ceramic composites [186].

REFERENCES

[1] Mildred S. Dresselhaus，Gene Dresselhaus，Ko Sugihara，Ian L. Spain，Harris A. Goldberg. (1988) Graphite Fibers and Filaments. *Springer Series in Materials Science, 5*.

[2] Sumio Iijima. (1991) Helical microtubules of graphitic carbon, *Nature,* 354, 56–58.

[3] Sumio Iijima, Toshinari Ichihashi. (1993) Single-shell carbon nanotubes of 1-nm diameter, *Nature,* 363, 603–605.

[4] Saito, R., G. Dresselhaus, M.S. Dresselhaus. (1998) Physical properties of carbon nanotubes. *World scientific*.

[5] M.S. Dresselhausa, G. Dresselhausb, R. Saitoc, A. Joriod. (2005) Raman spectroscopy of carbon nanotubes, *Physics Reports*, 409, 47-99.

[6] Chunming Niu, Enid K. Sichel, Robert Hoch, David Moy, and Howard Tennent. (1997) High power electrochemical capacitors based on carbon nanotube electrodes, *Appl. Phys. Lett.* 70.

[7] K. Cui, T. Chiba, S. Omiya, T. Thurakitseree, P. Zhao, S. Fujii, H. Kataura, E. Einarsson, S. Chiashi, S. Maruyama. (2013) Self-Assembled Micro-Honeycomb Network of Single-Walled Carbon Nanotubes for Solar Cell, *J. Phys. Chem. Lett.*,4, 2571-2576.

[8] K. Cui, Y. Qian, I. Jeon, A. Anisimov, Y. Matsuo, E. I. Kauppinen, S. Maruyama. (2017) Scalable and Solid-State Redox Functionalization of Transparent Single-Walled Carbon Nanotube Films for Highly Efficient and Stable Solar Cells. Adv. Energy Mater, 7, 1700449.

[9] Savas Berber, Young-Kyun Kwon, and David Tománek. (2000) Unusually High Thermal Conductivity of Carbon Nanotubes. *Phys. Rev. Lett.* 84, 4613.

[10] K.M. Liew, Z.X. Lei, L.W. Zhang. (2015) Mechanical analysis of functionally graded carbon nanotube reinforced composites: A review, *Composite Structures*, 120, 90-97.

[11] Balandin A A, Ghosh S, Bao W, Calizo I, Teweldebrhan D, Miao F, Lau C. (2008) Superior thermal conductivity of single-layer graphene. *Nano Lett.* 8, 902-907.

[12] Ghosh S, Calizo I, Teweldebrhan W, Pokatilov E P, Nika D L, Balandin A A, Bao W, Miao F, Lau C N (2008) Extremely high thermal conductivity of graphene: Prospects for thermal management applications in nanoelectronic circuits. *Appl. Phys. Lett*. 92, 151911.

[13] Amy M. Marconnet, Matthew A. Panzer, and Kenneth E. Goodson. (2013) Thermal conduction phenomena in carbon nanotubes and related nanostructured materials, *Rev. Mod. Phys*. 85, 1295

[14] K.I.Tserpes, P.Papanikos. (2005) Finite element modeling of single-walled carbon nanotubes, *Composites Part B: Engineering*,36, 5 468-477.

[15] M. S. Dresselhaus, P. C. Eklund. (2010) Phonons in carbon nanotubes, *ADV PHYS*,49, 6, 705, 814.

[16] Steven H. Simon. (2013) The Oxford Solid State Basics.

[17] J. HoneM.C. LlagunoM.J. BiercukA.T. JohnsonB. BatloggZ. BenesJ.E. Fischer, (2002) Thermal properties of carbon nanotubes and nanotube-based materials. *Applied Physics A: Materials Science &*

Processing, 2002. 74(3): p. 339-343.

[18] Charles Kittel, Herbert Kroemer. (1980) Thermal physics.

[19] Wang, J., J.-S. Wang. (2006) Carbon nanotube thermal transport: Ballistic to diffusive, *Appl. Phys. Lett.* 88, 111909.

[20] Shang, L., L. Ming, and W. Wang, (2007) Diameter-dependant thermal conductance models of carbon nanotubes, *7th IEEE Conference on Nanotechnology*. 206–210.

[21] Roham Rafiee,Reza Maleki Moghadam, (2014) On the modeling of carbon nanotubes A critical review, *Composites Part B: Engineering*, 56, 435-449.

[22] J. Tersoff, (1988) New Empirical Approach for the Structure and Energy of Covalent Systems, *Phys. Rev. B,* 37, 12, 6991-7000.

[23] J. Tersoff, (1988) Empirical Interatomic Potential for Silicon with Improved Elastic Properties, *Phys. Rev. B*, 38, 14, 9902-9905.

[24] J. Tersoff (1989) Modeling Solid-State Chemistry: Interatomic Potentials for Multicomponent Systems, *Phys. Rev. B*, 39, 8, 5566-5568,

[25] D. W. Brenner. (1992) Empirical Potential for Hydrocarbons for Use in Simulating the Chemical Vapor Deposition of Diamond Films, *Phys. Rev. B*, vol. 42, pp.9458-9471.

[26] Y. Yamaguchi, S. Maruyama, (1998) A Molecular Dynamics Simulation of the Fullerene Formation Process, *Chem. Phys. Lett.,* vol. 286, no. 3-4, pp. 336-342,.

[27] Maruyama. S, (2009) Molecular Dynamics Method for Micro/Nano Systems, *Handbook of Numerical Heat Transfer*, 2 nd, 21.

[28] Jennifer R. Lukes, Hongliang Zhong,(2007) Thermal Conductivity of Individual Single-Wall Carbon Nanotubes, *J. Heat Transfer*, 129, 6, 705-716.

[29] X. Lü, J. H. Chu, and W. Z. Shen, (2003) Modification of the lattice thermal conductivity in semiconductor rectangular nanowires, *Journal of Applied Physics* 93, 1219

[30] Maruyama, S. (2002) A molecular dynamics simulation of heat conduction in finite length SWNTs, *Physica B: Condensed Matter*, 323B, 193.

[31] Maruyama, S., (2003) A Molecular Dynamics Simulation of Heat Conduction of A Finite Length Single-walled Carbon Nanotube, *Microscale Therm. Eng*. 7, 41.

[32] Yao, Z., J.-S. Wang, B. Li, and G.-R. Liu, (2005) Thermal conduction of carbon nanotubes using molecular dynamics, *Phys. Rev. B* 71, 085417.

[33] Che, J., T. Cagin, and W. A. Goddard, III, (2000) Thermal conductivity of carbon nanotubes, *Nanotechnology*,11, 65

[34] Osman, M. A. and D. Srivastava, (2001) Temperature dependence of the thermal conductivity of single-wall carbon nanotubes *Nanotechnology,* 12, 21.

[35] Zhang, W., Z. Zhu, F. Wang, T. Wang, L. Wun, and Z. Wang, (2004)Chirality dependence of the thermal conductivity of carbon nanotubes, *Nanotechnology* , 15, 936.

[36] Grujicic, M., G. Cao, and B. Gersten, Mater.(2004) Atomic-scale computations of the lattice

contribution to thermal conductivity of single-walled carbon nanotubes, *Sci. Eng. B*, 107, 204.

[37] Grujicic, M., G. Cao, and W. N. Roy, Computational analysis of the lattice contributionto thermal conductivity of single-walled carbon nanotubes, *J. Mater. Sci*. 40, 1943 (2005).

[38] J. F. Moreland, J. B. Freund, G. Chen, (2004)The disparate thermal conductivity of carbon nanotubes and diamond nanowires studied by atomistic simulation, *Microscale Thermophysical Engineering,* 8:61–69.

[39] Padgett, C. W., D. W. Brenner, (2004)Influence of Chemisorption on the Thermal Conductivity of Single-Wall Carbon Nanotubes, *Nano Lett*. 4, 1051.

[40] Zhang, G. and B. Li, (2005) Thermal conductivity of nanotubes revisited: Effects of chirality, isotope impurity, tube length, and temperature, *J. Chem. Phys.* 123, 114714.

[41] Davide Donadio, Giulia Galli, Thermal Conductivity of Isolated and Interacting Carbon Nanotubes Comparing Results from Molecular Dynamics and the Boltzmann Transport Equation, *Phys. Rev. Lett*. 99, 255502.

[42] L. Lindsay, D. A. Broido, and Natalio Mingo, (2010) Diameter dependence of carbon nanotube thermal conductivity and extension to the graphene limit *Phys. Rev. B*, 82, 161402(R).

[43] Cuilan Ren, Zijian Xu, Wei Zhang, Yong Li, Zhiyuan Zhu, Ping Huai, Theoretical study of heat conduction in carbon nanotube hetero-junctions, *Physics Letters A*, 374, 17–18,2010,1860-1865,

[44] B. Qiu, Y. Wang, Q. Zhao, X. Ruan, (2012) The effects of diameter and chirality on the thermal transport in free-standing and supported carbon-nanotubes, *Appl. Phys. Lett.* 100, 233105.

[45] J. Shiomi, S. Maruyama, (2008) Molecular dynamics of diffusive-ballistic heat conduction in single-walled carbon nanotubes, *Jpn. J. Appl. Phys*. 47 2005–2009.

[46] J.A. Thomas, R.M. Iutzi, A.J.H. (2010) McGaughey, Thermal conductivity and phonon transport in empty and water-filled carbon nanotubes, *Phys. Rev. B*, 81, 045413

[47] R.-Q. Pan, Z.-J. Xu, Z.-Y. Zhu, (2007) Length dependence of thermal conductivity of single-walled carbon nanotubes, *Chin. Phys. Lett*. 24, 1321–1323

[48] M. Alaghemandi, E. Algaer, M.C. Bohm, F. Muller-Plathe, (2009)The thermal conductivity and thermal rectification of carbon nanotubes studied using reverse non-equilibrium molecular dynamics simulations, *Nanotechnology* 20, 115704.

[49] A. Cao, J. Qu, (2012) Size dependent thermal conductivity of single-walled carbon nanotubes, *J. Appl. Phys*. 112, 013503.

[50] Richard N.Salaway, Leonid V.Zhigilei, (2014) Molecular dynamics simulations of thermal conductivity of carbon nanotubes Resolving the effects of computational parameters, *International Journal of Heat and Mass Transfer,*70, 954-964.

[51] Zhun-Yong Ong, Eric Pop, (2010) Molecular dynamics simulation of thermal boundary conductance between carbon nanotubes and SiO_2, *Phys. Rev. B,* 81, 155408

[52] Cem Sevik, Alper Kinaci, Justin B. Haskins, Tahir Çağın, (2011) Characterization of thermal transport in low-dimensional boron nitride nanostructures, *Phys. Rev. B*, 84, 085409.

[53] H. F. Zhan, G. Zhang, J. M. Bell, and Y. T. Gu, (2014)Thermal conductivity of configurable two-dimensional carbon nanotube architecture and strain modulation, *Appl. Phys. Lett*. 105, 153105.

[54] Junhua Zhao, Jianyang Wu, Jin-Wu Jiang, Lixin Lu, Zhiliang Zhang, and Timon Rabczuk, (2013) Thermal conductivity of carbon nanocoils, *Appl. Phys. Lett.* 103, 233511.

[55] Philip B. Allen (2013) Improved Callaway model for lattice thermal conductivity, *Phys. Rev. B*, 88, 144302.

[56] D. T. Morelli, J. P. Heremans, and G. A. Slack,(2002) Estimation of the isotope effect on the lattice thermal conductivity of group IV and group III-V semiconductors, *Phys. Rev. B*, 66, 195304.

[57] Chantrenne, P., J.-L. Barrat, (2004) Analytical model for the thermal conductivity of nanostructures, *Superlattices Microstruct*. 35, 173.

[58] David G. Cahill1, Paul V. Braun, Gang Chen, David R. Clarke, Shanhui Fan, Kenneth E. Goodson, Pawel Keblinski, William P. King, Gerald D. Mahan, Arun Majumdar, Humphrey J. Maris, Simon R. Phillpot, Eric Pop, and Li Shi, (2014)Nanoscale thermal transport. II. 2003–2012,*Appl. Phys. Rev,* 1, 011305.

[59] Lucas Lindsay,(2016) First Principles Peierls-Boltzmann Phonon Thermal Transport A Topical Review, *NANOSC MICROSC THERM,*20,2, 67-84.

[60] X. H. Yan, Y. Xiao, Z. M. Li (2006) Effects of intertube coupling and tube chirality on thermal transport of carbon nanotubes, *J.Appl. Phys.*, 99, 124305.

[61] Wang. Tang. Zheng(2007) Length-dependent thermal conductivity of single-wall carbon nanotubes: prediction and measurements, *Nanotechnology,* 18, 475714.

[62] Mingo, N., D. A. Broido, (2005) Length Dependence of Carbon Nanotube Thermal Conductivity and the “Problem of Long Waves”. *Nano Lett*. 5, 1221.

[63] D.A.Broido, M. Malorny, G. Birner, M. Malorny and G. Birner, D. A. Stewart, (2007) Intrinsic lattice thermal conductivity of semiconductors from first principles, *Appl. Phys. Lett*. 91, 231922.

[64] Lindsay, L. and D. A. Broido, (2010) Optimized Tersoff and Brenner empirical potential parameters for lattice dynamics and phonon thermal transport in carbon nanotubes and graphene. *Phys. Rev. B*, 81, 205441.

[65] Esfarjani, K., Stoles, H. T., (2008)Method to extract anharmonic force constants from first principles calculations, *Physical Review B*, 77, 144112.

[66] Esfarjani, K., Chen, G., Stokes, H. T., (2011) Heat transport in silicon from first-principles calculations, *Physical Review B*, 84, 085204.

[67] Sebastian Volz, Junichiro Shiomi, Masahiro Nomura, Koji Miyazaki, Heat conduction in nanostructured materials, *Journal of Thermal Science and Technology*, Vol. 11, 1-15 (2016).

[68] Zhiting Tian, Keivan Esfarjani, Junichiro Shiomi, Asegun S. Henry, and Gang Chen, (2011) On the importance of optical phonons to thermal conductivity in nanostructures, *Appl. Phys. Lett*. 99, 053122

[69] Tian, Z., Garg, J., Esfarjani, K., Shiga, T., Shiomi, J. and Chen, G., (2012) Phonon conduction in

PbSe, PbTe, and PbTe1-xSexfrom first-principles calculations, *Physical Review B*, 85, 184303.

[70] H. J. Maris, S. Tamura, (2012) Heat flow in nanostructures in the Casimir regime, *Phys. Rev. B,* 85, 054304.

[71] 2004-Yamamoto, T., S. Watanabe, and K. Watanabe, (2004) Low-temperature thermal conductance of carbon nanotubes, *Thin Solid Films* 464–465, 350.

[72] Rego, L. G. C., G. Kirczenow, (1998) Quantized Thermal Conductance of Dielectric Quantum Wires, *Phys. Rev. Lett*. 81, 232.

[73] Yamamoto, T., S. Watanabe, and K. Watanabe, (2004) Universal Features of Quantized Thermal Conductance of Carbon Nanotubes, *Phys. Rev. Lett*. 92, 75502.

[74] Jishi, R. A., L. Venkataraman, M. S. Dresselhaus, G. Dresselhaus, (1993) Phonon modes in carbon nanotubules, *Chem. Phys. Lett*. 209, 77.

[75] Saito, R., T. Takeya, T. Kimura, G. Dresselhaus, M. S. Dresselhaus, (1998) Raman intensity of single-wall carbon nanotubes, *Phys. Rev. B*, 57, 4145.

[76] Daniel Sánchez, Portal, D., E. Artacho, J. M. Soler, A. Rubio, P. Ordejón, (1999) Ab initio structural, elastic, and vibrational properties of carbon nanotubes, *Phys. Rev. B* 59, 12 678

[77] V. N. Popov, V. E. Van Doren, M. Balkanski, (2000) Elastic properties of single-walled carbon nanotubes, *Phys. Rev. B,* 61, 3078.

[78] Valentin N. Popov, (2002)Low-temperature specific heat of nanotube systems, *Phys. Rev. B* 66, 153408.

[79] Popov, V. N., (2004) Theoretical evidence for $T^{1/2}$ specific heat behavior in carbon nanotube systems, *Carbon* 42, 991.

[80] Mahan, G. D. and G. S. Jeon, (2004) Flexure modes in carbon nanotubes, *Phys. Rev. B*, 70, 075405.

[81] J. Hone, M. Whitney, C. Piskoti, A. Zettl, (1999) Thermal conductivity of single-walled carbon nanotubes, *Phys. Rev. B*, vol. 59, pp R2514-2516.

[82] T. Borca-Tasciuca, S. Vafaei, D.-A. Borca-Tasciuc, B. Q. Wei, R. Vajtai, P. M. Ajayan, (2005) Anisotropic thermal diffusivity of aligned multiwall carbon nanotube arrays. *J. Appl. Phys.* 98, 054309.

[83] Yamamoto, T., S. Konabe, J. Shiomi, S. Maruyama, (2009) Crossover from Ballistic to Diffusive Thermal Transport in Carbon Nanotubes, *Appl. Phys. Express* 2, 095003.

[84] P. Kim, L. Shi, A. Majumdar, P. L. McEuen, (2001)Thermal transport measurement of individual multiwalled nanotubes, *Phys. Rev. Lett*. 87, 215502.

[85] Alexander A. Balandin, (2011) Thermal properties of graphene and nanostructured carbon materials, *Nat. Mater*. 10, 569.

[86] J. Hone,B. Batlogg,Z. Benes, A. T. Johnson1, J. E. Fische, (2000) Quantized phonon spectrum of single-walled carbon nanotube, *Science* 289, 1730.

[87] D. V. Chalin, M. V. Avramenko, and S. B. Rochal. (2017) Simple theory of low-temperature thermal conductivity in single- and double-walled carbon nanotubes, Phys. Rev. B 96, 155413.

[88] Pop, E., D. Mann, Q. Wang, K. E. Goodson, and H. Dai, (2006) Thermal Conductance of an

Individual Single-Wall Carbon Nanotube above Room Temperature, *Nano Lett.* 6, 96.

[89] Tomoyuki Hata, Hiroki Kawai, Tatsuhiko Ohto, Koichi Yamashita, (2013) Chirality dependence of quantum thermal transport in carbon nanotubes at low temperatures A first-principles study, *J Chem Phys,* 139, 044711.

[90] Ilia Ivanova, Alexander Puretzky, Gyula Eres, Hsin Wang, Zhengwei Pan, Hongtao Cui, Rongying Jin, Jane Howe, and David B. Geohegan, (2006) Fast and highly anisotropic thermal transport through vertically aligned carbon nanotube arrays, *Appl. Phys. Lett*. 89, 223110.

[91] Denis L Nika1, Alexander A Balandin., (2017) Phonons and thermal transport in Graphene and Graphene-based materials, *Rep Prog Phys*, 80, 3

[92] Junichiro Shiomi, Shigeo Maruyama, (2008) Diffusive-Ballistic Heat Conduction of Carbon Nanotubes and Nanographene Ribbons, *INT J THERMOPHYS*, 31, 10, 1945-1951.

[93] Junichiro Shiomi, (2014) Nonequilirium molecular dynamics methods for lattice, *Annual Rev Heat Transfer.*

[94] Takahiro Yamamoto, Kazuyuki Watanabe, Eduardo R. Hernández, (2008) Mechanical Properties, Thermal Stability and Heat Transport in Carbon Nanotubes, *Carbon Nanotubes,* pp. 165-195.

[95] Jihong Ma, Yuxiang Ni, Sebastian Volz, Traian Dumitrică (2015) Thermal Transport in Single-Walled Carbon Nanotubes Under Pure Bending, *Phys. Rev. Applied* 3, 024014.

[96] V.Vijayaraghavana, A.Garga, C.H.Wong, K.Tai, Pravin M.Singru, Liang Gao, K.S.Sangwan (2014) A molecular dynamics based artificial intelligence approach for characterizing thermal transport in nanoscale material. *Thermochimica Acta*, 594, 20, pp. 39-49.

[97] Xin Wang, QianJiang Wei, zong Xu, Wei Cai, Yoku Inoue, Yuntian Zhu. (2013) Effect of carbon nanotube length on thermal, electrical and mechanical properties of CNT bismaleimide composites. *Carbon*,53, pp.145-152.

[98] L. Lindsay, D. A. Broido, Natalio Mingo, (2009) Lattice thermal conductivity of single-walled carbon nanotubes Beyond the relaxation time, *Phy. Rev. B*,80,125407.

[99] Victor Lee, Chi-Hsun Wu, Zong-Xing Lou, Wei-Li Lee, and Chih-Wei Chang, (2017)Divergent and Ultrahigh Thermal Conductivity in Millimeter-Long Nanotubes, *Phys. Rev. Lett.* 118, 135901.

[100] Shiomi. J, Maruyama. S (2007) Diameter and length effect on diffusive-ballistic phonon transport in a carbon nanotube, 2007 ASME-JSME Thermal Engineering Summer Heat Transfer Conference.

[101] J. X. Cao, X. H. Yan, Y. Xiao,J. W. Ding, (2004) Thermal conductivity of zigzag single-walled carbon nanotubes Role of the umklapp process, *Phys Rev B*.69.073407

[102] Sheng-Ying Yue, Tao Ouyang, Ming Hu, (2015) Diameter Dependence of Lattice Thermal Conductivity of Single-Walled Carbon Nanotubes Study from Ab Initio, *Scientific Reports,*5, 15440.

[103] Feng Ya, Zhu Jie, Tang Da-Wei (2014) Influence of chirality on the thermal conductivity of single-walled carbon nanotubes, *Chinese Physics B*, 23, 8.

[104] Cem Sevik, Hâldun Sevinçli, Gianaurelio Cuniberti, Tahir Çağın (2011) Phonon Engineering in Carbon Nanotubes by Controlling Defect Concentration, *Nano Letters* 11, 4971.

[105] Abhishek Chaudhuri, Anupam Kundu, Dibyendu Roy, Abhishek Dhar, Joel L. Lebowitz, Herbert Spohn. (2010) Heat transport and phonon localization in mass-disordered harmonic crystals. *Phys. Rev. B* 81, 064301.

[106] V. Meunier, A. G. Souza Filho, E. B. Barros, and M. S. Dresselhaus, (2016) Physical properties of low-dimensional sp2-based carbon nanostructures, *Rev. Mod. Phys*. 88, 025005.

[107] Masato Ohnishi, Takuma Shiga, Junichiro Shiomi (2017)-Effects of defects on thermoelectric properties of carbon nanotubes, *Phys. Rev. B* 95, 155405.

[108] Shigeo Maruyama, Yasuhiro Igarashi, Yuki Taniguchi, Junichiro Shiomi, (2006) Anisotropic Heat Transfer of Single-Walled Carbon Nanotubes, *Journal of Thermal Science and Technology*.

[109] Xiuqiang Li, Jie Chen, Chenxi Yu, Gang Zhang, (2013) Comparison of isotope effects on thermal conductivity of graphene nanoribbons and carbon nanotubes, *Appl. Phys. Lett*. 103, 013111.

[110] Ivana Savić, Natalio Mingo, Derek A. Stewart, (2008) Phonon Transport in Isotope-Disordered Carbon and Boron-Nitride Nanotubes: Is Localization Observable? *Phys. Rev. Lett*. 101, 165502.

[111] Feng Dai-Li, Feng Yan-Hui, Chen Yang, Li Wei, Zhang Xin-Xin, (2013) Effecte of doping, stone-wales and vacancy defects on thermal conductivity of single-walled carbon nanotubes, *Chin. Phys. B*, 22, 1.

[112] Li Shi, Deyu Li, Choongho Yu, Wanyoung Jang, Dohyung Kim, Zhen Yao, Philip Kim and Arunava Majumdar, J. Heat Transfer 125(5), 881-888,2003

[113] Pettes, M. T. and Shi, L. (2009), Thermal and Structural Characterizations of Individual Single-, Double-, and Multi-Walled Carbon Nanotubes. *Adv. Funct. Mater.*, 19: 3918-3925.

[114] Motoo Fujii, Xing Zhang, Huaqing Xie, Hiroki Ago, Koji Takahashi, Tatsuya Ikuta, Hidekazu Abe, Tetsuo Shimizu, (2005) Measuring the thermal conductivity of a single carbon nanotube, *Phys. Rev. Lett*. 95, 065502

[115] Jaehyun Kim, Eric Ou, Daniel P. Sellan, Li Shi. (2015) A four-probe thermal transport measurement method for nanostructures. *Rev Sci Instrum* 86, 044901.

[116] Z. Wang, N. Mingo, (2010) Diameter dependence of SiGe nanowire thermal conductivity, *Appl. Phys. Lett*. 97, 101903.

[117] Jaehyun Kim, Evan Fleming, Yuanyuan Zhou, Li Shi, (2018) Comparison of four-probe thermal and thermoelectric transport measurements of thin films and nanostructures with microfabricated electro-thermal transducers, *Journal of Physics D: Applied Physics*, 51, 10.

[118] Tae-Youl Choi, Dimos Poulikakos, Joy Tharian, Urs Sennhauser, (2006) Measurement of the Thermal Conductivity of Individual Carbon Nanotubes by the Four-Point Three-ω Method, *Nano Lett.*, 6 (8), pp 1589–1593

[119] Tae Y. Choi, Dimos Poulikakos, Joy Tharian and Urs Sennhauser (2005) Measurement of thermal conductivity of individual multiwalled carbon nanotubes by the 3-ω method, *Appl. Phys. Lett*. 87, 013108.

[120] A. Bachtold, M. S. Fuhrer, S. Plyasunov, M. Forero, Erik H. Anderson, A. Zettl, and Paul L.

McEuen, (2000) Scanned Probe Microscopy of Electronic Transport in Carbon Nanotubes, *Phys. Rev. Lett.* 84, 6082

[121] L. Lu, W. Yi, D. L. Zhang, (2001)3ω method for specific heat and thermal conductivity measurements, *Review of Scientific Instruments* 72, 2996.

[122] Hsiao-Fang Lee, Benedict A. Samuel, M. A. Haque, (2009) In-plane thermal conductance measurement of one-dimensional, *J Therm Anal Calorim* 99(2):495-500.

[123] Chris Dames, Gang Chen, (2005)1ω, 2ω, and 3ω methods for measurements of thermal properties, *Review of Scientific Instruments*, 76:12

[124] Jinbo Hou, Xinwei Wang, Pallavi Vellelacheruvu, Jiaqi Guo, (2006)Thermal characterization of single-wall carbon nanotube bundles using the self-heating 3ω technique, *J. Appl Phys*,100, 124314

[125] I-Kai Hsu, Michael T. Pettes, Adam Bushmaker, Mehmet Aykol, Li Shi, Stephen B. Cronin, Optical Absorption and Thermal Transport of Individual Suspended Carbon Nanotube Bundles, Nano Lett., 2009, 9 (2), pp 590–594

[126] S. Chiashi, Y. Murakami, Y. Miyauchi and S. Maruyama*, (2008) Temperature Dependence of Raman Scattering from Single-walled Carbon Nanotubes -Undefined Radial Breathing Mode Peaks at High Temperatures-, *Jpn. J. Appl. Phys*., 47-4, 2010-2015.

[127] I-Kai Hsu, Michael T. Pettes, Mehmet Aykol, Chia-Chi Chang, Wei-Hsuan Hung, Jesse Theiss, Li Shi, Stephen B. Cronin, (2011) Direct observation of heat dissipation in individual suspended carbon nanotubes using a two-laser technique, *Journal of Applied Physics,* 110, 044328.

[128] Qingwei Li, Changhong Liu, Xueshen Wang, Shoushan Fan, (2009) Measuring the thermal conductivity of individual carbon nanotubes by the raman shift method, *Nanotechnology*, 20, 14.

[129] Vikram V. Deshpande, Scott Hsieh, Adam W. Bushmaker, Marc Bockrath, Stephen B. Cronin, (2009) Spatially Resolved Temperature Measurements of Electrically Heated Carbon Nano, *Phys. Rev. Lett.* 102, 105501.

[130] Eric Pop, David Mann, Jien Cao, Qian Wang, Kenneth Goodson, and Hongjie Dai (2005) Negative Differential Conductance and Hot Phonons in Suspended Nanotube Molecular Wires, Phys. Rev. Lett. 95, 155505.

[131] Eric Pop, David A. Mann, Kenneth E. Goodson, Hongjie Dai, (2007) Electrical and thermal transport in metallic single-wall carbon nanotubes on insulating substrates, *Journal of Applied Physics* 101:9.

[132] Michele Lazzeri, S. Piscanec, Francesco Mauri, A. C. Ferrari, J. Robertson, (2005)Electron Transport and Hot Phonons in Carbon Nanotubes,phys. *Rev. Lett.* 95, 236802.

[133] Adam W. Bushmaker, Vikram V. Deshpande, Marc W. Bockrath, Stephen B. Cronin, (2007) Direct Observation of Mode Selective Electron−Phonon Coupling in Suspended Carbon Nanotubes, *Nano Lett.*, , 7 (12), pp 3618–3622.

[134] Takashi Kodama, Masato Ohnishi, Woosung Park, Takuma Shiga, Joonsuk Park, Takashi Shimada, Hisanori Shinohara, Junichiro Shiomi, Kenneth E. Goodson, (2017)Modulation of thermal and

thermoelectric transport in individual carbon nanotubes by fulleren encapsulation, *Nature Materials*,16, pps 892–897.

[135] Yang, J., Yang, Y., Waltermire, S. W., Gutu, T., Zinn, A. A., Xu, T. T., Chen, Y. and Li, D. (2011), Measurement of the Intrinsic Thermal Conductivity of a Multiwalled Carbon Nanotube and Its Contact Thermal Resistance with the Substrate. *Small*, 7: 2334-2340.

[136] Matthew A. Panzer, Hai M. Duong, Jun Okawa, Junichiro Shiomi, Brian L. Wardle, Shigeo Maruyama, Kenneth E. Goodson, (2010) Temperature-Dependent Phonon Conduction and Nanotube Engagement in Metalized Single Wall Carbon Nanotube Films, *Nano Lett*., 10 (7), pp 2395–2400.

[137] Choongho Yu, Li Shi, Zhen Yao, Deyu Li, and Arunava Majumdar, (2005) Thermal Conductance and thermopower of an individual single-walled carbon nanotube, *Nano Lett*., 5 (9), pp 1842–1846.

[138] L. Jiao, B. Fan, X. Xian, Z. Wu, J. Zhang, Z. Liu, (2008) Creation of Nanostructures with Poly(methyl methacrylate)-Mediated Nanotransfer Printing, *J. Am. Chem. Soc*. 130, 38, 12612-12613.

[139] Pettes M T, Jo I, Yao Z, Shi L, (2011) Influence of polymeric residue on the thermal conductivity of suspended bilayer graphene, *Nano Lett*. 11 1195-1200.

[140] Jang W, Bao W, Ling L, Lau C N, Dames C, (2013) Thermal conductivity of suspended fewlayer graphene by a modified T-bridge method. *Appl. Phys. Lett*. 103 133102.

[141] Li H, Ying H, Chen X, Nika D L, Cocemasov A I, Cai W, Balandin A A, Chen S, (2014) Thermal conductivity of twisted bilayer graphene, *Nanoscale,* 6 13402.

[142] Young Jin Heo, Chang HunYun, Woo Nyon Kim, Heon Sang Lee, (2011)The effect of mesoscopic shape on thermal properties of multi-walled carbon nanotube mats, *Current Applied Physics*, 11, 5,1144-1148.

[143] Prasher, R. S., X. J. Hu, Y. Chalopin, N. Mingo, K. Lofgreen, S. Volz, F. Cleri, P. Keblinski, (2009) Turning Carbon Nanotubes from Exceptional Heat Conductors into Insulators, *Phys. Rev. Lett.* 102, 105901.

[144] Thess, A.; Lee, R.; Nikolaev, P.; Dai, H.; Petit, P.; Robert, J.; Xu, C.; Lee, Y. H.; Kim, S. G.; Rinzler, A. G.; Colbert, D. T.; Scuseria, G. E.;Toma´nek, D.; Fischer, J. E.; Smalley, R. E. (1996) Crystalline Ropes of Metallic Carbon Nanotubes, *Science* 1996, 273, 483.

[145] Alexey N. Volkov, Leonid V. Zhigilei, (2010) Mesoscopic Interaction Potential for Carbon Nanotubes of Arbitrary Length and Orientation, *J. Phys. Chem. C,* 114 (12), pp 5513–5531

[146] Y. Feng, T. Inoue, H. An, R. Xiang, S. Chiashi, S. Maruyama. (2018) Quantitative study of bundle size effect on thermal conductivity of single-walled carbon nanotubes, *Appl. Phys. Lett.* , submitted.

[147]] Hennrich, F.; Lebedkin, S.; Malik, S.; Tracy, J.; Barczewski, M.;Ro¨sner, H.; Kappes, M.. (2002) Preparation, characterization and applications of free-standing single walled carbon nanotube thin films, *Phys Chem. Chem. Phys*., 4, 2273.

[148] Ma, W.; Song, L.; Yang, R.; Zhang, T.; Zhao, Y.; Sun, L.; Ren, Y.; Liu, D.; Liu, L.; Shen, J.; Zhang, Z.; Xiang, Y.; Zhou, W.; Xie, S. (2007) Directly Synthesized Strong, Highly Conducting, Transparent Single-Walled Carbon Nanotube Films, *Nano Lett.* 7, 2307.

[149] J.-L. Sauvajol , E. Anglaret, S. Rols , L. Alvarez (2002) Phonons in carbon nanotube bundles, *Carbon* 40, 1697–1714

[150] Lu JP, Yang W. (1994) Shape of large single- and multiple-shell fullerenes, *Phys Rev B*;49:11421–4.

[151] Rols S. PhD thesis, University of Montpellier II, 2000.

[152] Kahn D, Ping Lu J. (1999) Vibrational modes of carbon nanotubes and nanoropes, *Phys Rev B*;60:6535–40.

[153] C. L. Kane, E. J. Mele, R. S. Lee, J. E. Fischer, P. Petit, H. Dai, A. Thess, R. E. Smalley, A. R. M. Verschueren, S. J. Tans, and C. Dekker (1998)Temperature-dependent resistivity of single-wall carbon nanotubes, *Europhys Lett*;41:683–8.

[154] Alexey N. Volkova), Richard N. Salaway, and Leonid V. Zhigilei, (2013) Atomistic simulations, mesoscopic modeling, and theoretical analysis of thermal conductivity of bundles composed of carbon nanotubes, *J. Appl Phys* 114, 104301.

[155] L. HenrardA. LoiseauC. JournetP. Bernier, (2000) Study of the symmetry of single-wall nanotubes by electron diffraction, *Eur Phys J B*;13:661–5.

[156] A.G. RinzlerJ. LiuH. DaiP. NikolaevC.B. HuffmanF.J. Rodríguez-MacíasP.J. BoulA.H. LuD. HeymannD.T. ColbertR.S. LeeJ.E. FischerA.M. RaoP.C. EklundR.E. Smalley, (1998) Large-scale purification of single-wall carbon nanotubes: process, product, and characterization, *Appl. Phys. A Mat. Sci. Process*. 67, 29.

[157] Chalopin, Y., S. Volz, and N. Mingo, (2009) Upper bound to the thermal conductivity of carbon nanotube pellets, *J. Appl. Phys.* 105, 084301.

[158] Yang, J., S. Waltermire, Y. Chen, A. A. Zinn, T. T. Xu, and D. Li, (2010) Enhanced and switchable nanoscale thermal conduction due to van der Waals interfaces, *Appl. Phys. Lett*. 96, 023103.

[159] S. Maruyama, Y. Igarashi, Y. Taniguchi and Y. Shibuta, (2004)Molecular Dynamics Simulation of Heat Transfer Issues in Carbon Nanotubes, 1st *Int. Symp. Micro. Nano. Technol*., Honolulu, XXIX-3-01.

[160] Zhong, H. and J. R. Lukes, (2006) Interfacial thermal resistance between carbon nanotubes: Molecular dynamics simulations and analytical thermal modeling, *Phys. Rev. B* 74, 125403.

[161] L. Hu and A. J. H. McGaughey, (2014) Thermal conductance of the junction between single-walled carbon nanotubes, *Appl. Phys.Lett.* 105, 193104.

[162] XuemingYang, Zhonghe Han, Yonghua Li, Dongci Chen, Pu Zhang, Albert C.To (2012) Heat welding of non-orthogonal X-junction of single-walled carbon nanotubes, *Physica E: Low-dimensional Systems and Nanostructures*, 46, 30-32

[163] Evans, W. J., M. Shen,P. Keblinski, (2012) Inter-tube thermal conductance in carbon nanotubes arrays and bundles: Effects of contact area and pressure, *Appl. Phys. Lett.* 100, 261908.

[164] Z. Xu and M. J. Buehler (2009) Nanoengineering heat transfer performance at carbon nanotube interfaces, *ACS Nano* 3, 2767.

[165] Alexey N. Volkov and Leonid V. Zhigilei, (2010) Scaling Laws and Mesoscopic Modeling of

Thermal Conductivity in Carbon Nanotube Materials, *Phys. Rev. Lett.* 104, 215902.

[166] Ali E Aliev, Marcio H Lima, Edward M Silverman and Ray H Baughman, (2010) Thermal conductivity of multi-walled carbon nanotube sheets: radiation losses and quenching of phonon mode, Nanotechnology, 21, 3.

[167] Jakubinek, M. B., M. A. White, G. Li, C. Jayasinghe, W. Cho, M. J. Schulz, and V. Shanov, (2010) Thermal and electrical conductivity of tall, vertically aligned carbon nanotube arrays, *Carbon 48,* 3947.

[168] M. I. Bagatskii, M. S. Barabashko, A. V. Dolbin, V. V. Sumarokov, (2012) The specific heat and the radial thermal expansion of bundles of single-walled carbon nanotubes, *Low Temperature Physics* 38, 523.

[169] J. Hone, M. C. Llaguno, N. M. Nemes, A. T. Johnson, J. E. Fischer, D. A. Walters, M. J. Casavant, J. Schmidt, and R. E. Smalley (2000) Electrical and thermal transport properties of magnetically aligned single wall carbon nanotube films, *Appl. Phys. Lett.* 77, 666.

[170] J. E. Fischer, W. Zhou, J. Vavro, M. C. Llaguno, C. Guthy, R. Haggenmueller, M. J. Casavant, D. E. Walters, R. E. Smalley (2003) Magnetically aligned single wall carbon nanotube films: Preferred orientation and anisotropic transport properties. *J. Appl Phys* 93, 2157

[171] Philippe Gonnet, Zhiyong Liang, Eun Sang Choi, Ravi Shankar Kadambala, Chuck Zhang, James. S. Brooks, BenWang, Leslie Kramer, (2005) Thermal conductivity of magnetically aligned carbon nanotube buckypapers and nanocomposites, *Current Applied Physics*, 6, 1.

[172] Ali E. Aliev, Csaba Guthy, Mei Zhang, Shaoli Fang, Anvar A.Zakhidov, John E.Fischer, Ray H.Baughman (2007)Thermal transport in MWCNT sheets and yarns. *Carbon*, 45, 15.

[173] Baratunde A. Cola, Xianfan Xu, Timothy S. Fisher, (2007) Increased real contact in thermal interfaces: A carbon nanotube/foil material, *Appl. Phys. Lett.* 90, 093513.

[174] Lin, W., J. Shang, W. Gu, and C. P. Wong, (2012) Parametric study of intrinsic thermal transport in vertically aligned multi-walled carbon nanotubes using a laser flash technique, *Carbon* 50, 1591.

[175] Alexey N. Volkov, Takuma Shiga, David Nicholson, Junichiro Shiomi, and Leonid V. Zhigilei (2012) Effect of bending buckling of carbon nanotubes on thermal conductivity of carbon nanotube materials, *J. Appl Phys*, 111, 053501.

[176] Alexey N. Volkov, Leonid V. Zhigilei (2010) Structural Stability of Carbon Nanotube Films: The Role of Bending Buckling, *ACS Nano,* 4 (10), pp 6187–6195.

[177] Jonathan N.ColemanaUmarKhanaWerner J.BlauaYurii K.Gun'ko, (2006) Small but strong A review of the mechanical properties of carbon nanotube–polymer composites. *Carbon*, 44, 9, 1624-1652.

[178] Michele T. Byrne and Yurii K. Gun'ko, (2010) recent advances in research on carbon annotube-polymer composite, Adv. Mater. 22, 1672–1688.

[179] Zdenko Spitalsky, Dimitrios Tasis, Konstantino sPapagelis, Costas Galiotis (2010) Carbon nanotube-polymer composites Chemistry, processing, mechanical and electrical properties, Progress in Polymer Science,35,3 357-401.

[180] Carlos Velasco-Santos, Ana L. Martínez-Hernández, Frank T. Fisher, Rodney Ruoff, and Victor M.

Castaño, (2003) Improvement of Thermal and Mechanical Properties of Carbon Nanotube Composites through Chemical Functionalization, *Chem. Mater*., 15 (23), pp 4470–4475.

[181] Ning Hu, Yoshifumi Karube, Masahiro Arai, Tomonori Watanabe, Cheng Yan, Yuan Li, Yaolu Liu, Hisao Fukunaga, Investigation on sensitivity of a polymercarbon nanotube composite strain sensor, *Carbon*, 48, 3, 680-687.

[182] P.J.F. Harris, (2003) Carbon nanotube composites, *Journal International Materials Reviews* 49,1, pp 31-43.

[183] O. Breuer, Uttandaraman Sundararaj, (2004) Big returns from small fibers A review of polymer-carbon nanotube composites. *Polymer Composite*, 25, 6, pp 630-645.

[184] M. Yudasaka, M. Zhang, C. Jabs, S. Iijima, (2000) Effect of an organic polymer in purification and cutting of single-wall carbon nanotubes, *Appl.Phys. A*., 71, 449.

[185] Zhidong Han, Alberto Fina. (2011) Thermal conductivity of carbon nanotubes and their polymer nanocomposites A review, *Progress in Polymer Science,* 36, 7, 914-944.

[186] Qiang Zhang, Jia-Qi Huang, Wei-Zhong Qian, Ying-Ying Zhang, Fei Wei, (2013) The Road for Nanomaterials Industry: A Review of Carbon Nanotube Production, Post-Treatment, and Bulk Applications for Composites and Energy Storage. *Small*, 9, 8, 1237-1265.

[187] J.-M. Moon, K. H. An, Y. H. Lee, Y. S. Park, D. J. Bae, G.-S. Park, (2001) High-Yield Purification Process of Single walled Carbon Nanotubes. *J. Phys. Chem. B*., 105, 5677.

[188] I. W. Chiang , B. E. Brinson , A. Y. Huang , P. A. Willis , M. J. Bronikowski , J. L. Margrave , R. E. Smalley , R. H. Hauge (2001) Purification and Characterization of Single-Wall Carbon Nanotubes (SWNTs) Obtained from the Gas-Phase Decomposition of CO (HiPco Process), *J. Phys. Chem. B* 105, 8297.

[189] Y. H. Wang , H. W. Shan , R. H. Hauge , M. Pasquali, R. E. Smalley, A Highly Selective, (2007) One-Pot Purification Method for Single-Walled Carbon Nanotubes. *J. Phys. Chem. B,* 111, 1249.

[190] Y. Y. Feng , H. B. Zhang , Y. Hou , T. P. McNicholas , D. N. Yuan , S. W. Yang , L. Ding , W. Feng , J. Liu, (2008) Room Temperature Purification of Few-Walled Carbon Nanotubes with High Yield, *ACS Nano*, 2, 1634.

[191] P. X. Hou , C. Liu , H. M. Cheng, (2008) Purification of carbon nanotubes, *Carbon* , 46, 2003.

[192] Coleman JN, Khan U, Gunko YK. (2006) Mechanical reinforcement of polymers using carbon nanotubes. Adv Mater;18:689–706.

[193] Thostenson ET, Ren ZF, Chou TW. (2001) Advances in the science and technology of CNTs and their composites: a review. *Compos Sci Technol* ;61:1899–912.

[194] Peng-Cheng Ma, Naveed A.Siddiqui, Gad Marom, Jang-Kyo Kim, (2010) Dispersion and functionalization of carbon nanotubes for polymer-based nanocomposites: A review. *Composites Part A: Applied Science and Manufacturing,* 41,10, 1345-1367.

[195] Gojny FH, Wichmann MHG, Köpke U, Fiedler B, Schulte K. (2004) Carbon nanotube reinforced epoxy-composites: enhanced stiffness and fracture toughness at low nanotube content. *Compos Sci*

Technol;64:2363–71.

[196] Thostenson ET, Chou TW. (2006) Processing-structure-multi-functional property relationship in carbon nanotube/epoxy composites. *Carbon*;44:3022–9.

[197] Gao B, Bower C, Lorentzen JD, L.Fleming A. Kleinhammes, X.P.Tang, L.E.McNeil,Y.Wu, O.Zhou. (2000) Enhanced saturation lithium composition in ball-milled single-walled carbon nanotubes. *Chem Phys Lett*;327:69–75.

[198] Sandler JKW, Shaffer MSP, Prasse T, Bauhofer W, Schulte K, Windle AH. (1999) Development of a dispersion process for carbon nanotubes in an epoxy matrix and the resulting electrical properties. *Polymer*;40:5967–71.

[199] Schmid CF, Klingenberg DJ. (2000) Mechanical flocculation in flowing fiber suspensions. *Phys Rev Lett*;84:290–3.

[200] Tasis D, Tagmatarchis N, Bianco A, Prato M. (2006) Chemistry of carbon nanotubes. *Chem Rev* ;106:1105–36.

[201] Park H, Zhao J, Lu JP. (2006) Effects of sidewall functionalization on conducting properties of single wall carbon nanotubes. *Nano Lett*;6:916–9.

[202] Chen J, Rao AM, Lyuksyutov S, Itkis ME, Hamon MA, Hu H, et al. (2001) Dissolution of full-length single-walled carbon nanotubes. *J Phys Chem B* ;105:2525-8

[203] Chen RJ, Zhang Y, Wang D, Dai H.(2001) Noncovalent sidewall functionalization of single-walled carbon nanotubes for protein immobilization. *J Am Chem Soc*;123:3838-9.

[204] Lordi V, Yao N. (2000) Molecular mechanics of binding in carbonnanotube-polymer composites. *J Mater Res* ;15:2770-9.

[205] A. Star, J. F. Stoddart, D. Steuerman, M. Diehl, A. Boukai, E. W. Wong, X. Yang, S.-W. Chung, H. Choi, and J. R. Heath, (2001) Preparation and Properties of Polymer-Wrapped Single-Walled Carbon Nanotubes, *Angew. Chem. Int. Ed*., 40, 1721.

[206] V. Georgakilas, K. Kordatos, M. Prato, D. M. Guldi, M. Holzinger, A. Hirsch, (2002) Organic Functionalization of Carbon Nanotubes, *J. Am. Chem. Soc.*, 124, 760.

[207] Baskaran D, Mays JW, Bratcher MS. (2005) Polymer adsorption in the grafting reactions of hydroxyl terminal polymers with multi-walled carbon nanotubes. *Polymer*;46:5050–7.

[208] Cui J, Wang WP, You YZ, Liu C, Wang P. (2004) Functionalization of multiwalled carbon nanotubes by reversible addition fragmentation chain-transfer polymerization. *Polymer*;45:8717–21.

[209] Hong CY, You YZ, Pan CY. (2006) A new approach to functionalize multiwalled carbon nanotubes by the use of functional polymers. *Polymer*;47:4300–9.

[210] Nanda Gopal Sahoo, Sravendra Rana, Jae Whan Cho, Lin Li, Siew Hwa Chan, (2010) Polymer nanocomposites based on functionalized carbon nanotubes, *Progress in Polymer Science*,35,7,837-867.

[211] Suslick KS. (1990) Sonochemistry. *Science* ;247:1439–45.

[212] Haggenmueller R, Gommans HH, Rinzler AG, Fischer JE, Winey I. (2000) Aligned single-wall carbon nanotubes in composites by melt processing methods. *Chem Phys Lett*;330: 219–25.

[213] Grossiord N, Loos J, Regev O, Koning CE. (2006) Toolbox for dispersing carbon nanotubes into polymers to get conductive nanocomposites. *Chem Mater*;18:1089–99

[214] Kosmidou TV, Vatalis AS, Delides CG, et al. (2008) Structural, mechanical and electrical characterization of epoxy-amine/carbon black nanocomposites. *Express Polym Lett*;2:364–72.

[215] Ma PC, Liu MY, Kim JK, Tang BZ, et al. (2009) Development of electrically conducting nanocomposites by employing hybrid fillers of carbon nanotubes and carbon black. *ACS Appl Mater Interfaces*;1:1090–6.

[216] C. W. Nan, (1993) Physics of inhomogeneousinorganic materials, *Prog. Mater. Sci*. 37,1.

[217] C. W. Nan, Z. Shi, Y. Lin. (2003) A simple model for thermal conductivity of carbon nanotube-based composites, *Chemical Physics Letters,* 175,5-6, 666-669.

[218] Aniruddha Bagchi, Seiichi Nomura. (2006) On the effective thermal conductivity of carbon nanotube reinforced polymer composites. *Composites Science and Technology*, 66, 11-12, 1703-1712.

[219] Chenyu Wei, Deepak Strivastava, Kyeongjae Cho. (2002)Thermal Expansion and Diffusion Coefficients of Carbon Nanotube-Polymer Composites, *Nano Letters*, 2 (6), pp 647–650.

[220] Hai M Duong, Dimitrios V Papavassiliou, Kieran J Mullen, Shigeo Maruyama,(2008) Computational modeling of the thermal conductivity of single-walled carbon nanotube–polymer composites, *Nanotechnology*, 19, 6.

[221] Fng Gong, Dimitrios V. Papavassiliou, Hai M. Doung, (2014) - Off-Lattice Monte Carlo Simulation of Heat Transfer through Carbon Nanotube Multiphase Systems Taking into Account Thermal Boundary Resistances, *Journal Numerical Heat Transfer, Part A: Applications*, 65, 11.

[222] Bryning M B, Milkie D E, Kikkawa J M and Yodh A G, (2005) Thermal conductivity and interfacial resistance in single-wall carbon nanotube epoxy composites. *Appl. Phys. Lett*. 87 161909

[223] Haggenmueller R, Guthy C, Lukes JR, Fischer JE, Winey KI. (2007) Single wall carbon nanotube/polyethylene nanocomposites: thermal and electrical conductivity. *Macromolecules*; 40:2417–21.

[224] M. Foyge, R. D. Morris, D. Anez, S. French, and V. L. Sobolev (2005)Theoretical and computational studies of carbon nanotube composites and suspensions Electrical and thermal conductivity, *Phys Rev B*.71.104201.

[225] Shiren Wang, Richard Liang, Ben Wang, Chuck Zhang, (2009) Dispersion and thermal conductivity of carbon nanotube composites, *Carbon* 47, 1, 53-57.

[226] S. Shenogin, A. Bodapati, L. Xue, R. Ozisik, P. Keblinski (2004) Effect of chemical functionalization on thermal transport of carbon nanotube composites, *Appl. Phys. Lett.* 85, 2229.

[227] Frank Garde, Dimitris C. Lagoudas, (2014) Characterization of electrical and thermal properties of carbon nanotube-epoxy composites, *Composites Part B: Engineering,* 56, 611-620.

[228] Ce-Wen Nan, Gang Liu, Yuanhua Lin, Ming Li, (2004) Interface effect on thermal conductivity of carbon nanotube composites, *Appl. Phys. Lett.* 85, 3549.

[229] C. W. Nan, R. Birringer, D. R. Clarke, H. Gleiter, (1997) Effective thermal conductivity of

particulate composites with interfacial thermal resistance, *J. Appl. Phys*. 81, 6692.

[230] C. W. Nan and R. Birringer, (1998) Determining the Kapitza resistance and the thermal conductivity of polycrystals: A simple model, *Phys. Rev. B* 57, 8264.

[231] E. T. Swartz and R. O. Pohl, (1988) Thermal resistance at interfaces, *Appl. Phys. Lett*. 51, 200 ~1987.

[232] Sergei Shenogin, Liping Xue, Rahmi Ozisik, and Pawel Keblinski, (2004) Role of thermal boundary resistance on the heat flow in carbon-nanotube composites. *J. Appl.Phys* 95, 8136.

[233] A.Moisala, Q.Li, I.A.Kinloch, A.H.Windle, (2006) Thermal and electrical conductivity of single- and multi-walled carbon nanotube-epoxy composites, *Composites Science and Technology,* 66, 10, 1285-1288.

[234] McNally T, Pötschke P, Halley P, Murphy M, Martin D, Bell SEJ, Brennan GP, Bein D, Lemoine P, Quinn JP. (2005) Polyethylene multiwalled carbon nanotube composites. *Polymer*;46:8222–32.

[235] Assouline E, Lustiger A, Barber AH, Cooper CA, Klein E, Wachtel E, Wagner HD. (2003) Nucleation ability of multiwall carbon nanotubes in polypropylene composites. *J Polym Sci B: Polym* Phys;41:520–7.

[236] Bonnet P, Sireude D, Garnier B, Chauvet O. (2007) Thermal properties and percolation in carbon nanotube–polymer composites. *Appl Phys Lett*;91:201910.

[237] E. S. Choi, J. S. Brooks, D. L. Eaton, M. S. Al-Haik, M. Y. Hussaini, H. Garmestani, D. Li, K. Dahmen. (2003) Enhancement of thermal and electrical properties of carbon nanotube polymer composites by magnetic field processing, *J. Appl.Phys* 94, 6034.

[238] Biercuk, M. J., Llaguno, M. C., Radosavljevic, M., Hyun, J. K., Johnson, A. T., & Fischer, J. E. (2002). Carbon nanotube composites for thermal management. *Appl. Phys. Lett.,* 80, pp. 2767-2769.

[239] Amy M. Marconnet, Namiko Yamamoto, Matthew A. Panzer, Brian L. Wardle, and Kenneth E. Goodson, (2011) Thermal Conduction in Aligned Carbon Nanotube–Polymer Nanocomposites with High Packing Density, *ACS Nano,* 5 (6), pp 4818–4825.

[240] P. C. Sun, Y. L. Wu, J. W. Gao, G. A. Cheng, G. Chen, R. T. Zheng, (2013) Room Temperature Electrical and Thermal Switching CNTHexadecane Composites, *Adv Mater* 25, 35, 4938-4943.

[241] Ketan S. Khare, Fardin Khabaz, Rajesh Khare, (2014) Effect of Carbon Nanotube Functionalization on Mechanical and Thermal Properties of Cross-Linked Epoxy–Carbon Nanotube Nanocomposites: Role of Strengthening the Interfacial Interactions, *ACS Appl. Mater. Interfaces,* 6 (9), pp 6098–6110.

[242] M. J. Biercuk, M. C. Llaguno, M. Radosavljevic, J. K. Hyun, A. T. Johnson, J. E. Fischer, (2002) Carbon nanotube composites for thermal management, *Appl. Phys. Lett.* 80, 2767.

[243] Park H, Zhao J, Lu JP. (2006) Effects of sidewall functionalization on conducting properties of single wall carbon nanotubes. *Nano Lett*;6:916–9.

[244] Zhou Z, Wang S, Lu L, Zhang Y, Zhang Y. (2007) Isothermal crystallization kinetics of polypropylene with silane functionalized multi-walled carbon nanotubes. *J Polym Sci B: Polym Phys*;45:

1616–24.
[245] Shen J, Hu Y, Qin C, Li C, Ye M. (2008) Dispersion behavior of single-walled carbon nanotubes by grafting of amphiphilic block copolymer. *Composites A*;39:1679–83
[246] Xiaoyi Gong, Jun Liu*, Suresh Baskaran, Roger D. Voise, James S. Young, (2000) Surfactant-Assisted Processing of Carbon Nanotube/Polymer Composites, *Chem. Mater.,* 12 (4), pp 1049–1052.
[247] Brandrup, J., Immergut, E. H., Grulke, E. A., Eds. (1999) Polymer Handbook, 4th edition; *Wiley: New York,* Vol. 17.
[248] Carlos Velasco-Santos, Ana L. Martínez-Hernández, Frank T. Fisher, Rodney Ruoff, and Victor M. Castaño,(2003) Improvement of Thermal and Mechanical Properties of Carbon Nanotube Composites through Chemical Functionalization, *Chem. Mater.,* 15 (23), pp 4470–4475.